المؤتمر العلمي الدولي الرابع عشر
لجمعية الرياضيات العراقية والمنعقد تحت شعار
الإبداع يلتقي بالتحديات من اجل التقدم العلمي والتكنولوجي
للمدة 4 - 5 اب 2024
دمشق - سورية

Comparing the Concentrations of Chromium, Iron and Manganese in the Serum of Prostate Cancer with the Control

Shaymaa Awad Kadhim[1] ,Allawi Hamead Harjan[2], Ahmed Ali Ghali Al-Khayfawee[3], Noor Ali Jaafar Al-Quraishi[4], *Naeema Hadi Ali*[5]

[1,3,4,5] Department of Physics /Faculty of Science/ University of Kufa /Iraq

allawi.alasadi@uokufa.edu.iq[a]

shaymaa.alshebly@uokufa.edu.iq[b]

Abstract

Prostate cancer is one of the most serious illness that threaten human life, but its his reason is still undetermined. Trace elements play diverse roles in life of society. Trace elements such as Cadmium, Iron, and Manganese are inherent to this type of cancer, although their roles are not evident. The research investigate and comparative serum concentrations of these elements in prostate cancer patients with a normal group. A total of 100 samples used in this work. The samples were divided into 50 for healthy with average age (62.8 ± 7) and 50 for those infected from males whose ages were (65.3 ± 4), family history, tobacco and alcohol status. Subsequent to sample preparation, serum levels of Cd, Fe and Mn were measured using Flame Atomic Absorption spectrophotometer (FAAS). Concentrations of Cd, Fe and Mn were elevated in prostate cancer patients compared to normal ($p<0.05$). This research supports the assumption that exposure to Cd, Fe and Mn increases the risk of prostate cancer. These discoveries have the potential to speed up the diagnosis and processing of prostate cancer. There is a need to conduct more studies and research with more samples to determine whether heavy metals have a role in causing prostate cancer.

Keywords: *Trace elements, Prostate cancer, Atomic absorption Spectrophotometer, Cancer risk.*

Introduction

Throughout hemopoiesis, trace elements play a significant role as necessary components or cofactors of enzymes. The metabolically significant enzymatic pathway[1], plays a vital role in most trace elements during hemopoiesis. Furthermore, trace elements may bond to red blood cells and be delivered to target organs as they enter the body. As a result, trace elements can affect not only the production of red blood cells, but also the distribution and

storage of blood cells in target organs, changing the state of blood parameters in the body[2] .

To organize data about the substance and physiological job of chemical elements in the body, a few characterizations has been proposed as of late. Without analyzing them exhaustively, One of the standards of characterization is division of chemical elements into three gatherings, contingent upon their items in the creature of vertebrates and people[3].

The first gathering in this order is "macro elements", whose focus in the body surpasses 0.01%. They are: N, Ca, P, K, O, Na, S, Cl, Mg, C, H. The outright body content of these components (For people with a weight of 70 kilograms) goes from a couple of grams (Mn) to above forty kilograms (O). A few components of this gathering are designated "organogens" (Oxygen, Hydrogen, Carbon, Sulphur, Nitrogen and Phosphorus) because of their driving job of tissues and organs[4].

The second gathering is "trace elements", and their focus scopes from 0.00001% to 0.01%. This gathering incorporates: Cu, Br, Si, Cs, I, Mn, Fe, Al, Pb, Rb, Cd, B, Zn, F, Sr, Mo. The body contains these elements in quantities from many milligrams to a few grams. In any case, in spite of the "little" satisfied, trace elements are not irregular elements of natural material, but rather parts of a confounded physiological framework associated with the guideline of indispensable capacities at all transformative phases of the living life form[5].

The last gathering is "ultratrace elements", and their levels is less than 0.000001%. These are Ba, Ti, Ag, Sn, Be, Ga, Se, Co, V, Cr, As, U, Th, Rh, Ni, Li, Ge, Hg, Sc, Zr, Bi, Sb. Its substance inside the human body is estimated at less than a gram. In this group there are elements necessary for the living organism, for example, Co, Se, C at the present time [6].

The elements that have been classified according to the opinion of the World Health Organization are 19 elements, including Cd, Ni, As, Zn, Se, which are necessary for a healthy body[7] .The evolution of cancer and its relationship to tratrace elements is still unknown[8].

The frequent use of the prostate specific antigen(PSA test) and the increasing tests in recent years for early detection of prostate cancer, weight gain, unhealthy diet, drinking, smoking, sexual and physical activity[9], Genetic and environmental factors increase the risk incidence of this disease, in addition to that it plays a major role in the growth and reproduction of malignant cells directly by stimulating the pathogenic pathways cancer or

by stimulating hereditary genes for disease[10]. Hormonal regulation or metabolism resulting from the involvement of carcinogenic factors, as indicated by indirect mechanisms[11].

Prostate cancer infect 2.78 people per 100,000 (Iraqi Cancer Council 2011), according to what was recorded by the Iraqi Cancer Council in Iraq, although the incidence of this disease is not fully known[12]

Trace elements, including Fe, Pd, and Co, are potentially carcinogenic to humans. This is confirmed by the epidemiological evidence. It was found that there is a large participation of cadmium in the increase in the number of deaths from prostate cancer[13].

It is possible that there is a link between the incidence of prostate cancer and the concentrations of minerals in the human body, which was shown by biochemical studies, and these minerals included a list of Mg, Se, Mn, B, Ca, Zn, Co, Cr, Fe [14, 15]

Recent studies have confirmed the importance of heavy metals in human blood components, so they should be used as biomarkers to detect many diseases, including cancer [16].

The main objective of the study was to conduct a practical study in the field of prostate cancer using physical techniques and then treat the results statistically using the SPSS statistical program, in the hope of finding a method through which to accurately diagnose this dangerous disease and take the necessary treatment measures to reduce the number of deaths. The novelty of research in collecting a group of blood serum samples for the Najaf area, the tumor center, and studying the relationship of these elements with some for the first time at the local level.

Material and methods

Three ml of blood samples were gathered from fifty (50) of people diagnosed with prostate cancer from Middle Euphrates Cancer Center and fifty (50) healthy control from Main Blood Bank in Najaf Governorate of Iraq where the average age (62.8 ± 7) for group health and infected from was (65.3 ± 4) for prostate cancer group. A centrifuge was used to centrifuge the blood samples and obtain the blood serum in 2000 cycles for 10 minutes and keep the serum in deep freezing at -20°C for use in preparing the samples for the purpose of measurement. To digest the protein particles in the serum samples, we added 2:1 ml of a mixture of NHO3 acid and HClO4 acid, respectively to serum under 85°C. Deionized water was used to dilute the fully digested samples with 20 ml per sample and filtered in 0.4 µm

type filter paper and measured using Flame Atomic Absorption Spectrophotometer (F-AAS) type 7000A Shimadzu, Japan . Measurement results are express it in ppm[17, 18] .

Statistical analysis

The data were statistically processed using the statistical program SPSS version 20.0, IBM, USA. Changes, linkages, and associations between variables in the groups were identified using analysis of variance (ANOVA), multiple regression, and Pearson's correlation, respectively. Statistical significance was defined as $P < 0.05$. Also, express the results using a mean plus or minus the standard deviation[19].

Results and Discussion

Trace element concentrations shown in table 1. According to statistical study, prostate cancer (PCa) patients have a very high level of iron (Fe) in their serum when compared to control persons (1.2960±0.5160, 0.6890±0.2810) with $p \leq 0.05$ indicating substantial differences There were significant differences at the $p \leq 0.05$ level. Several epidemiological and clinical trials showed that low Fe levels could decrease cancer incidence including prostate cancer [20-22], On contrary, [23] reported results indicating that increased iron stores weren't associated with prostate cancer. Cadmium (Cd) levels in the serum of PCa patients were higher than in healthy people respectively (0.0787±0.0147, 0.0344±0.0262) with inequalities in significance .

In addition manganese (Mn) In comparison to healthy persons, the results showed a high amount in prostate cancer patients' serum respectively (0.0333±0.0312, 0.0040±0.002582) comparison with international studies[24].

Also the concentrations of Cd, Fe and Mn elements measured in ppm. The maximum value of the concentration of elements measured in this study were (0.111, 3.566 and 0.1608) and the minimum values was (0.0500, 0.8840 and 0.0041) for prostate cancer patients respectively. Also the maximum value of the concentration of elements were (0.1230, 1.4320 and 0.0091) and the minimum values was (0.0097, 0.1010 and 0) for healthy. In addition, the highest mean value of the concentration was noted at Iron 3.566 in patient samples and the lowest mean value was at Manganese 0 for healthy.

Table1:Shows the trace element concentration in prostate cancer and healthy (mean and standard deviation).

Concentration(ppm)	Number	Prostate cancer				Healthy			
		Mean± Std. Deviation	Std. Error	Minimum	Maximum	Mean± Std. Deviation	Std. Error	Minimum	Maximum
Cd	50	.078714±.0146539	.0020724	.0500	.1111	.034368±.0261665	.0037005	.0097	.1234
Fe	50	1.296206±.5160677	.0729830	.8842	3.5661	.688614±.2811291	.0397577	.1006	1.4321
Mn	50	.033282±.0311622	.0044070	.0041	.1608	.004000±.0025819	.0003651	.0000	.0091
Total	150	.469401±.6575846	.0536916	.0041	3.5661	.242327±.3558472	.0290548	.0000	1.4321

Also from table(1), we note that the comparative among Cd, Fe and Mn concentration (ppb) for health group and prostate cancer group ,where was the concentration of iron was higher than the another elements but the concentration of cadmium was the less than the other elements,

Table 2: It shows some statistical indications such as Mean Square, F leven;s test and Sig.

		Sum of Squares	df	Mean Square	F	Sig.
Healthy	Between Groups	14.961	2	7.480	281.485	.000
	Within Groups	3.907	147	.027		
	Total	18.867	149			
Prostate cancer	Between Groups	51.322	2	25.661	287.775	.000
	Within Groups	13.108	147	.089		
	Total	64.430	149			

From table 2, Shown the Concentrations of trace elements in this study iron, cadmium and manganese were significant by using Anova test for prostate cancer patients compared to controls , increased in concentration of serum heathy, as shown in figure 1 below.

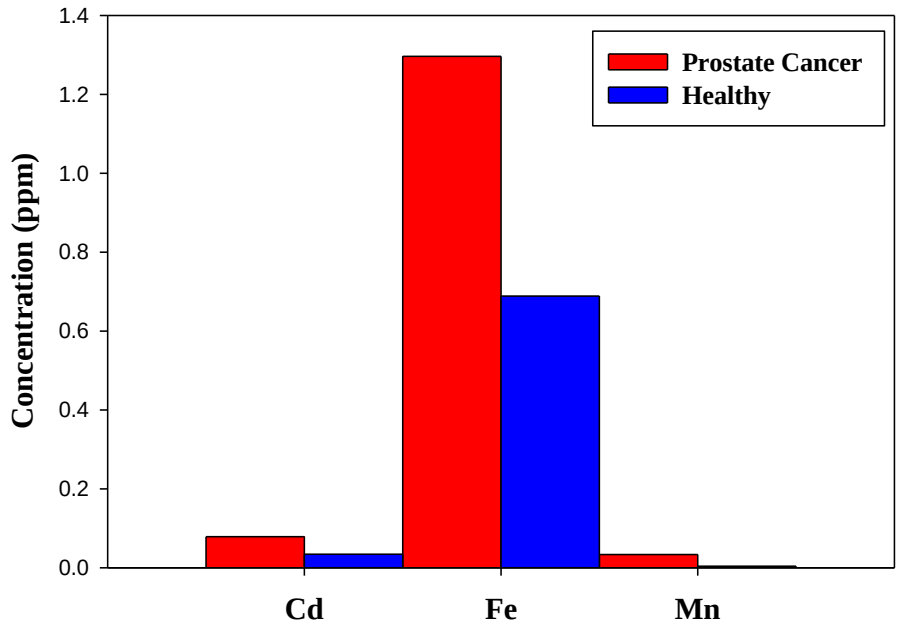

Figure 1: Comparison the iron, cadmium and manganese concentration in prostate cancer patients is compared to healthy controls.

Table 3. A study of the interrelationships between the three studied elements

		Cd(ppb)H.	Cd(ppb) P.C	Fe(ppb)H.	Fe(ppb) P.C	MN(PPB)H.	Mn(ppb) P.C
Cd(ppb) H.	Pearson Cor.	1					
	P value						

Cd(ppb) P.C	Pearson Cor.	-.043-	1				
	P value	.767					
Fe(ppb) H.	Pearson Cor.	.104	-.002-	1			
	P value	.474	.990				
Fe(ppb) H.	Pearson Cor.	-.001-	.033	-.126-	1		
	P value	.993	.822	.385			
MN(PPB)H.	Pearson Cor.	.123	-.076-	.128	.146	1	
	P value	.393	.602	.377	.311		
Mn(ppb) P.C	Pearson Cor.	.006	-.155-	-.039-	-.105-	-.076-	1
	P value	.968	.283	.788	.467	.600	

It is clear from the Pearson factor comparison table that the relationship is not positive and weak and not statistically significant among the studied trace element where the value of Pearson factor was note found equal 1, the value on which the extent of the bonding strength is compared in the light of this study and according to the samples, number and area

Conclusions

Through this study, the concentrations of the elements selected in this research were high for all prostate cancer patients, whereas these concentrations were low for healthy people, indicating the effect of these elements on the serum of the disease, which can be a catalyst for this malignant tumor .This research backs up the theory that exposure to iron, cadmium, and manganese raises the risk of prostate cancer. These discoveries could help doctors diagnose and treat prostate cancer more quickly. There is a need to conduct more studies and research with more samples to determine whether heavy metals have a role in causing prostate cancer.

Acknowledgment

We extend our thanks to all the Middle Euphrates Cancer Centre and Main Blood Bank employees, in Najaf Governorate of Iraq, especially the centre director, the working doctors, and the calculator unit, for their assistance in completing the research.

REFERENCES

1. Garnica, A.D., *Trace metals and hemoglobin metabolism.* Annals of Clinical & Laboratory Science, 1981. **11**(3): p. 220-228.
2. Janicka, M., et al., *Cadmium, lead and mercury concentrations and their influence on morphological parameters in blood donors from different age groups from southern Poland.* Journal of Trace Elements in Medicine and Biology, 2015. **29**: p. 342-346.
3. Nagel, T., *Conceiving the impossible and the mind-body problem.* Revista Română de Filosofie Analitică, 2012. **6**(1): p. 5-21.
4. Ryerson, E., *First Lessons on Agriculture for Canadian Farmers and Their Families*. 1871: Copp, Clark.
5. Vandecasteele, C. and C.B. Block, *Modern methods for trace element determination*. 1997: John Wiley & Sons.
6. Haraguchi, H., *Metallomics: Integrated biometal science*, in *Metallomics*. 2017, Springer. p. 3-39.
7. Lv, J., et al., *Effects of several environmental factors on longevity and health of the human population of Zhongxiang, Hubei, China.* Biological trace element research, 2011. **143**(2): p. 702-716.
8. Circuncisão, A.R., et al., *Minerals from macroalgae origin: Health benefits and risks for consumers.* Marine Drugs, 2018. **16**(11): p. 400.
9. Kristal, A.R., et al., *Associations of demographic and lifestyle characteristics with prostate-specific antigen (PSA) concentration and rate of PSA increase.* Cancer: Interdisciplinary International Journal of the American Cancer Society, 2006. **106**(2): p. 320-328.
10. Olumi, A.F., et al., *Carcinoma-associated fibroblasts stimulate tumor progression of initiated human epithelium.* Breast Cancer Research, 2000. **2**(1): p. 1-1.

11. Niu, B., et al., *In vivo genome-wide binding interactions of mouse and human constitutive androstane receptors reveal novel gene targets.* Nucleic acids research, 2018. **46**(16): p. 8385-8403.
12. Hussain, A.M. and R.K. Lafta, *Cancer Trends in Iraq 2000–2016.* Oman medical journal, 2021. **36**(1): p. e219.
13. Kaba, M., et al., *Serum levels of trace elements in patients with prostate cancer.* Asian Pacific Journal of Cancer Prevention, 2014. **15**(6): p. 2625-2629.
14. Zaichick, V. and S. Zaichick, *Dietary intake of minerals and prostate cancer: insights into problem based on the chemical element contents in the prostate gland.* J Aging Res Clin Practice, 2015. **4**(3): p. 164-171.
15. Diniz, W.J., et al., *Detection of co-expressed pathway modules associated with mineral concentration and meat quality in nelore cattle.* Frontiers in Genetics, 2019. **10**: p. 210.
16. Ventura, C., et al., *Biomarkers of effect as determined in human biomonitoring studies on hexavalent chromium and cadmium in the period 2008–2020.* Environmental Research, 2021. **197**: p. 110998.
17. Alshebly, S.A.K., et al. *Serum levels of lead, cadmium and silver in patients with breast cancer compared with healthy females in Iraq*. in *AIP Conference Proceedings*. 2019. AIP Publishing LLC.
18. Hussein, H.H., et al., *Study the Impact of the Trace Elements between the Healthy Females and who take Chemotherapy for samples of Sera.* Research Journal of Pharmacy and Technology, 2017. **10**(10): p. 3323-3325.
19. Pituch, K.A. and J.P. Stevens, *Applied multivariate statistics for the social sciences: Analyses with SAS and IBM's SPSS*. 2015: Routledge.
20. Knekt, P., et al., *Antioxidant vitamin intake and coronary mortality in a longitudinal population study.* American journal of epidemiology, 1994. **139**(12): p. 1180-1189.
21. Liszka, H.A., et al., *Prehypertension and cardiovascular morbidity*. Annals of family Medicine, 2005. **3**(4): p. 294.
22. Zacharski, L.R., et al., *Decreased cancer risk after iron reduction in patients with peripheral arterial disease: results from a randomized trial.* JNCI: Journal of the National Cancer Institute, 2008. **100**(14): p. 996-1002.
23. Kuvibidila, S.R., T. Gauthier, and W. Rayford, *Serum ferritin levels and transferrin saturation in men with prostate cancer.* Journal of the National Medical Association, 2004. **96**(5): p. 641.
24. Arinola, O., *Essential trace elements and metal binding proteins in Nigerian consumers of alcoholic beverages.* Pak. J. Nutr, 2008. **7**(6): p. 763-765.

المؤتمر العلمي الدولي الرابع عشر
لجمعية الرياضيات العراقية والمنعقد تحت شعار
الإبداع يلتقي بالتحديات من اجل التقدم العلمي والتكنولوجي
للمدة 4 - 5 اب 2024
دمشق - سورية

Finite difference time domain as a tool to solve light interaction problems

Dana .S.Akil

Abstract

Optics and photonics are exciting, rapidly developing fields building their success largely on use of more and more elaborate artificially made, nanostructured materials. To further advance our understanding of light-matter interactions in these complicated artificial media, numerical modeling is often indispensable. Examples of the use of the finite-difference frequency-domain method in this thesis range from simulating localized modes in a three-dimensional photonic-crystal membrane-based cavity, a quasi-one-dimensional nanobeam cavity and arrays of side-coupled nanobeam cavities, to modeling light propagation through metal films with single or periodically arranged multiple subwavelength slits.

Introduction

Numerical analysis is the study of algorithms that use numerical approximation for the problems of mathematical analysis .Almost no modern physics can be studied without computer simulations .Even analytical calculations ,often require computer algebra systems are not fully analytical, but “numerically exact calculations”. Typical problems in physics, which can be solved numerically: Linear systems. Eigenvalue and eigenvector problems. Integration in one or more dimensions. Differential equations.Root finding (Nullstellensuche), optimization (finding minima or maxima). Different numerical software are used by the scientist including COMSOL,Lumerical , Matlab)

The finite difference time domain(FTDT)

Optics and photonics are exciting, rapidly developing fields building their success largely on use of more and more elaborate artificially made, nanostructured materials.

Finite-difference method, a very general tool to solve Maxwell’s equations in arbitrary geometries in three dimensions, with an emphasis on the frequency-domain formulation. Examples of the use of the finite-difference frequency-domain method range from simulating localized modes in a three-dimensional photonic-crystal membrane-based cavity, a quasi-one-dimensional nanobeam cavity and arrays of side-coupled nanobeam cavities, to modeling light propagation through metal films with single or periodically arranged multiple subwavelength slits. Manipulating light at the micro- and nanoscale was hardly possible or even imaginable. By now progress in fabrication techniques and our understanding of light-matter interactions have turned optics into one of the most dynamic, rapidly developing and promising fields of mesoscopic physics; even the new term, photonics, was invented and

widely accepted to emphasize numerous new developments and directions such as image resolution below diffraction limit [1,2] and superfocusing [3,4]; optical cloaking [5,6]; ultrafast photonic chips [7,8]; lossless, nonlinear and gain materials [9]; optical modulators [10], couplers [11], switches [12] and light sources on nanoscale [13]. This is naturally followed by a multitude of applications to technology [14], biophysics [15], energy harvesting [16], lightning [17], and medical science [18].

And like fifty years ago it was hard to envisage the perspectives of semiconductor transistors in building computers and all of that today's electronic equipment, it is in the same way unpredictable what current research activity in nanophotonics will lead to. What we can say with confidence yet is that in order to utilize the tremendous potential of classical and quantum optics phenomena in real-life applications, a systematic understanding and deep intuition for the behavior of light in various nanostructured arrangements should be developed by each practitioner in the field. To develop such intuition for light-matter interactions in complex photonic bandgap or plasmonic structures, to design nontrivial devices and to explore new phenomena, efficient numerical modeling is the key..

Reference

[1] E. Ozbay, "Plasmonics: merging photonics and electronics at nanoscale dimensions," Science, vol. 311, pp. 189–193, 2006.

[2] S. A. Ramakrishna, "Physics of negative refractive index materials," Reports on Progress in Physics, vol. 68, pp. 449–521, 2005.

[3] N. Kundtz and D. R. Smith, "Extreme-angle broadband metamaterial lens," Nature Materials, vol. 9, pp. 129–132, Feb. 2010

[4] X. Zhang, "Electromagnetic waves in 2d photonic crystals," Materials Today, vol. 12, pp. 44–51, 2009.

[5] J. Valentine, J. Li, T. Zentgraf, G. Bartal, and X. Zhang, "An optical cloak made of dielectrics," Nature Materials, vol. 8, pp. 568–571, July 2009.

[6] J. Zhang, Y. Luo, and N. A. Mortensen, "Minimizing the scattering of a nonmagnetic cloak," Applied Physics Letters, vol. 96, p. 113511, 2010.

[7] M. Paniccia and N. Photonics, "Integrating silicon photonics," Nature Photonics, vol. 4, pp. 498–499, Aug. 2010.

[8] H.-W. H¨ubers, "Terahertz technology: Towards THz integrated photonics," Nature Photonics, vol. 4, pp. 503–504, Aug. 2010.

[9] J. Leuthold, C. Koos, and W. Freude, "Nonlinear silicon photonics," Nature Photonics, vol. 4, pp. 535–544, July 2010.

[10] H.-T. Chen, W. J. Padilla, M. J. Cich, A. K. Azad, R. D. Averitt, and A. J. Taylor, "A metamaterial solid-state terahertz phase modulator," Nature Photonics, vol. 3, pp. 148–151, 2009.

[11] F. Lopez-Tejeiro, S. G. Rodrigo, L. Martin-Moreno, F. J. Garcia-Vidal, E. Devaux, T. W. Ebbesen, J. R. Krenn, I. Radko, S. I. Bozhevolnyi, M. U. Gonzalez, J. C. Weber, and A. Dereux, "Efficient unidirectional nanoslit couplers for surface plasmons," Nature Physics, vol. 3, pp. 324– 328, 2007.

[12] S. Carretero-Palacios, A. Minovich, D. N. Neshev, Y. S. Kivshar, F. J. Garcia-Vidal, L. Martin-Moreno, and S. G. Rodrigo, "Optical switching in metal-slit arrays on nonlinear dielectric substrates," Optics Letters, vol. 35, pp. 4211–4213, Dec. 2010.

[13] A. J. Shields, "Semiconductor quantum light sources," Nature Photonics, vol. 1, pp. 215–223, Apr. 2007.

[14] H. J. Caulfield and S. Dolev, "Why future supercomputing requires optics," Nature Photonics, vol. 4, pp. 261–263, May 2010.

[15] M. Celebrano, P. Kukura, A. Renn, and V. Sandoghdar, "Single-molecule imaging by optical absorption," Nature Photonics, pp. 95–98, January 2011

[16] A. P. Kulkarni, K. M. Noone, K. Munechika, S. R. Guyer, and D. S. Ginger, "Plasmon-enhanced charge carrier generation in organic photovoltaic films using silver nanoprisms," Nano Letters, vol. 10, pp. 1501–1505, Apr. 2010.

[17] D. Cyranoski, "Seeing the light," Nature, vol. 94, p. 726, 2003

[18] N. I. Smith, "Biophotonics: A light to move the heart," Nature Photonics, vol. 4, pp. 587–589, Sept. 2010.

المؤتمر العلمي الدولي الرابع عشر
لجمعية الرياضيات العراقية والمنعقد تحت شعار
الإبداع يلتقي بالتحديات من اجل التقدم العلمي والتكنولوجي
للمدة 4 - 5 اب 2024
دمشق - سورية

ديناميكيات تغيرات سبين نواة ^{57}Fe باستخدام مطيافية ميوسباور

د. مصطفى ديلو

جامعة البعث – كلية العلوم – فسم الفيزياء.

ملخص البحث

لقد أتاحت أحدث التحليلات الطيفية لميوسباور تقدماً لا يرقى إليه الشك في دراسة البنية المجهرية الصلبة. إذ تم في هذا العمل دراسة ديناميكية تحولات سبين النووي لنواة ^{57}Fe باستخدام مطيافية ميوسباور. لإجراء ذلك لا بد من فعل تحريضي حيث يطبق حقل ترددات راديوية rf مغنطيسي مهتز، ذات آثار قوية مترابطة ، على نواة ميوسباور .لقد تم كموسياً دراسة التأثير المتبادل لنواة ميوسباور ^{57}Fe مع إشعاع γ وحقول فوق دقيقة. وأيضاً في هذا المضمار درست تغيرات ديناميكية مغنطيسية لـ^{57}Fe في حقول rf مغنطيسية مهتزة. ومن ثم تمت دراسة الانتقالات الديناميكية السبينية لمنظومة نواة ميوسباور ^{57}Fe في حقل rf مهتزة وفق مفهوم الحالات شبه الطاقية. ومن خلال ذلك نم التوصل لحالات التحولات السبين الانتقالية الزمنية .

الكلمات المفتاحية: حقل الترددات الراديوية rf المغنطيسي المهتز- المطيافية موسباورية – تحولات السبين النووي الانتقالية – الحالات شبه الطاقية – لهملتونيان – معادلة الحركة.

Dynamics of spin conversion of the ^{57}Fe nucleus using Mossbauer spectroscopy

Dr. M. Dilo

Al-Baath university - faculty of science - department of physics.

Abstract

The state of the art Mossbauer spectroscopy has made unquestionable advance possible in the solid micro- structure study. In this work, the dynamics of nuclear spin transformations of the ^{57}Fe nucleus were studied using Musebauer spectroscopy. To do this, an inductive action is required, in which an alternating magnetic rf field, with strong coherent effects, is applied to the Mossbauer nucleus. The interactions of the Mossbauer nucleus ^{57}Fe with γ radiation and superfine fields has been quantitatively studied. Also, in this regard, I studied the dynamic magnetic conversions of ^{57}Fe in alternating magnetic rf fields. Then, the dynamic spin transformations of the ^{57}Fe Mossbauer nucleus system were studied in an alternating rf field according to the concept of quasi-energy states. During this, the cases of temporal transitional spin transitions were achieved.

المؤتمر العلمي الدولي الرابع عشر
لجمعية الرياضيات العراقية والمنعقد تحت شعار
الإبداع يلتقي بالتحديات من اجل التقدم العلمي والتكنولوجي
للمدة 4 - 5 اب 2024
دمشق - سورية

الهدف البحث (Aim of research)

1-دراسة ديناميكية تحولات السبين النووي لنواة ميوسباور ^{57}Fe تحت تأثير حقل قوي rf مغنطيسي خارجي مهتز.

2- دراسة المغنطة خلال تغيرات ديناميكية مغنطيسية لـ^{57}Fe في حقول rf مهتزة.

3- دراسة الحالات شبه الطاقية لأجل تحولات ديناميكية لسبين نواة ^{57}Fe

مقدمة

بنيت مطيافية ميوسباور على ميكانيك الكم إذ توفر هذه المطيافية ارتباطاً بين الفيزياء النووية والحالة الصلبة. تقيس مطيافية ميوسباور الطاقات التي تمتصها نوى محددة عندما تسقط عليها أشعة غاما. من الغريب ان تصدر نواة واحدة أشعة غاما وتمتصها نواة ثانية بنفس الكفاءة باعتبار أن الجزيئات المحتوية على نواتين يجب أن تكون مترابطة كيميائياً بالحالة الصلبة [1]. إن معظم تطبيقات مطيافية ميوسباور في استخدام علوم المواد تعتمد على التأثيرات المتبادلة الفوق الدقيقة التي فيها تحرض الالكترونات حول النواة السويات الطاقية النووية أو يتم تحرضها بفعل تطبيق حقل كهرطيسي خارجي على النواة . تبدو مطيافية ميوسباور أكثر فعالية في دراسة التأثيرات المتبادلة فوق الدقيقة في المواد الصلبة، خاصة بالنسبة للعديد من المواد المغناطيسية. ليس فقط بواسطة مطيافية ميوسباور ممكناً تحديد خصائص المادة في حالة ثابتة، ولكن أيضاً ممكن دراسة عينات من المادة واقعة تحت تأثير حقول خارجية متغيرة [2-5]. تحدث التغييرات الأكثر اهتماماً في أطياف ميوسباور في الحالة، التي عندها تكون هذه الحقول مترابطة. إن أثر الحقل المترابط يمكن أن يكون مثلاً حقلاً مغنطيسياً ذا ترددات راديوية (rf) [6, 7].

من جهة أخرى فإن تجارب Mössbauer في حقول خارجية متغيرة هي أدوات لضوء غاما ميوسباور، الذي في إطاره لا ينحصر التركيز الأساسي للحصول على معلومات حول المادة، ولكن ينحصر للحصول على تعديلات، ويتم التركيز على تغيير متحولات إشعاع غاما. إن التجارب ميوسباور التي تم إجراءها في حقول خارجية تستخدم الآن كطريقة لمثل هذه التغييرات المقصودة. لذلك يعتبر من المهم دراسة الحالة المغناطيسية-السبينية لمادة مغناطيسية عند وجود تطبيق مغناطيسي ديناميكي في حقول مغناطيسية ذي ترددات راديوية rf. تم دراسة عينات بارا مغناطيسية (Fe^{3+}) في غياب حقل rf خارجي. حيث جعل استرخاء السبين الالكتروني و مخطط السويات النووية الالكترونية شروط التجربة صعبة جداً [8-9]. لوحظ أيضاً اقتراح تحقيق تجاوب مضاعف غاما الراديوي DGR في المواد الديومغناطيسية مبنياً على تأثير متبادل مع رباعي القطب الكهربائي للنواة. تجذب فيزياء ظاهرة تجاوب مضاعف غاما الراديوي DGR انتباه الباحثين باستمرار حيث يتم التعامل مع ديناميكيات السبين الكمومي في حقول نووية مرتبطة [10-11]. إن أفعال rf المغناطيسية الديناميكية على أطياف ميوسباور مهمة أيضاً لا غنى عنها تظهر فيها تأثيرات فوق دقيقة للحقل rf على نوى ميوسباور [12]. تم إجراء تجارب مثيرة للاهتمام لإيضاح إمكانية تطبيق حقول واسعة النطاق rf على رقائق الفولاذ المقاوم للصدأ [13]. كل هذا يجعل الأبحاث في مجال مطيافية ميوسباور لمنظومات سبين لا متوازنة أكثر واقعية. من الضروري دراسة التأثيرات الديناميكية المغناطيسية في أطياف ميوسباور دون التقيد بشروط التجاوب DGR. نفترض أنه تم تطبيق حقل مغناطيسي rf خارجي على نواة حديد ^{57}Fe (نظير ميوسباوري) لتتجاوز عرض الخط الطبيعي لإشعاع غاما حيث يتم تضخيم الحقل الخارجي للنواة بواسطة التأثير المتبادل فوق الدقيق و بالتالي الحقول الموجودة في النواة تبدو أنها تعتمد بشدة على حدود المغنطة الزمنية للعينة.

تأثير متبادل لنواة ميوسباور ^{57}Fe مع إشعاع γ وحقول فوق دقيقة

إن الخلط التجاوبي لسويات زيمن الفرعية بواسطة الحقل المغنطيسي RF هو آلية فعالة تؤدي إلى ديناميكية مترابطة لسبين نواة ميوسباور في المواد المغناطيسية. يتضح انه يمكن التعبير عن تحليل تأثيرات التداخل الكمي التي قد تحدث في مثل هذا الترابط من خلال مجموع مؤثر هاملتون لكل على حدى[7] ويمكن التعبير عن الهاميلتونيان الكلي بالشكل:

$$\hat{H} = \hat{H}_N^0 + \hat{H}_g^0 + \hat{H}_e^0 + \hat{H}_Q + \hat{H}_\gamma^0 + \hat{H}_{rf}^0 + \hat{H}_\gamma + \hat{H}_{rf}. \quad (1)$$

حيث تعني هذه الحدود، $\hat{H}_N^0$ و $\hat{H}_{g,e}^0$ التأثير المتبادل النووي الداخلي والتأثير المتبادل للحقل المغناطيسي فوق الدقيق مع الحالة الأساسية والمتحرضة للنواة ، ويصف الحد $\hat{H}_Q$ تأثير متبادل رباعي القطب الكهربائي. يمكن كتابة الحدود الأربعة الأولى في العلاقة (1) كالآتي:

$$\hat{H}_N^0 = \varepsilon_0 \sum_M \hat{a}_M^+ \hat{a}_M, \qquad \hat{H}_g^0 = \sum_m \varepsilon_m \hat{a}_m^+ \hat{a}_m,$$

$$\hat{H}_e^0 = \sum_M \varepsilon_M \hat{a}_M^+ \hat{a}_M, \quad \hat{H}_Q = \sum_{M,M'} Q_{MM'} \hat{a}_M^+ \hat{a}_{M'}. \qquad (2)$$

حيث $\hat{a}_m^+$ و$\hat{a}_m$، $\hat{a}_M^+$ و$\hat{a}_M$ – مؤثرات فيرمي للتوالد والفناء بقيم معينة(m, M) للمؤثر $\hat{I}_z^{g,e}$ وε_0 هي طاقة تحول ميوسباور. و تعبر الحدود التالية: $\hat{H}_\gamma^0$ و$\hat{H}_{rf}^0$ في (1) عن حقل الفوتونات غاما وحقل rf في حدود مؤثرات بوزه والترددات الموافقة: $\hat{c}_k^+$، $\hat{c}_k$ وω_k، $\hat{b}$ و$\hat{b}^+$، ω_0، على التوالي (نفترض أن$\hbar = 1$):

$$\hat{H}_\gamma^0 = \sum_k \omega_k \hat{c}_k^+ \hat{c}_k, \quad \hat{H}_{rf}^0 = \omega_0 \hat{b}^+ \hat{b}. \qquad (3)$$

يعبر الحد $\hat{H}_\gamma$ عن التأثير المتبادل بين النواة و فوتون غاما (k, σ, L) – الشعاع الموجي والاستقطابية والتعددية القطبية على التوالي و(α, β, γ) – زوايا أولر التي تحدد اتجاه انتشار فوتون غاما:

$$\hat{H}_\gamma = \hat{H}_\gamma(k, \sigma, L, \alpha, \beta, \gamma)$$

$$= K \sum_{M,m} \sigma^{\Delta(\pi)} D_{\mu\sigma}^L(\alpha, \beta, \gamma) \langle I_g m L \mu | I_e M \rangle \hat{c}_k \hat{a}_M^+ \hat{a}_m \qquad (4)$$

$\Delta(\pi) = 0 \; or \; 1$ (اشعاع متعدد أقطاب كهربائي أو مغناطيسي)؛ $D_{\mu\sigma}^L(\alpha, \beta, \gamma)$ – هي مصفوفة الدوران؛ $\langle I_g m L \mu | I_e M \rangle$ – هي معاملات غليبش-غوردن؛ وK – ثابت يتبع لـL، I_e وI_g. أيضاً يمكن التعبير عن هاملتونيان التأثير المتبادل لسبينات النواة (I_e, I_g) مع الحقل rf المغنطيسي بالشكل:

$$\hat{H}_{rf}(t) = \Omega_{M,M'} \hat{a}_M^+ \hat{a}_{M'} e^{-i\omega_0 t}$$

$\Omega_{M,M'}$ - تردد رابي للحقل rf.

لندرس عملية التحريض النووي بسبب الامتصاص الكمي K_1، متبوعاً بالإصدار الكمي K_2 لفوتونات غاما بواسطة هذه النواة. لنستخدم معادلة الحركة في حالة التأثير المتبادل.

$$i\frac{d\tilde{\varphi}}{dt} = \tilde{H}_{\text{ɣ}}\,\tilde{\varphi},$$

$$\tilde{\varphi} = V^{+}(t)\varphi\,,$$

$$\tilde{H}_{\text{ɣ}} = V^{+}(t)H_{\text{ɣ}}V(t),$$

$$V(t) = V_0(t) \times V_1(t)$$

$$V_0(t) = V_0(t,t_0) = \exp\left[-i\left(H_N + H_\gamma^0\right)(t-t_0)\right] \qquad (6)$$

$$V_1(t) = V_1(t,t_0) = Texp[-i\int_{t_0}^{t} H^{e,g}(t')dt']$$

تعبر العبارتان H_{hf} و $V_1 = V^{e,g}$ (مؤثر فائق التحول super-operator evolution) عن السويتين الأساسية (E_0 الطاقة) والمتحرضة على الترتيب لنواة ميوسباور. وتعبر φ عن التابع الموجي بالأساس لحالات خاصة لـH_N مع احتمالات معينة لـ$|I_g,m\rangle$ و$|I_e,M\rangle$ للسبينات النووية والحالات الخاصة لـ $\widehat{H}_\gamma^0$ و$|0\rangle$ بدون تكميم و$|K_2\rangle$ مع تكميم K_2 على التوالي:

$$\tilde{\varphi} = V^{+}(t)\varphi = \sum_{M} b_M|M,0\rangle + \sum_{M,K_2} b_{mK_2}\ |m,K_2\rangle,$$

$$|I_e,M\rangle|0\rangle = |M,0\rangle,$$

$$|I_g,m\rangle|K_2\rangle \equiv |m,K_2\rangle. \qquad (7)$$

جملة المعادلات لأجل الثوابت b_i تعطى كالتالي:

$$ib_M = \sum_{m,K_2} \langle M,O|\tilde{H}_{\text{ɣ}}(t)|m,K_2\rangle b_{mK_2} \times$$

$$\langle M,O|\tilde{H}_{\text{ɣ}}(t)|m,K_1\rangle b_{m_iK_1}, \qquad (8)$$

$$ib_{mK_2} = \sum_{M} \langle m,k_2|\tilde{H}_{\text{ɣ}}(t)|M,0\rangle b_{M.} \qquad (9)$$

$$mK_2 \neq mK_1.$$

إن الحالة الأولية $|m,K_1\rangle$ تكون منفردة تبعاً للشروط الابتدائية:

$$b_{\mathrm{m}K_2}(t_0) = \delta_{mm_i}\delta_{K_1K_2}\ , \qquad b_M(t_0) = 0$$

بتقريب عرض الخط الطبيعي(عرض الخط غاما للحالة النووية المتحرضة):

$$b_M(t) = (-i)\int_{t_0}^{t} dt' \exp\left(-\frac{\gamma(t-t')}{2}\right)\langle M, O|\tilde{H}_\gamma(t')|m_i, K1\rangle b_{m_iK_1}(t'). \quad (10)$$

لنعوض المعادلة (10) في المعادلة (9) ونكاملها بافتراض أن: $b_{m_iK_1}(t') \approx 1$ و $t_0 \to -\infty$.

$$b_{mK_2}(t) = (-i)^2 \int_{-\infty}^{t} dt' \sum_{M,M',m'} \langle m, k2|\tilde{H}_\gamma(t')|M, 0\rangle$$

$$\times U^{(t')}_{Mm_iM'm'}(p)\langle M', 0|\tilde{H}_\gamma(t')|m', K_1\rangle, \qquad (11)$$

حيث يمكن كتابة مؤثر التحول الدقيق كالآتي:

$$U(p,t) = U^{(t)}(p) = \int_{-\infty}^{0} d\tau \exp(p\,\tau)\, U^{(t)}(\tau), \qquad (12)$$

$$p = -i(E_{k1} - E_0) + \gamma/2$$

إن المصفوفة $U^{(1)}_{MmM'm'}(p)$ في المعادلة (11) معرفة على الحالات المنزاحة زمنياً $V(t)|\mathrm{m}\rangle$ و $V(t)|M\rangle$. يشير الدليل العلوي (t) إلى الزمن الخارجي. بما أننا نتعامل مع عملية امتصاص أو اصدار فوتون غاما، فيجب أن نعبر من خلال تكامل (12) عن عملية التحول غاما التابعة للزمن. لنعتبر أن اللحظة t=0 تقابل اللحظة t في جملة مرجعية مخبرية. لذلك فإن طور الاضطراب الخارجي الدوري في اللحظة t هو

$\omega t = \varphi(t) = 2\pi t/T$ ، حيث T – دور الاهتزاز.

وهكذا من خلال هذه العلاقات بمكن وصف التغيرات الزمنية لأطياف ميوسباور في نظام مؤشر الزمن الخارجي. يجب الإشارة إلى انه يجب أن يتحقق الشرط $\Delta t \ll T$، وذلك عندما تكون Δt صغيرة بما يكفي. ينكن ملاحظة أن المعلومة عن التأثير المتبادل فوق الدقيق تكمن في المؤثر فوق الدقيق $U^{(t)}_{Mm_iM'm'}(p)$.

تغيرات ديناميكية مغنطيسية لـ^{57}Fe في حقول rf مهتزة

يتعلق العديد من الأبحاث الميوسباورية بحالة الحقول الخارجية المهتزة عالية التردد (مقارنة بتردد Larmour للسبين النووي). ومع ذلك، كانت هناك أيضاً بعض المحاولات لمراقبة الأطياف مع تغيير اتجاه (دوران) الحقل الخارجي عند تردد منخفض(مقارنة بترددLarmour) [14].

إن الحقول في حالة ترددات منخفضة هي الحقول المطلوبة وفقًا للنظرية في المرجع[15]،على الرغم من اختلافات واسعة النطاق للحقل فوق الدقيق حيث لا يحدث تخريب بالبنية، كما يمكن أن يحدث في الترددات العالية. وهكذا، في وضع منخفض التردد، يمكن أن يحدث اختلاف في مواضع الخطوط الطيفية حتى في حقول عالية السعة. أيضاً يؤدي التأثير المتبادل المترابط على نواة ميوسباور ^{57}Fe بواسطة حقول rf إلى تشكيل زمني (مغنطة) لقابليتها للتحول في مجال غاما[16] . في هذه الحالة، غالباً يكون دور حقول rf كبير ما يكفي للحصول على ذلك و أيضاً بمكن حدوث ذلك في حالة التأثير غاما الضوئي. بداية تشمل مسألة تشكيل الترددات الراديوية لتحولات غاما، كامل تقنية توليد الحقول المتناوبة الكبيرة السعة على النواة. لأجل نظير الحديد ^{57}Fe ، يوفر التأثير المتبادل المغناطيسي فوق الدقيق تضخيمًا لحقل ترددات راديوية rf خارجي إلى

مرتبتين أو ثلاث مراتب. ليس من الصعب الحصول على الحقول المتناوبة على نواة (30-10Koe). مثل هذه الحقول كافية لملاحظة الأفعال التجاوبية.

ولكن وجود تباين الحقول المغناطيسية (بسبب حالة التبلور أو شكل العينة) ينتج عنه بعض الصعوبات في توليد حقول مهتزة فوق دقيقة. إلا أنه يمكن تطبيق حقول خارجية قوية rf على نوى ^{57}Fe من ثم إجراء عمليات تحويل حقل خارجيrf إلى حقل مهتز(متناوب) على النوى آخذين بعين الاعتبار خصائص منظومة مغناطيسية ^{57}Fe. سيتم تحليل نظام حركة المغنطة في منظومة ^{57}Fe المغناطيسية [17]. يمكن صياغة هذا التحليل حيث تتم دراسة تبعية سلوك المغنطة الديناميكية للتردد وسعة الحقل المهتز. بمعنى آخر، من أجل جميع ترددات الحقل المهتز، تتبع المغنطة للحقل المهتز بشكل مترابط. هذا السؤال يصبح مهمًا لحقول النوى لمعرفة تبعية المغنطة للحقل المهتز و ذلك إذا كانت السرعة الزاوية التي تغير اتجاهها أقل من تواتر Larmour الدوار المتعلق بسعة الحقل المهتز. سيتم في هذه الحالة اعتبار المغنطة كحركة دائرية حول الاتجاه المباشر للحقل الخارجي. وهذا سيجعل عمليات التبدد لأجل المغنطة متزامنة مع اتجاه الحقل اللحظي. في مثل هذه الحركة، يكون للحقل فوق الدقيق تقريبًا نفس التبعية الزمنية كما هي للحقل الخارجي. و ذلك ممكناً إما بسبب زيادة تردد الحقل الخارجي أو بسبب تناقص سعته. قد يكون الأمر نفسه بسبب التباين البلوري للحقول والحقول الداخلية للعينة. لا تتعلق المغنطة في هذه الحالة بالحقل الخارجي. ولا يمكن استخدام مثل هذا الترتيب لأجل تعديل محكم لحقل فوق دقيق. لأجل ذلك يمكن تحليل المنظومة المغناطيسية ^{57}Fe باستخدام معادلة حركة المغنطة M كتابع للزمن وفق نموذج Landau-Lifshits:

$$\frac{dM}{dt} = \gamma[MH] - \frac{\alpha}{M^2}[M[MH]], \quad (13)$$

حيث $H = H_e(t) + H_a + H_i$ – مجموع الحقل الخارجي وحقل التباين المغناطيسي والحقل الداخلي في العينة على الترتيب، γ – النسبة الجيرو-مغناطيسية و α – معامل التبدد. ويمكن التعبير عن متجهة المغنطة M كتابع لـ (t) حسب العلاقة:

$$M = \frac{\alpha}{\gamma}\frac{[n[nH]]}{[nH]} + \frac{A\alpha}{\omega}[n[nH]]\exp\left(-\frac{\gamma}{\omega}[nH]\cos\omega t\right). \quad (14)$$

حيث n متجهة واحدة وفق M. لنعتبر الحالة التالية: $H_a = 0$ و $H_i = 0$. و $H_e(t)$ –الحقل الدوار ذي سعة H_1 و تردده ω، وبالتالي $H_1 = H$.

وفق هذه القيم تمت محاكاة هذه العلاقة (14) حسب برنامج حاسبة الرسوم البيانية GeoGebra. يمكن عرض نتائج المحاكاة العددية لأجل حركة المغنطة حسب العلاقة (14) بالجدول (1) الشكل 1. و ذلك باعتبار الافتراضات الموضحة أعلاه.

t	m
0	1.367879
0.01	1.367898
0.02	1.367953
0.03	1.368045
0.04	1.368174
0.05	1.368339
0.06	1.368542
0.07	1.368781
0.08	1.369058
0.09	1.369371
0 1	1 369722
0 11	1 37011
0 12	1 370535
0 13	1 370997
0 14	1 371496
0.15	1.372034
0.16	1.372608
0.17	1.373221
0.18	1.373871
0.19	1.37456
0.2	1.375286
0.21	1.376051
0.22	1.376854
0.23	1.377696
0.24	1.378576
0.25	1.379496
0.26	1.380454

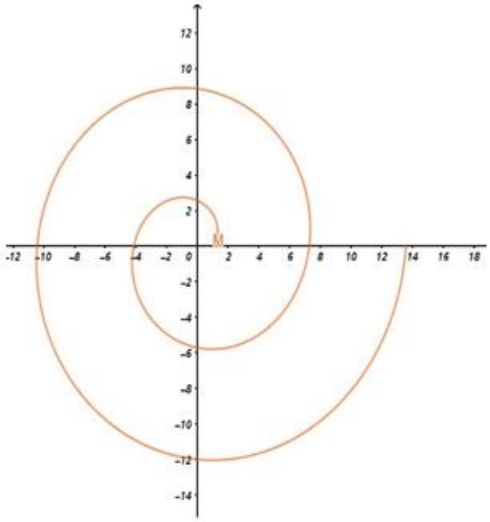

الشكل (1): تبعية M إلى ωt. باعتبار أن التردد 2,8 MHz.

للحصول على صورة واضحة لحركة المغنطة ، من المناسب أن ننسب هذه المنظومة لجملة إحداثيات متحركة دائرياً فيها المحور X متوافقاً لحظياً مع اتجاه حقل rf والمحور z المتعامد بدايةً مع مستوي دوران الحقل. نرى في الشكل 1 تعاظم سلوك المغنطة كمثل تزايد تواتر الحقل الدوار. لاحظ أن المحور الذي يميل إليه متجه المغنطة ينحرف عن اتجاه الحقل الدوار وفي حدود الترددات الكبيرة جدًا فإنه يتوافق تقريباً مع الاتجاه العمودي على الحقل الدوار. هذا يعني أن المغنطة تخرج عن الاتجاه المباشر للحقل. لنعرف الحد الترددي حسب العلاقة $\omega_b = \gamma H_1$. لذلك لأجل قيمة الحقل 1oe تكون قيمة التردد حوالي 2.8MHz. ومن ثم بالنسبة للمادة الفيرومغنطيسية متماثلة المناحي ^{57}Fe يتبع التردد لسعة الحقل التي فوقها يختلف الحقل المتحرض على النواة إلى حد كبير عن الحقل الخارجي [18]. وبالتالي عند تحليل سلوك المغنطة يجب الأخذ بالحسبان التأثيرات المتبادلة للمواد المغناطيسية ،حيث أن هذه التأثيرات المتبادلة تصف الحقول المغناطيسية المتباينة.

حالات السبين شبه الطاقية.

ان التفسير الدقيق للآثار التي تظهر في أطياف ميوسباور في ظل شروط ديناميكية مترابطة مع العزوم السبينية النووية يمكن أن يتم على أساس مفهوم شبه الطاقة [19]. وفقاً لهذا المفهوم [20-21] إن حالة المنظومة ذي هاملتونيان

يتبع الى الزمن دورياً تكون متميزة بحالات شبه طاقية. يمكن الحصول على هذه الحالات بالنسبة لسبين النواة في حقل فوق دقيق متناوب كيفي. تعرف هذه الحالات من خلال احتمالات التحولات الطيفية بينها. و يتم تعريفها من خلال هذه الاحتمالات في وضعية ثبات الحالات. سيتم استخدام الطريقة الموضحة في [20-21] كنموذج قابل للحل لأجل حقل دوار، التي من خلالها يمكن تعريف حالات السبين شبه الطاقية في هذه الحالة:

$$\Psi^{\alpha} = (\exp(-iE_{\alpha}t)) \times$$

$$\sum_{M} d'_{\alpha M}|M\rangle \exp(i(M-\alpha)\omega t)\exp(-iM\varphi), \qquad (15)$$

$$E_{\alpha} = -\omega M' + M'((\omega_0+\omega)^2+\omega_1^2)^{1/2} = -\omega M' + E_{\alpha}^0 \ , \qquad \alpha \equiv M' \ ,$$

$$\omega_1 = -\gamma H_1 \qquad , \qquad \omega_0 = -\gamma H_0$$

حيث $d^i_{\alpha M} = d^i_{\alpha M}(t)$ - مصفوفة الدوران، وω ، φ – تردد وطورالحقل الدوار. H_0 - حقل فوق دقيق ثابت عمودي على مستوى دوران الحقل الدوار. ولكن يمكن الإشارة الآن إلى أنه بدلاً من الحالة الأساسية الثابتة يتم استخدم الحالات شبه الطاقية. إن احتمال انتقال النواة بسبب التأثير المتبادل مع حقل إشعاع غاما، H_{γ} ، من الحالة المثارة a إلى الحالة الأساسية $\acute{a}$ في الحظة τ :

$$|A_{a\acute{a}}(\tau)|^2 = \left| \int_0^{\tau} dt \sum_{Mm} d^{ie}_{aM} * \langle M|H_{\gamma}|m\rangle d^{ig}_{\acute{a}m} \exp\left[i(E^0_a - E^0_{\acute{a}} - \omega_{\gamma})t - i(M-m)\omega t - i(M-m)\varphi\right] \right|^2$$

$$|A_{a\acute{a}}(\tau)|^2 = \left| \sum_{M-m} \left(\sum_{M-m=const} d^{ie}_{aM} * d^{ig}_{\acute{a}m} \langle M|H_{\gamma}|\acute{m}\rangle \right) \right.$$

$$\left. \exp(-i(M-m)\varphi)\Phi(E_{aM} - E_{a\acute{m}} - \omega_{\gamma}) \right|^2 \quad (16)$$

$$\Phi(E_{aM} - E_{a\acute{m}} - \omega_{\gamma}) = \frac{\exp[i(E_{aM} - E_{a\acute{m}} - \omega_{\gamma})\tau] - 1}{i(E_{aM} - E_{a\acute{m}} - \omega_{\gamma})}$$

إذ تم الأخذ بالحسبان: $E_{aM} = E^0_a - \omega' M$، $E_{a'M} = E^0_{a'} - \omega' m$ وهكذا يسمح التعبير المعطى بالحصول على احتمال اصدار غاما المتحرض. إذا تم استخدام المعدل الزمني لتسجيل فوتونات غاما فإن هذا الاحتمال لكل وحدة زمنية هو:

$$P_{aa'}(k,\Sigma) = 2\pi \sum_{M-m} \left| \sum_{M-m=const} \langle I^e, M|H_{\gamma}(k,\Sigma)|I^g, m\rangle \, d^{Ie}_{aM} * d^{Ig}_{a'm} \right|^2 .$$

$$\delta(E^0_a - E^0_{a'} - \omega_{\gamma} - (M-m)\omega). \qquad (17)$$

يشير $\sum$ إلى حالة الاستقطاب للكم الذي يحرض هذا الانتقال.

تحدد الصيغة (17) العدد الإجمالي للخطوط الطيفية و مواضعهم.

لنكتب العبارة الخاصة باحتمالية انتقال غاما لكل وحدة زمن كالآتي:

$$P_{a\acute{a}}(k,\sum) = \int_0^\infty d\tau \frac{d|A_{a\acute{a}}(\tau)|^2}{d\tau}.$$

في الواقع، يمكن التعبير عن شدة الإشعاع المتحرض في اللحظة t المعتبرة من قبل عدد انتقالات غاما النووية في فترة الزمنية محددة.

لنوضح سلوك المحرضات لأجل النظير ^{57}Fe يمكننا فقط إثبات التحولات المغناطيسية ثنائية القطب وذلك في حالة تحولات غاما المتحرضة . يمكن التعبير عن شدة الاشعاع المتحرض في هذه الحالة بالعبارة:

$$P_{aa'} = P^0_{aa'} + P_{aa'}(t),$$

$$P^0_{aa'} \propto \sum_{\Delta M=\pm 1} \frac{1}{\left(E^0_a - E^0_{a'} - \Delta M\omega - \omega_\gamma\right)^2 + \gamma^2/4},$$

$$P_{aa'}(t) \propto \frac{sin\, 2\omega t}{\gamma}\left\{\frac{-\left[\left(E^0_a - E^0_{a'}\right)^2 - \omega^2 + \gamma^2/4\right]4\omega + 2\omega\gamma^2}{\left[\left(E^0_a - E^0_{a'}\right)^2 - \omega^2 + \gamma^2/4\right]^2 + \omega^2\gamma^2}\right\}.$$

يتم الحصول على نتيجة مختلفة لإصدار غاما العفوي و بعد ذلك يتم احداث الانتقال من خلال اهتزازات صفرية للفضاء الكهرطيسي. ونحصل على اشعاع غاما كتركيب خطي لطاقات واستقطابات مختلفة لحالات الفوتون. وهكذا يمكن تخيل حالة الفوتون المركب كتعميم لحالات الفوتون المعروفة كونها تراكيب خطية لحالات الفوتون ذات الاستقطابات المختلفة لكن لها نفس الطاقات.

لندرس النظير الميوسباوري الأكثر شيوعاً - ^{57}Fe . لنفترض أنه لا يوجد تدرج حقل كهربائي في العينة. إن المستويات الفرعية للحالة المثارة للنواة في هذه الحالة تشكل بنية زيمن المتساوية البعد $(I_e = 3/2)$. عند الأخذ بعين الاعتبار سبين الحالة الأساسية للنواة $(I_g = 1/2)$ وقاعدة اصطفاء انتقال غاما، $(M - m = 0, \mp 1)$، الانتقالات الميوسباورية الممكنة ستة (انظر الشكل 2).

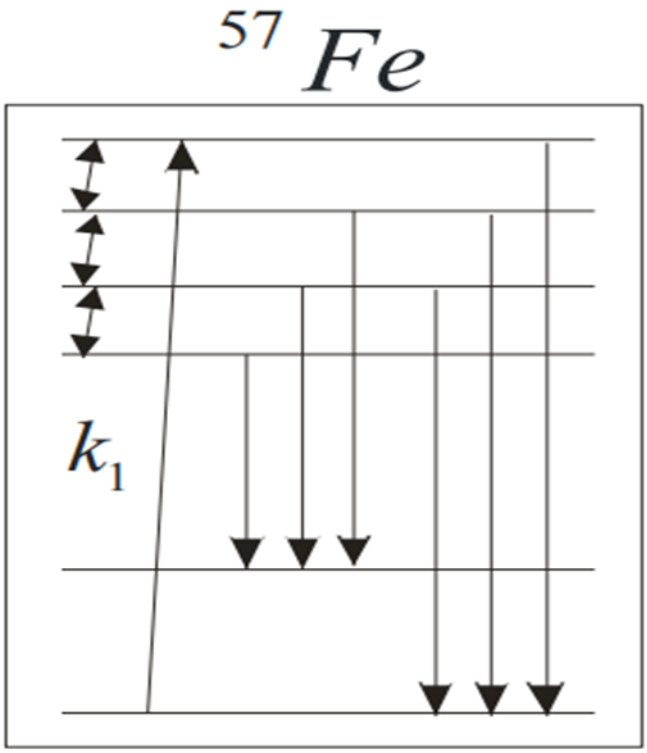

الشكل (2) الانتقالات الميوسباورية الممكنة لـ^{57}Fe

يُفترض في هذه الحالة، وجود ترابط في منظومة حقلr.f قوي على نواة ^{57}Fe تحريضي يؤثر على السويات الفرعية السبينية. يمكن الحصول على هذه النتيجة بطريقة أخرى بإدخال الحالات السبين شبه االطاقية Ψ^{α} في الحقل الدوار r.f بالنسبة لنواة ^{57}Fe. يمكن من خلال العلاقة (15) والمخطط المدرج بالشكل (3) ملاحظة أن التحولات السبينية شبه االطاقية لنواة^{57}Fe يحصل فيها انزياح ترددي مكمم يتبع للحقل فوق الدقيق.

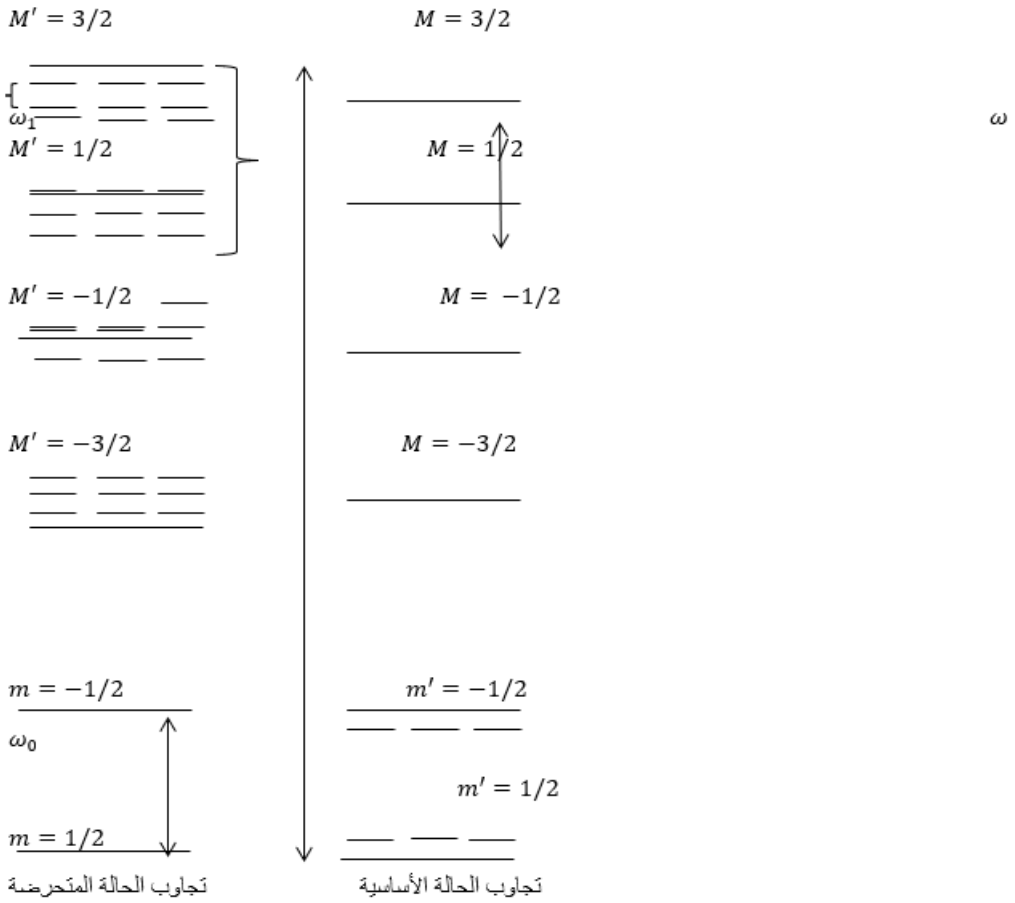

شكل (3) مخطط تحول نواة ^{57}Fe $\quad I_e = \frac{3}{2} \quad \rightarrow I_g = \frac{1}{2}$

الاستنتاجات:

1- تبين أنه من خلال هذه العلاقات بمكن وصف التغيرات الزمنية لأطياف ميوسباور وذلك وفق مؤشر الزمن الخارجي أخذين بعين الاعتبار الشرط $\Delta t \ll T$.

2- يظهر بالنسبة لمادة فيرومغنطيسية ^{57}Fe تنامي سلوك المغنطة مع تزايد تواتر الحقل الدوار . وينتج من العلاقة (14) أن متجه المغنطة ينحرف عن اتجاه الحقل الدوار وفي حدود الترددات الكبيرة إلى أن يتوافق تقريباً مع الاتجاه العمودي على الحقل الدوار.

3- يمكن من خلال العلاقة (15) والمخطط المدرج بالشكل (3) ملاحظة أن التحولات السبينية شبه االطاقية لنواة ^{57}Fe يحصل فيها انزباح ترددي يتبع للحقل فوق الدقيق.

References:

1. Brent Fultz, "Mossbauer Spectrometry", in Characterization of Materials. Elton Kaufmann, Editor (John Wiley, New York, 2011).

2. Molins, E.; Gich, M.; Tejada, J.; Grenèche J., M.; Macià, F. Zero-field quantum tunneling relaxation of the molecular spin in Fe8 observed by 57Fe Mössbauer spectrometry. Europhys. Lett. 2014, 108, 47004. [CrossRef].

3. E. Solano-Carrillo. Chiral Phonons and Electrical Resistivity of Ferromagnetic Metals at Low Temperatures. Department of Physics. Columbia University, New York, NY 10027, USA 2018.

4. ^{57}Fe Mössbauer Spectroscopy as a Tool for Study of Spin States and Magnetic Interactions in Inorganic Chemistry. Molecules 2021, 26, 1062

5. Coronado, E. Molecular magnetism: From chemical design to spin control in molecules, materials and devices. Nat. Rev. Mater. 2019. [CrossRef].

6. O. A. Kocharovskaya, , , F. G. Vagizova, b, V. V. Arinina ,and E. K. Sadykova. Controllable Quantum Interference in Mössbauer Spectroscopy: "Valve" Effect. ISSN 1062-8738, Bulletin of the Russian Academy of Sciences: Physics, 2007, Vol. 71, No. 9, pp. 1205–1210. © Allerton Press, Inc., 2007

7. V. V. Arinina, effects of coherence and controlled quantum interference in spectra resonance florescence Mossbauer radiation, Russia 2010.

8. A.V. Mitin and G.P. Chugunova, Phys. Lett. A49 (1974) 111.

9. A.M. Afanasev, P.A. Alexandrov and S.S. Jakimov, Preprint of Inst. Atom. Energy, N3337/9 (1980) p. 25.

10. Yu.V. Baldochin, S.A. Borsch, L.M. Klinger and V.A. Povitsky, JETF 63 (1972) 708.

11. S. Olariu, Phys. Rev. B37 (1988) 7698.

12. G.V. Smirnov, Yu.V. Shvydko, O.S. Kolotov, V.A. Pogozhev, M. Kotrbova, S. Kadechkova and I. Novak, JETF 86 (1984) 1495.

13. T.W. Sinor, P.W. Reitinger and C.B. Collins, Phys. Rev. Lett. 62 (1989) 2547.

14. G.J. Perlow , Phys. Rev. 1 72, N 2, 31 9 (1 969).

15. E.K. Sadykov, A.G. Isavnin, Laser Physics 5, N 2, 411 (1995).

16. A.V. Mitin, Phys. Lett. A, 84, 278 (1981).

17.A. Abragam , Principles of Nuclear Magnetism , Oxford , 1961.

18. G.V. Smirnov, Hyp. Int.,27, 203 (1986).

19. E.K. Sadykov, A.G. Isavnin, A.I.Skvortsov, Hyp. Int. 108/3-4, 257, 1997.

20. H. Sambe, Phys. Rev. A, 7, 2203 (1973).

21. M.Z. Smirnov Phys. Rev. A, 52, 2195 (1995).

الأثر الحراري لأيونات الهيليوم الصادرة عن جهاز البلازما المحرقية الكثيفة AECS-PF1

أ.د. وليد صهيوني: رئيس وحدة أبحاث البلازما–قسم الفيزياء– كلية العلوم– جامعة البعث

wsahyouni@albaath-univ.edu.sy

د. علاء ناصيف: مدرس في كلية الصيدلة – الجامعة الوطنية الخاصة

alaa.nassif.85@hotmail.com alaa.nassif@wpu.edu.sy

ملخص

تمّ في هذا البحث دراسة الأثر الحراري لأيونات الهيليوم الصادرة عن جهاز البلازما المحرقية الكثيفة AECS-PF1 من خلال اصطدامها بعينات من التنغستن، القصدير، الفولاذ والنحاس ، تمّ **أولاً** تحديد مميزات حزمة الأيونات الصادرة باستخدام كود Lee حيث كانت أعلى طاقة للحزمة 18.8 keV عند الضغط 2 Torr، ثمّ باستخدام برنامج SRIM تمّ تحديد مقدار فقدان طاقة الأيونات حيث أظهرت النتائج أن الأيونات تفقد معظم طاقتها من خلال التصادم مع السحابة الإلكترونية للمواد المدروسة. تمّ حساب مقدار الحرارة الناتجة في العينات حيث تبيّن انصهار القصدير والفولاذ عند وضع العينات مكان تشكّل قبضة البلازما لذلك تمّ تحديد البعد اللازم لتجنب انصهار هذه المواد $5 \times 10^{-7} m$ للفولاذ، $2.94 \times 10^{-6}\ m$ للقصدير.

الكلمات المفتاحية: الأثر الحراري، أيونات الهيليوم، البلازما المحرقية الكثيفة، قدرة الإيقاف.

Thermal effect of helium ions emitted by the AECS-PF1 dense plasma focus device

المؤتمر العلمي الدولي الرابع عشر
لجمعية الرياضيات العراقية والمنعقد تحت شعار
الإبداع يلتقي بالتحديات من اجل التقدم العلمي والتكنولوجي
للمدة 4 - 5 اب 2024
دمشق - سورية

Prof. Walid Sahyouni: Head of the Plasma Research Unit - Department of Physics - Faculty of Science - Al-Baath University. wsahyouni@albaath-univ.edu.sy

Dr. Alaa Nassif: Lecturer at Faculty of Pharmacy - Alwataniya Private University. alaa.nassif.85@hotmail.com, alaa.nassif@wpu.edu.sy

Abstract

In this research, the thermal effect of helium ions emitted by AECS-PF1 dense plasma focus device was studied by colliding with samples of tungsten, tin, steel and copper. First, The characteristics of ion beam emitted using Lee code were determined, the highest value of ions beam energy was 18.8 keV at 2 Torr. Then, using SRIM, the amount of ions energy loss was determined, the results showed that the ions lose most of their energy through collision with the electronic cloud of the studied materials. The amount of heat produced in the samples was calculated, it was found that tin and steel melted when were placed where the plasma pinch was formed. Therefore, the necessary dimension was determined to avoid the melting of these materials, $5 \times 10^{-7} m$ m for steel, $2.94 \times 10^{-6}\ m$ m for tin.

Keywords: thermal effect, helium ions, dense plasma focus , stopping power.

مقدمة:

يكمن التحدي الرئيسي في أبحاث الاندماج النووي في اختيار المواد المناسبة لمكونات مفاعل الاندماج وذلك بسبب تعرّض هذه المكونات لأحمال حرارية مختلفة تصل إلى عدة MeV/m^2 ناتجة عن اصطدام الحزم الأيونية والنيوترونية بها في وقت قصير جداً [1] ، لذلك يجب أن تتمتع هذه المواد بمواصفات مميزة من ناحية الناقلية الحرارية المرتفعة ومقاومة الضرر الإشعاعي الناتج، وبالتالي من الضروري اختبار ومعرفة سلوك هذه المواد عند تعرّضها لظروف مشابهة لتلك الموجودة في مفاعلات الاندماج مما يساعد على اختيارها وتطوير مواد جديدة. تعتبر أجهزة البلازما المحرقية أجهزة محاكاة ممتازة لفحص سلوك المواد في ظروف الاندماج النووي نظراً لطبيعة الإصدارات الإشعاعية بحيث يمكن الحصول على التدفق الحراري المطلوب لأبحاث الاندماج بتكلفة أقل كثيراً ، حيث سجّل Pimenov إصدار حزم أيونية بكثافة طاقية تصل إلى $\sim 10^{12} W/m^2$ بطاقة 100 keV وبيّن أن هذه الأيونات تحدث تغيرات كبيرة في خصائص المواد [2] ، ودرس Bhuyan [3] الضرر الناتج في التنغستن بسبب التعرّض لحزم بروتونات ناتجة عن جهاز 2.2 kJ وحزم أيونات الهيليوم [4] . كما تمّ إجراء العديد من الأبحاث والدراسات لدراسة الحزم الأيونية الصادرة عن أجهزة البلازما المحرقية الكثيفة

وتغيّر خصائصها بتأثير عوامل مختلفة مثل نوع وضغط الغاز المستخدم [5] [6] أو طاقة تشغيل الجهاز [7] ، كما تمّ دراسة سلوك المواد عند تعرّضها لحزم الجسيمات الناتجة عن أجهزة البلازما المحرقية والتغيرات في خصائص هذه المواد [8] .

تفاعل الأيونات مع المادة:

عندما تصطدم الأيونات مع المادة فإنها تتباطأ وذلك بسبب فقدان طاقتها من خلال التفاعل مع الكترونات ونوى المادة وذلك تبعاً لطاقة الأيون الوارد ونوع المادة، حيث تفقد الأيونات منخفضة الطاقة طاقتها من خلال التصادم المرن مع النوى بما يطلق عليه "التوقف النووي" بحيث في حال كانت الطاقة المنقولة إلى النواة أكبر من طاقة الإزاحة تنزاح الذرة من موضعها الشبكي وينشأ عيب نقطي ضمن الشبكة البلورية للمادة أما اذا كانت طاقة الأيون أقل من طاقة الازاحة فتتولد الفونونات. أما الأيونات مرتفعة الطاقة فتفقد طاقتها من خلال التصادم غير المرن مع الإلكترونات "التوقف الالكتروني" مما يؤدي إلى تأيين ذرات الهدف. يعبّر عن هذا الفقد الطاقي بـ " قدرة الإيقاف Stopping Power" التي تعطى با لعلاقة [9] :

$$S(E) = -\left(\frac{dE}{dx}\right)_{total} = -\left(\left(\frac{dE}{dx}\right)_{nuclear} + \left(\frac{dE}{dx}\right)_{electronic}\right) \quad .....(1)$$

يتحول فقدان طاقة الحزم الأيونية ضمن المادة إلى حرارة ضمن المادة، يتم حساب تغيّر درجة حرارة العينة بتأثير الحزم الأيونية من العلاقة [10] :

$$\Delta T = Flux\left(\frac{ions}{m^2 s^{-1}}\right) \times [\Delta E_{el} + \Delta E_{phonon}] \times \frac{R_{proj}}{\kappa} \quad .....(2)$$

حيث: $\Delta E_{phonon}(J)$: كمية الطاقة المفقودة من كل أيون بسبب التصادم مع النوى وبالتالي توليد الفونونات

$\Delta E_{el}(J)$: فقدان الطاقة بسبب التصادمات غير المرنة مع الالكترونات.

$\kappa\left(\frac{W}{m.K}\right)$: الناقلية الحرارية للعينة [11] .

$R_{proj}(A^0)$: المسافة المتوقعة لمسار الأيونات ضمن المادة.

تمّ في هذا البحث اختبار أربع مواد وهي: التنغستن، القصدير، الفولاذ والنحاس لدراسة الأثر الحراري الناتج عند تعرّضها لأيونات الهليوم الصادرة عن جهاز البلازما المحرقية الكثيفة AECS-PF1.

النتائج والمناقشة:

تمّ استخدام كود Lee [12] لمحاكاة جهاز البلازما المحرقية الكثيفة AECS-PF1 لإيجاد خصائص حزمة الأيونات وذلك عند تغيّر ضغط غاز الهيليوم باستخدام بارامترات الجهاز الآتية [13] :

بارامترات بنك المكثفات: $r_0 = 46\ m\Omega$ ، $C_0 = 25\ \mu F$ ، $L_0 = 1330\ nH$

بارامترات الأنبوب: $z_0 = 16\ cm$ ، $b = 3.2\ cm$ ، $a = 0.95\ cm$

بارامترات التشغيل: $P_0 = Variable$ ، $V_0 = 15\ kV$

يظهر من الجدول 1 ازدياد طاقة حزمة أيونات الهيليوم لتبلغ قيمة عظمى 1.2 J عند الضغط 2 Torr، وتدفق الأيونات $3.233 \times 10^{27}\ ions.m^{-2}.s^{-1}$، والطاقة التي يحملها أيون الهليوم 18.8 keV.

جدول 1: خصائص حزمة الأيونات المتشكلة في جهاز البلازما المحرقية الكثيفة AECS-PF1

Pressure Torr	Ions Flux J_b ($\times 10^{27}$ ions. $m^{-2}s^{-1}$)	Energy flux ($\times 10^{13}$ W.m^{-2})	Ions Beam Energy E_b (J)	Ions Number ($\times 10^{14}$ Ions)
0.5	2.413	1.3	0.75	1.4
1	3.004	1.3	1.02	2.4
1.5	3.227	1.2	1.15	3.2
2	3.233	0.97	1.20	4
2.5	3.029	0.77	1.19	4.7
3	2.681	0.58	1.14	5.3
3.5	2.233	0.4	1.05	5.9
4	1.735	0.26	0.95	6.3
4.5	1.259	0.16	0.82	6.7
5	0.842	0.084	0.69	6.9
5.5	0.521	0.041	0.55	7
6	0.296	0.018	0.42	7

6.5	0.153	0.0067	0.30	6.9

تحديد تفاعل أيونات الهيليوم مع المواد:

باستخدام برنامج SRIM2013 [14] تمّ تحديد مقدار فقدان الطاقة ومدى الأيونات عند أكبر قيمة لطاقة أيون الهيليوم 18.8 keV لتحديد فقدان طاقة الأيونات ضمن المواد المدروسة.

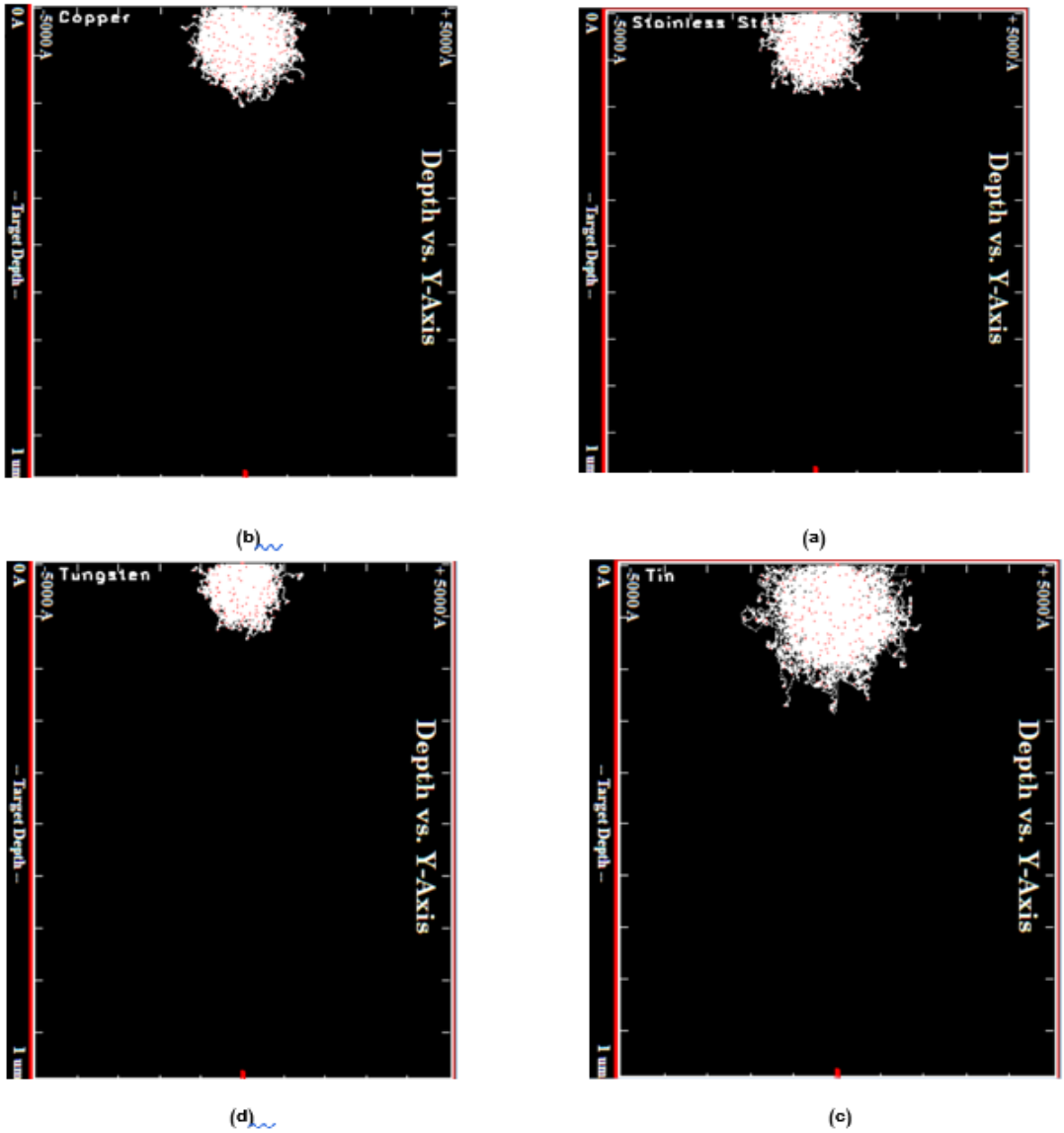

الشكل1: اختراق أيونات الهيليوم بطاقة 18.8 keV ضمن a الفولاذ، b النحاس، c القصدير، d لتنغستن

تشير النقاط باللون الأحمر في الأشكال السابقة إلى ذرات المواد التي انزاحت من مكانها بسبب تصادم أيونات الهيليوم معها، نلاحظ عددها المنخفض وبالتالي فإن معظم الأيونات تفقد طاقتها من خلال التصادم مع الكترونات مادة الهدف وهذا ما أكدته النتائج الموضحة في الجدول 2:

الجدول2: نتائج SRIM توضح فقدان الطاقة بالفونونات والتأين لكل أيون هيليوم بطاقة 18.8 keV للمواد المدروسة

	Energy losses to ionisation per ion ΔE_{el} [keV]	**Energy losses to phonons per ion ΔE_{phonon} [keV]**	**Ion range [A°]**	**projected range [A⁰]**	**Thermal conductivity $\kappa(\frac{W}{m.K})$**
SS	14.519	0.554	805	353	175
Cu	13.773	0.644	880	507	66
Sn	15.892	0.449	1079	512	19
W	15.909	0.498	520	325	398

باستخدام العلاقة 2 تمّ إيجاد الحرارة التي تنقلها أيونات الهيليوم إلى المواد المدروسة (الجدول 3) وذلك عند وضع عينات المواد المدروسة في مكان تشكل قبضة البلازما ومقارنتها مع درجة انصهار لكل مادة:

الجدول3: درجة الحرارة المنقولة بواسطة أيونات الهيليوم ودرجة انصهار المواد المدروسة

	ΔT K	**Melting point K**
SS	**14460.9**	**1823**
Cu	948.3262	**1356.4**
Sn	**6545.67**	**778.08**
W	1573.322	**3968**

يتضح من هذه النتائج أن كلاً من الفولاذ والقصدير سوف ينصهر بسبب طاقة أيونات الهليوم المتفاعلة معها، بينما التنغستن بسبب الناقلية الحرارية المرتفعة وعدد الكترونات السحابة الالكترونية له (50 الكترون) سوف يقوم بامتصاص طاقة الأيونات الواردة من خلال التصادمات مع هذه الالكترونات. لذلك تم تحديد الموضع المناسب لوضع عينة الفولاذ والقصدير بحيث لا تنصهر وفق المنهج الآتي:

باستخدام العلاقة $f_i = \frac{N_i}{\pi(Rtan\theta)^2}$ حيث R المسافة بين منبع الأيونات والعينة [8] .

باعتبار زاوية إصدار الأيونات 40^0 ، كانت أقل مسافة للفولاذ من قبضة البلازما $5 \times 10^{-7}\ m$ وللقصدير $2.94 \times 10^{-6}\ m$ وأي مسافة أكبر من هاتين المسافتين لا تنصهر العينة.

الاستنتاجات:

أظهرت نتائج هذه الدراسة الأثر الحراري لأيونات الهيليوم الصادرة عن جهاز البلازما المحرقية الكثيفة AECS-PF1 على عدد من المواد من خلال حساب كمية الحرارة الناتجة بسبب اصطدام الأيونات بها، كما تم تحديد أن الأيونات تفقد معظم طاقتها من خلال التصادم مع الكترونات المواد. كما تمّ تحديد المسافة عن قبضة البلازما (منبع الأيونات) لتجنب انصهار الفولاذ والقصدير.

المراجع

[1] Schoofs, F., & Gorley, M. (2019). **A route to standardised high heat flux testing: An example for tungsten.** Fusion Engineering and Design, 139, 132-136.

[2] Pimenov, V. N., Demina, E. V., Ivanov, L. I., Gribkov, V. A., Dubrovsky, A. V., Ugaste, U., ... & Tartari, A. (2008). **Damage and modification of materials produced by pulsed ion and plasma streams in Dense Plasma Focus device.** Nukleonika, 53, 111-121.

[3] Bhuyan, M., Mohanty, S. R., Rao, C. V. S., Rayjada, P. A., & Raole, P. M. (2013). **Plasma focus assisted damage studies on tungsten.** Applied surface science, 264, 674-680.

[4] mohammadreza Seyyedhabashy, M., Tafreshi, M. A., Shafiei, S., & Nasiri, A. (2020). **Damage studies on irradiated tungsten by helium ions in a plasma focus device.** Nuclear Engineering and Technology, 52(4), 827-834.

[5] Nassif, A., & Sahyouni, W. (2024). **Effect of Gas Type on Characteristics of Ion Beam Emitted by Plasma Focus.** Iraqi Journal of Applied Physics, 20(2A), 261-264.

[6] Sahyouni, W., & Nassif, A. (2021). **Effect of atomic number on plasma pinch properties and radiative emissions.** Advances in High Energy Physics, 2021(1), 6611925.

[7] Walid, S., & Alaa, N. (2019). **Ions beam properties produced by NX2 plasma focus device with helium and nitrogen gas**. American Journal of Modern Physics, 8(1), 1-4.

[8] Akel, M., Salo, S. A., Ismael, S., Saw, S. H., & Lee, S. (2017). **Comparison of measured and computed beam ion current densities emitted from two 2 kJ plasma focus machines**. Vacuum, 136, 163-167.

[9] Prosvetov, A. (2020). **Ion-beam induced modifications of structural and thermophysical properties of graphite materials**.

[10] Wolff, A., Klingner, N., Thompson, W., Zhou, Y., Lin, J., Peng, Y. Y., ... & Xiao, Y. (2018). **Modelling of focused ion beam induced increases in sample temperature: a case study of heat damage in biological samples**. Journal of Microscopy, 272(1), 47-59.

[11] ToolBox, E. (2005). **Metals, metallic elements and alloys-thermal conductivities**.

[12] Plasma Focus (Radiative) Computation Model, http://plasmafocus.net/IPFS/modelpackage/File1RADPF.htm.

[13] Akel, M., AL-Hawat, S., Ahmad, M., Ballul, Y., & Shaaban, S. (2022). **Features of Pinch Plasma, Electron, and Ion Beams That Originated in the AECS PF-1 Plasma Focus Device.** Plasma, 5(2), 184-195.

[14] James Ziegler - SRIM & TRIM, http://www.srim.org/.

Calculation the Hartree-Fock Energies for Ten Electron Systems (Ne , Na^{+1},Mg^{+2},Al^{+3})

Qassim Shamkhi AL-Khafaji[1], Ameer F. Shamkhi[2], shaymaa awad kadhim[3], Inass Abdulah Zgair[4] ,Hayder H. Hussein[5] , Maryam Hakim AL-Quraishi[6]

[1,2,3,4,5]Department of physics/ Faculty of science/ University of Kufa/ Iraq

[3]shaymaa.alshebly@uokufa.edu.iq

Abstract:

In this research the Hartree- Fock energies were calculated for ten-electron systems (Ne , Na^{+1},Mg^{+2},Al^{+3}) are obtained by an account the atomic properties by using the Hartree-Fock method and Mathcad 14 program, the total expectation value energy $\langle E_{HF} \rangle$ is important property account in this research and when comparing the result with published results. It was found that there is a good agreement; this present work is first study in Iraq.

Key words: Hartree- Fock, atomic properties, Hamiltonian operator, ten electrons system.

حساب طاقة هارتري-فوك للنظام عشر الالكترونات $(Al^{+3}, Mg^{+2}, Na^{+1}, Ne)$

1. Introduction

The Hartree –Fock (HF) approximation were first proposed by Fock in 1930 .Since then ,the HF method has taken a central role in studying the atomic and molecular electronic properties[1].the Hartree –Fock(HF) method enables calculation not only of the ground state but also excited states of atoms and ions

2. Theory

the Hartree-Fock method is the main idea of to solve the Schrodinger equation for a many-electron system can by choosing an appropriate wave function. As the exact solution for one-electron systems (like the Hydrogen-atom) are known, a first way for an approximate many-electron wave function is the Hartree-product. The total wave function Φ is then the simple product of one-electron hydrogen wave functions φ (orbitals)[2]

$$\Phi(\vec{x}1, \vec{x}2, ..., \vec{x}n) = \varphi_1(\vec{x}1)\cdot\varphi_2(\vec{x}2)\cdot...\cdot\varphi_n(\vec{x}n) \quad \text{.....(1)}$$

As electrons never only vary in the three spatial coordinates $\vec{r}$ but also have an intrinsic spin variable ω, which is either α or β, a special space-spin coordinate $\vec{x} = \{\vec{r}, \omega\}$ is used for the description of the spin orbitals $\varphi(\vec{x})$. These orbitals consist of a spacial orbital φ(ω) and a spin function $\sigma(\vec{r})$[3]

$$\Phi(\vec{x}) = \sigma(\vec{r})\cdot\varphi(\omega) \quad \text{.....(2)}$$

whereas electrons are fermions ,so the wave function must be antisymmetric (change sign) under ex-change of two electrons. The simple Hartree-product wave function (Eqn. 1) do not check the anti-symmetry principle (example with 2 electrons) in general

$$\Phi(\vec{x}1, \vec{x}2) = -\Phi(\vec{x}2, \vec{x}1) \quad \text{.....(3)}$$

$$\varphi1(\vec{x}1)\cdot\varphi2(\vec{x}2) \neq -\varphi1(\vec{x}2)\cdot\varphi2(\vec{x}1)$$

.

To fulfill the anti-symmetry principle a linear combination of the two products can be chosen

$$\Phi(\vec{x}1,\vec{x}2) = \frac{1}{\sqrt{2}}\,[\,\varphi1(\vec{x}1)\cdot\varphi2(\vec{x}2) - \varphi1(\vec{x}2)\cdot\varphi2(\vec{x}1)] \qquad \ldots\ldots(4)$$

The one-electron radial density function $D(r_1)$ represents the probability density function of finding an electron at a distance between r_1 and $r_1 + dr_1$ from the coordinate origin defined as [4]:

$$D(r_1) = \int_0^\infty D(r_1, r_2)dr_2 \qquad \ldots (5)$$

The radial electron-electron distribution function $f(r_{12})$, which describes the probability of locating two electrons separated by distance r_{12} from each other, [5,6].

The pair distribution function can be written as [8]:

$$f(r_{12}) = 8\pi^2 r_{12}\left[\int_0^{r_{12}} r_1 d\, r_1 \int_{r_1-r_{12}}^{r_1+r_{12}} \Gamma(r_1, r_2)r_2 dr_2 + \int_{r_{12}}^{\infty} r_1 dr_1 \int_{r_{12}-r_1}^{r_{12}+r_1} \Gamma(r_1, r_2)r_2 dr_2\right] \ldots\ldots\ldots (6)$$

The one-electron expectation value $\langle r_1{}^n\rangle$ is determined by the expression [8]:

$$\langle r_1^n\rangle = \int_0^\infty D(r_1) r_1^n\, dr_1 \qquad \ldots\ldots\ldots\ldots\ldots (7)$$

The inter-electron expectation values $\langle r_{12}^n\rangle$ is given by the relation [9]:

$$\langle r_{12}^n\rangle = \int_0^\infty f(r_{12}) r_{12}^n\, dr_{12} \qquad \ldots\ldots\ldots\ldots\ldots (8)$$

The virial theorem is a necessary condition for any stationary state. From the theorem, one is led to [10]:

$$\langle E\rangle = \langle T\rangle + \langle V\rangle \qquad \ldots\ldots\ldots\ldots(9)$$

$$\langle E\rangle = -\langle T\rangle = {}^{\langle V\rangle}/_{2} \qquad \ldots\ldots\ldots\ldots\ldots(10)$$

The expectation value of potential energy is proportional to the expectation values of $\langle r_1^{-1}\rangle$ and $\langle r_{12}^{-1}\rangle$ respectively, where [11]:

$$\langle V_{en}\rangle = -Z.\langle r_1^{-1}\rangle \qquad \ldots\ldots\ldots\ldots\ldots(11)$$

$$\langle V_{ee}\rangle = \langle r_{12}^{-1}\rangle \qquad \ldots\ldots\ldots\ldots\ldots(12)$$

المؤتمر العلمي الدولي الرابع عشر
لجمعية الرياضيات العراقية والمنعقد تحت شعار
الإبداع يلتقي بالتحديات من اجل التقدم العلمي والتكنولوجي
للمدة 4 - 5 اب 2024
دمشق - سورية

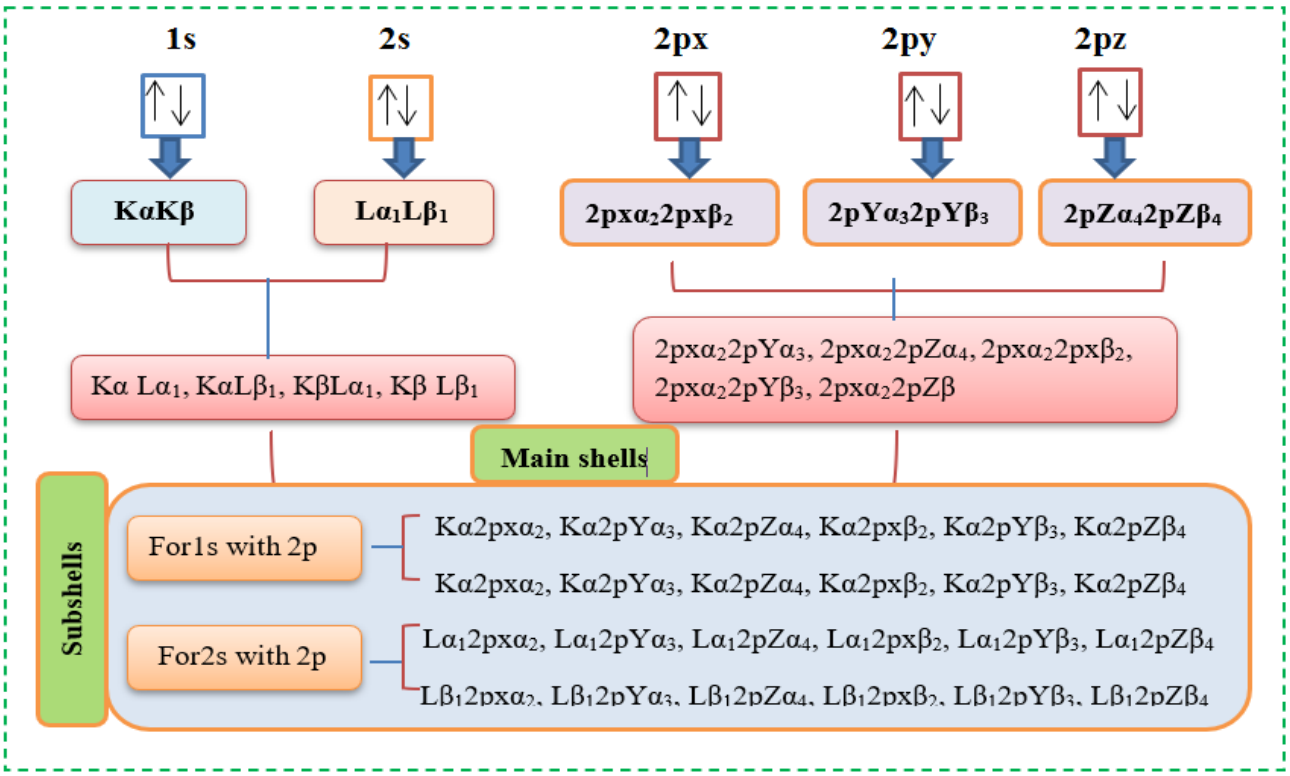

Shape explain the pairs electrons for ten electrons system

3. Results:

Table (1): Expectation values $\langle r_1^n \rangle$ of one particle position for different values of n $\{-2 < n < 2\}$ for ten-electron systems

Atom or ion	Expectation values o r1	shells						
		k-shell	L-shell	2p-shell	KαLα KβLβ	KαLβ KβLα	1s with 2p	2s with 2p
Ne	$< r_1^{-2} >$	187.1906	11.0770	3.0586	99.1333	99.1337	95.1246	7.0678
	$< r_1^{-1} >$	9.6181	1.6326	1.4353	5.6253	5.6253	5.5267	1.5339
	$< r_1^{0} >$	1	1	1	1	1	1	1
	$< r_1^{1} >$	0.1576	0.8920	0.9653	0.5248	0.5248	0.5615	0.9287
	$< r_1^{2} >$	0.0334	0.9665	1.2292	0.5000	0.5000	0.6313	1.0979

Na^{+1}	$< r_1^{-2} >$	227.5309	14.4522	4.1972	120.9918	120.9915	115.8640	9.3247
	$< r_1^{-1} >$	10.6073	1.8669	1.6991	6.2371	6.2371	6.1532	1.7830
	$< r_1^{0} >$	1	1	1	1	1	1	1
	$< r_1^{1} >$	0.1428	0.7790	0.7962	0.4609	0.4609	0.4695	0.7876
	$< r_1^{2} >$	0.0274	0.7312	0.8158	0.3793	0.3793	0.4216	0.7735
Mg^{+2}	$< r_1^{-2} >$	271.8590	18.3701	5.5011	145.1958	145.1192	138.6814	11.9356
	$< r_1^{-1} >$	11.6006	2.1071	1.9587	6.8567	6.8544	6.7802	2.0329
	$< r_1^{0} >$	1	1	1	1	1	1	1
	$< r_1^{1} >$	0.1307	0.6903	0.6809	0.4107	0.4107	0.4060	0.6856
	$< r_1^{2} >$	0.0230	0.5708	0.5885	0.2970	0.2971	0.3059	0.5797
Al^{+3}	$< r_1^{-2} >$	320.1334	22.8169	6.9715	170.5461	170.6412	163.5518	14.8760
	$< r_1^{-1} >$	12.5894	2.3406	2.2159	7.4297	7.4322	7.4027	2.2725
	$< r_1^{0} >$	1	1	1	1	1	1	1
	$< r_1^{1} >$	0.1202	0.6164	0.5960	0.3680	0.3680	0.3581	0.6046
	$< r_1^{2} >$	0.0194	0.4557	0.4468	0.2375	0.2375	0.2331	0.4501

Table (2): Expectation values $\langle r_{12}^{n} \rangle$ of inter- particle position for different values of n $\{-2 \leq n \leq 2\}$ for ten-electron systems

Atom or ion	Expectation values of r12	shells						
		k-shell	L-shell	2p-shell	KαLα KβLβ	KαLβ KβLα	1s with 2p	2s with 2p
Ne	$< r_{12}^{-2} >$	61.2498	1.7215	1.5641	2.3417	4.3756	3.2332	1.5873
	$< r_{12}^{-1} >$	5.9718	1.0219	0.9682	1.3532	1.4565	1.4173	0.9914
	$< r_{12}^{0} >$	1	1	1	1	1	1	1

	$< r_{12}^{1} >$	0.2303	1.2684	1.3997	0.9111	0.9085	0.9812	1.3350
	$< r_{12}^{2} >$	0.0669	1.9331	2.4585	1.00006	1.00006	1.2627	2.1958
Na^{+1}	$< r_{12}^{-2} >$	74.5249	2.2442	2.2304	2.9949	5.6580	4.4409	2.1547
	$< r_{12}^{-1} >$	6.588247	1.1673	1.1637	1.5352	1.6576	1.6757	1.1609
	$< r_{12}^{0} >$	1	1	1	1	1	1	1
	$< r_{12}^{1} >$	0.2087	1.1059	1.1484	0.7970	0.7945	0.8116	1.1274
	$< r_{12}^{2} >$	0.0549	1.4624	1.6317	0.7587	0.7587	0.8433	1.5470
Mg^{+2}	$< r_{12}^{-2} >$	89.1588	2.8493	2.9996	3.7436	7.1400	5.8271	2.8030
	$< r_{12}^{-1} >$	7.2106	1.3153	1.3546	1.7211	1.8635	1.9305	1.3283
	$< r_{12}^{0} >$	1	1	1	1	1	1	1
	$< r_{12}^{1} >$	0.1911	0.9787	0.9790	0.7077	0.7053	0.6961	0.9792
	$< r_{12}^{2} >$	0.0460	1.1417	1.1770	0.5941	0.5942	0.6118	1.1594
Al^{+3}	$< r_{12}^{-2} >$	105.0508	3.4957	3.8729	4.5477	8.7901	7.3842	3.5117
	$< r_{12}^{-1} >$	7.8241	1.4485	1.5430	1.8953	2.0592	2.1806	1.4861
	$< r_{12}^{0} >$	1	1	1	1	1	1	1
	$< r_{12}^{1} >$	0.1756	0.8687	0.8552	0.6325	0.6300	0.6102	0.8624
	$< r_{12}^{2} >$	0.0389	0.9067	0.8937	0.4751	0.4750	0.4663	0.9002

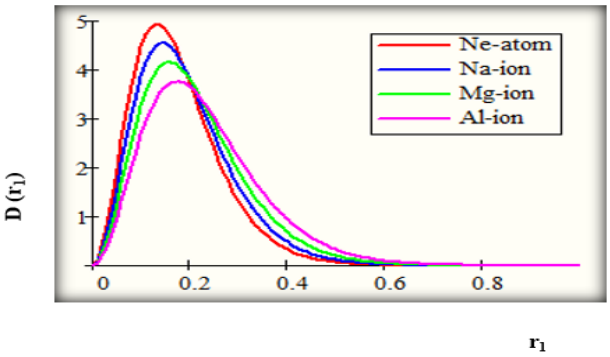

Fig. 1: The relation between $D(r_1)$ with the position (r_1) for K -shell

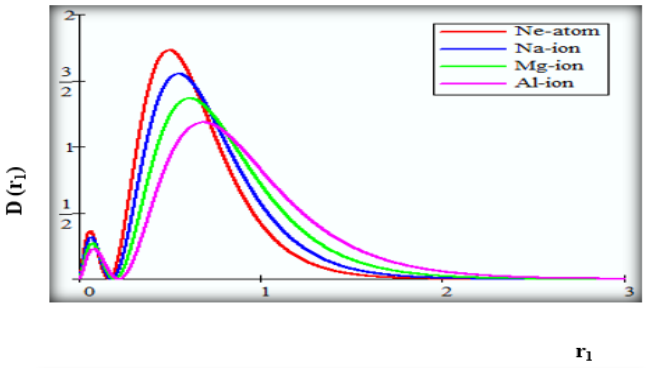

Fig. 2: The relation between $D(r_1)$ with the position(r_1) for L -shell

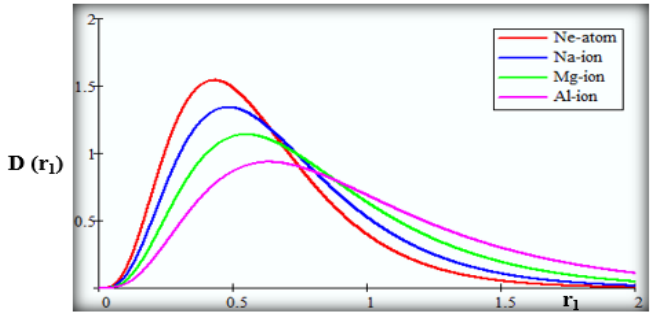

Fig. 3: The relation between $D(r_1)$ with the position(r_1) for 2p -shell

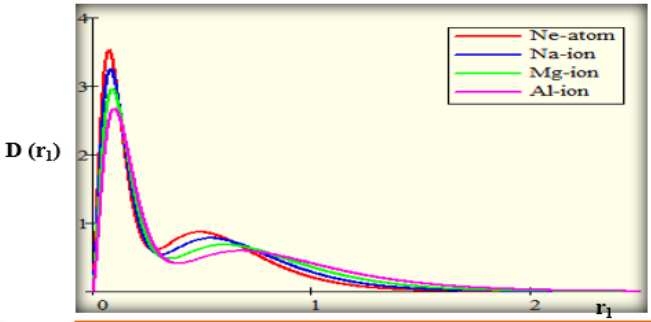

Fig. 4: The relation between $D(r_1)$ with the position(r_1) for KαLβ= KβLα -shells

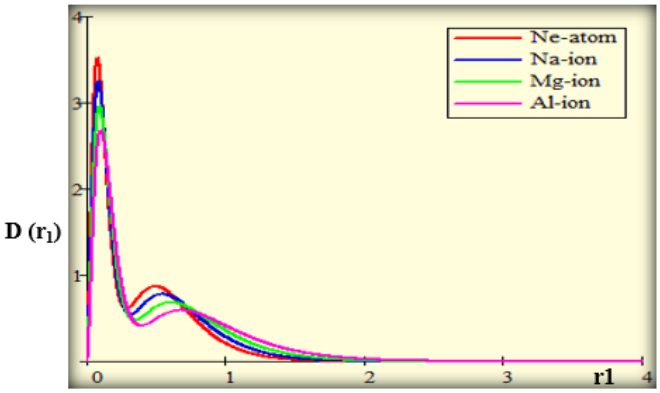

Fig. 5: The relation between $D(r_1)$ with the position(r_1) for KαLα= KβLβ -shells

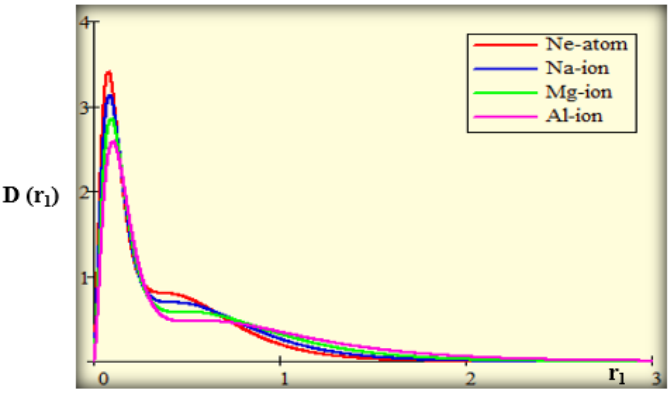

Fig. 6: The relation between $D(r_1)$ with the position(r_1) for 1s and 2p -shells

المؤتمر العلمي الدولي الرابع عشر
لجمعية الرياضيات العراقية والمنعقد تحت شعار
الإبداع يلتقي بالتحديات من اجل التقدم العلمي والتكنولوجي
للمدة 4 - 5 اب 2024
دمشق - سورية

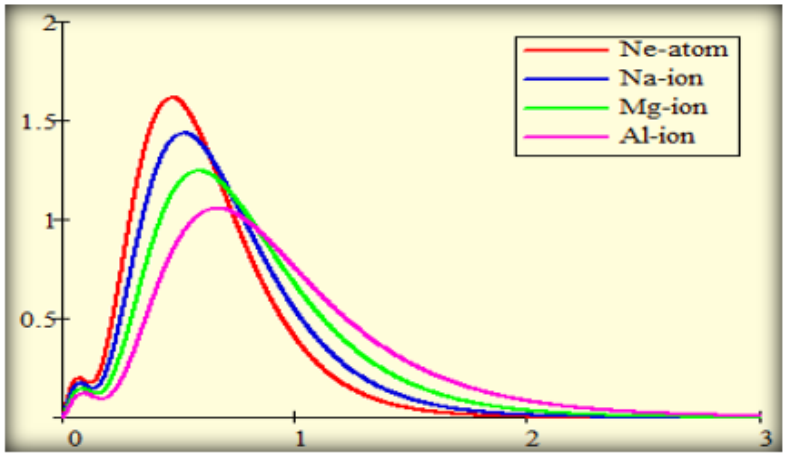

Fig. 7: The relation between $D(r_1)$ with the position(r_1) for 2s and 2p -shells

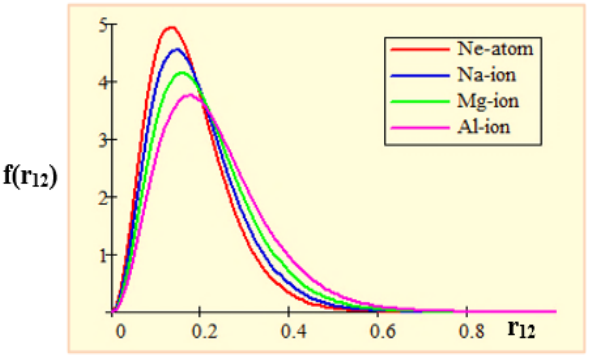

Fig. 8: The relation between $f(r_{12})$ with the position (r12) for K -shell

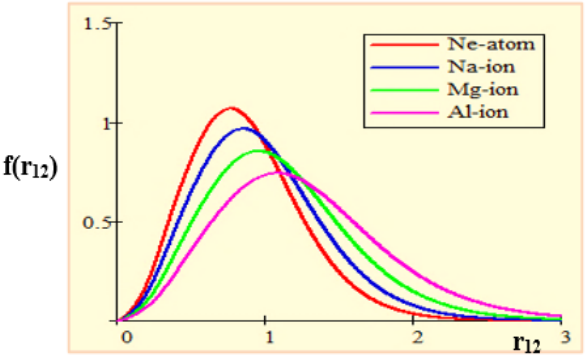

Fig. 9: The relation between $f(r_{12})$ with the position (r12) for L -shell

المؤتمر العلمي الدولي الرابع عشر
لجمعية الرياضيات العراقية والمنعقد تحت شعار
الإبداع يلتقي بالتحديات من اجل التقدم العلمي والتكنولوجي
للمدة 4 - 5 اب 2024
دمشق - سورية

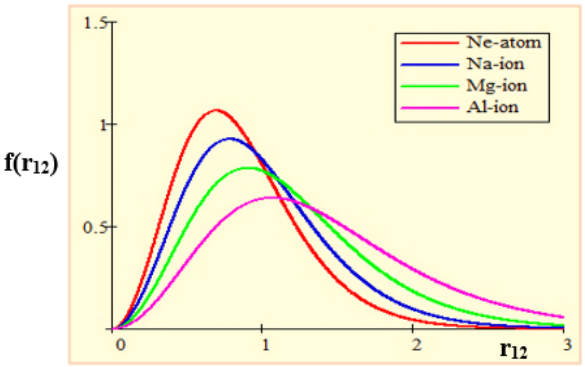

Fig. 10: The relation between $f(r_{12})$ with the position (r12) for 2p -shell

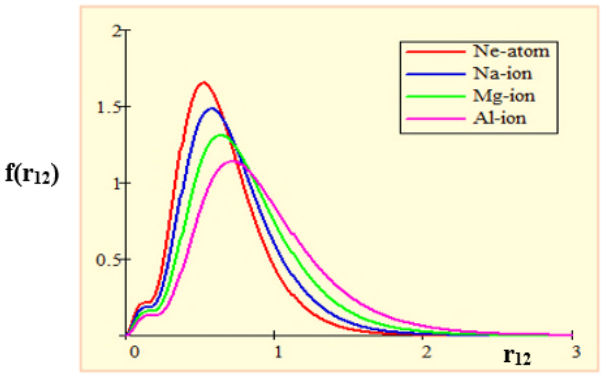

Fig. 11: The relation between $f(r_{12})$ with the position (r_{12}) for KαLβ= KβLα -shells

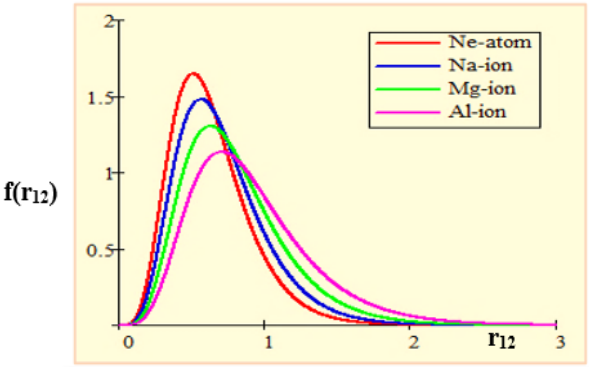

Fig. 12: The relation between $f(r_{12})$ with the position (r_{12}) for KαLα= KβLβ -shells

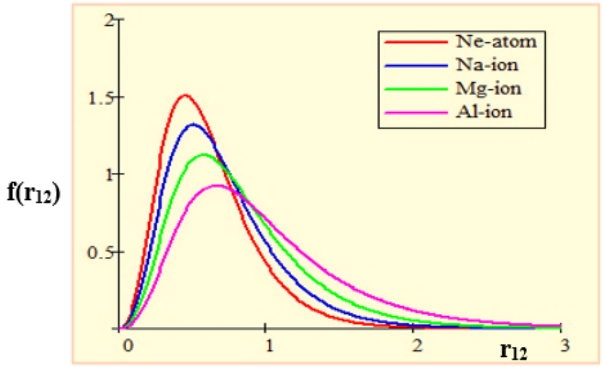

Fig. 12: The relation between $f(r_{12})$ with the position (r_{12}) for 1s and 2p -shells

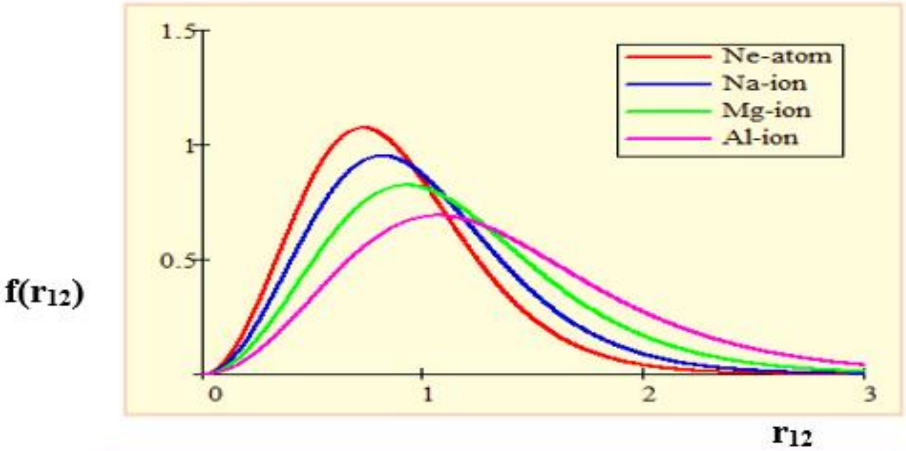

Fig. 14: The relation between $f(r_{12})$ with the position (r_{12}) for 2s and 2p -shells

Table (3): The expectation values for all attraction, repulsion, kinetic and Hartree- Fock energies for ten-electron systems.

	Expectation values of energies	shells							Total values of energies
		k-shell	L-shell	2p-shell	KαLα KβLβ	KαLβ KβLα	1s with 2p	2s with 2p	
Ne	$< V_{en} >$	-192.3625	-32.6526	-86.1188	.....	.....	.....	.....	-311.134
	$< V_{ee} >$	5.9718	1.0219	14.5234	1.3532	1.4565	1.4173	0.9914	26.7355
	$< V >$	-186.3906	-31.6307	-71.5954	2.7065	2.9132	17.0079	-11.8971	-255.0923
	$< T >$	-93.1953	-15.8153	-35.7977	1.3532	1.4565	8.5039	5.9485	-127.5461
	$< E_{HF} >$	93.1953	15.8153	35.7977	-1.3532	-1.4565	-8.5039	-5.9485	127.5461 128.54[12]
Na^{+} 1	$< V_{en} >$	-233.3619	-41.0737	-112.1863	.....	.....	.....	.....	-386.6219
	$< V_{ee} >$	6.5882	1.1673	17.4564	1.5352	1.6576	1.6757	1.1609	31.2415

	< V >	-226.7736	-39.9063	-94.7299	3.0704	3.3152	20.1085	13.9317	-320.9841
	< T >	-113.3868	-19.9531	-47.3649	1.5352	1.6576	10.0542	6.9658	-160.4920
	$< E_{HF} >$	113.3868	19.9531	47.3649	-1.5352	-1.6576	-10.0542	-6.9658	160.4920 161.67[12]
Mg^{+2}	$< V_{en} >$	-278.4151	-50.5717	-141.03	.....	.....	.....	.....	-470.0168
	$< V_{ee} >$	7.2106	1.3153	20.3197	1.7211	1.8635	1.9305	1.3283	35.6893
	< V >	-271.2045	-49.2563	-120.7102	3.4423	3.7271	23.1661	15.9397	-394.8959
	< T >	-135.6022	-24.6281	-60.3551	1.7211	1.8635	11.5830	7.9698	-197.4479
	$< E_{HF} >$	135.6022	24.6281	60.3551	-1.7211	-1.8635	-11.5830	-7.9698	197.4479 198.83[12]
Al^{+3}	$< V_{en} >$	-327.3267	-60.8564	-172.8437	.....	.....	.....	.....	-561.0268
	$< V_{ee} >$	7.8241	1.4485	23.1462	1.8953	2.0592	2.1806	1.4861	40.0400

	< V >	-319.5025	-59.4078	-149.6975	3.7906	4.1185	26.1676	17.8339	-476.6973
	< T >	-159.7512	-29.7039	-74.8487	1.8953	2.0592	13.0838	8.9169	-238.3486
	$< E_{HF} >$	159.7512	29.7039	74.8487	-1.8953	-2.0592	-13.0838	-8.9169	238.3486
									240.03 [12]

3. Discussion:

From all above figures It is observed that the maximum values of $D(r_1)$ and $f(r_{12})$ increases as Z increases, while the locations of these peaks are contracted toward the nucleus where It is noted that the maximum values of $D(r_1)$ and $f(r_{12})$ for Al^{+3} is closer to the nucleus from $D(r_1)$ and $f(r_{12})$ for Ne .This difference occurs because the Al^{+3} nucleus Z=13 exerts a much stronger attractive force on electrons than does the Ne nucleus (Z=10), also found that the probability of finding an electron in the K-shell is larger than another shells because K- shell is the nearest to nucleus, so that the attraction force between the nucleus and the electron is larger for K-shell according to Coulomb law..

it is also observed from figures (1,2,3,4,5,6 and 7) when the distance is equal to zero the probability of finding an electron equal to zero (when r =0 , $D(r1) = 0$) this means that the electron is cannot be existed inside the nucleus and when the distance is far away the probability of finding an electron equal to zero also (when $r = \infty$, $D(r1) = 0$) this means that it is not possible of the electron to be existed outside the atom while note that when $r_{12} = 0$ the probability of the inter particle distribution function $f(r_{12}) = 0$ this means that the electron not be closed to another electron and when the distance is far away ($r_{12} = \infty$) the probability of the inter particle distribution function $f(r_{12})$ equal to zero also, This means that the diameter is not found out the atom..

According to the Fig (2), it is found that there are two peaks for L- shell. The first peak represents the probability of finding the electron in the K-shell, the second peak represents the probability of finding the electron in the L-shell also It is note in the Fig (4 and 5), it is found

that there are two peaks, the first peak represents the probability of finding the electron in the L-shell, the second peak represents the probability of finding the electron in the K-shell, and Fig (6) the first peak represents the probability of finding the electron in the K-shell, the second peak represents the probability of finding the electron in the 2p-shell also Fig (7) the first peak represents the probability of finding the electron in the L-shell, the second peak represents the probability of finding the electron in the 2p-shell.

Fig. (11) It is noted that two peaks, the first peak represent the probability of finding two electrons in small distance r_{12} and the second peak represent the probability of finding two electrons in the larger distance between them (r_{12}).

From table (1) it is noted that when n takes the values (-2,-1) the one-particle expectation value $\langle r_1^n \rangle$ increases where the atomic number Z increases, this is due to the attraction energy between the nucleus and electron increases . While when n takes the values(+1,+2) the one-expectation value $\langle r_1^n \rangle$ decreases by atomic number (Z) increases ,where the $\langle r_1^{-1} \rangle$ which represents the attraction energy expectation value $\langle V_{en} \rangle = -Z[\langle r_1^{-1} \rangle]$ and the $\langle r_1^1 \rangle$ represents the distance between the nucleus and electron. When n equal to zero the one-particle expectation value $\langle r_1^n \rangle$ equal to unity for all studied systems this represented the normalization condition because the one-particle radial density distribution function $D(r_1)$ is normalized [$\int_0^\infty D(r_1) r_1^n \, dr_1 = 1$], the one-expectation value $\langle r_1^n \rangle$ in the K-shell is larger than the another shells because effect electrons in this shells. From tables (2) when Z increases the inter-particle expectation value $\langle r_{12}^n \rangle$ increases when n takes values -2,-1 this leads to increases of the repulsion energy between two electrons, whereas decreases when n takes values +1,+2 this means the distance between pair electron increases.

Table (3) shows the expectation value energies of ten-electron systems it is noted that all energies increase as nuclear charge increases. It is note that the attraction energy expectation values $\langle V_{en} \rangle$ are larger than the repulsion energy expectation value $\langle V_{ee} \rangle$ because the distances between the electrons and the nucleus are smaller than the distances between the electrons.

Conclusions

1.When the atomic number Z increases , the one-particle radial density distribution function $D(r_1)$ and the inter-particle distribution function $f(r_{12})$ are increased for two and three electrons systems.

2.For both one-particle expectation $\langle r_1^n \rangle$, and inter-particle expectation $\langle r_{12}^n \rangle$ are increased when Z increase for two and three electrons systems.

3. All the expectation values of the energies $\langle V_{en} \rangle$, $\langle V_{ee} \rangle$, $\langle V \rangle$, $\langle T \rangle$ and $\langle E_{HF} \rangle$ are increased when the atomic number increases for two and three electrons systems.

References

[1] S L.Saito,2009 .Hartree–Fock–Roothaan energies and expectation values for the neutral atoms He to Uuo: TheB-spline expansion method.J.Atomic Data and Nuclear Data Tables, V. 95.No.6.p.836-870.

[2] Q A. Szabo, N. S. Ostlund, Modern Quantum Chemistry, Dover Publications, Mineola, New York,1996

[3] M. Born, R. Oppenheimer,Ann. Physik,V.389,p.p. 457–484,(1927).

[4]T. Koga and H. Matsuyama , J. Theor Chem Acc ,V.115,p59–64, (2006).

[5]P. Dressel and F. King , J. Chemical physics, V. 100, No. 10 ,p7515–7522, (1994).
[6]R . Benesch and Vedene H. Smith , J. Chemical Physics, V. 55, No. 2 ,p 482-488, (1971).
[8]N.Moiseyev, J.Katriel and R. Boyd , J. Theoretica Chimica Acta, V. 45, p61 –67, (1977).
[9]A. Gupta and R. J. Boyd , J. Chemical physics, V. 68, No. 4 ,p1951 –1957, (1978).
[10] R . Jaber. and Q. shamkhi 2014. " Study of Energy and some atomic properties for electronic shells at ground state of three electron systems by analysis Hartree-Fock-Roothaan wavefunction".J. Of Kufa –Physics.V.5.No.1.P.91-102,2013.

[11]K. Sen and V. Reddy , J. Chemical Physics, V. 81, No. 5213 . p5213-5214, (1984).
[12] E.Clement and C.Roetti, J.Atomic Data and Nuclear Data Tables Vol.14,No.3-4(1974) 177- 478.

$Cd_{1-x}Zn_xS$ composites thin films: synthesis and characterization

Hamsa N. Naser[a], Wasan M. Mohamed[b], Jinan A. Abd[c], and Asmahan A. Muhmood[d]

[a,b,c] Department of Laser Physics, College of Science for Women, University of Babylon, Iraq.
[d] Department of Physics, College of Science, University of Kufa, Iraq.

Abstract

Pulsed laser deposition technique was used to synthesize the $Cd_{1-x}Zn_xS$ composites, x= (0.25, 0.5, 0.75). Scanning Electron Microscopy (SEM), Atomic Force Microscopy (AFM), X-ray Diffraction (XRD) and UV-visible Spectroscopy have been utilized to examine the effects of

ZnS ratio on the crystalline structure, morphological and optical properties of $Cd_{1-x}Zn_xS$ composites thin films, respectively. XRD patterns show the films of polycrystalline and hexagonal structure of three distinguished peaks corresponding to diffraction of the (100), (002), and (101) planes. ZnS content led to increase the peaks intensity and decrease the crystallite size. The AFM and SEM analysis images indicate that the films surface consists of spherical shaped grains without creaks or pinholes, homogeneous structure, and well covered to the substrates. The absorbance edge of the composite films lies in the visible region and have been shifted towards the shorter wavelengths with respect increasing of ZnS concentration. The energy gap values increase up to 2.78 eV as ZnS content increasing to 0.75. The optical studies showed that the fabricated films are more appropriate for solar cells fabrication.

Key words: ($Cd_{1-x}Zn_xS$) films, crystalline structure, morphology, optical.

Introduction

$Cd_{1-x}Zn_xS$ x= (0.25, 0.5, 0.75) composite has attracted technological interest. This is due to the possibility of variation of energy gap and lattice parameters. Adding ZnS to CdS can improve the optical properties. The $Cd_{1-x}Zn_xS$ ternary compound provides the wide band gap and high optical transmittance which makes the material much more appealing for solar cells manufacturing. It has been widely used as a wide band gap material in heterojunction photovoltaic, photoconductive devices and solar cell. From $Cd_{1-x}Zn_xS$ composite films, can be producing good quality thin film for inclusive studies and their several applications [1]. $Cd_{1-x}Zn_xS$ thin films can be prepared by physical methods including sputtering [2], thermal evaporation [3], pulsed laser deposition [4, 5] and chemical methods such as SILAR [6], spray pyrolysis [7, 8], chemical bath deposition [9, 10], chemical vapor deposition [11, 12]. This work aims to study ZnS content effects on structural, morphological, and optical properties of $Cd_{1-x}Zn_xS$ composites films prepared by pulsed laser deposition.

Materials and Methods

PLD technique has been accomplished to study the effects of ZnS ratio on the $Cd_{1-x}Zn_xS$ characteristics, x= (0.25, 0.5, 0.75), composites films. The laser pulse energies were (900 mJ). The Q –Switched Nd:YAG laser was used with (6 Hz, 1064 nm, 10 ns) . A pellet of (1.51,

2.75, 3.72) gm of x= (0.25, 0.5, 0.75), respectively pressed powder (purity of 99.9 %) was used to deposit $Cd_{1-x}Zn_xS$ thin films on glass substrates.

XRD- 6000 SHIMADZU has been applied to study the crystallite structure and also in the calculations of the important structural parameters. AFM Device of SPM AA3000 / Angstrom, Advanced Inc, Type Company U.S.A. The purpose of AFM analysis is to know the surface topography, grain distribution, and roughness of surface for thin films prepared under fixed conditions. The (SEM) device of type (Inspect S50). The device provides study the topography of the surface and gives the internal structure of composites films [13]. The optical properties have been examined using UV/VIS, Cez200, Cecil, 7000Series, Metertec.

Result and discussion

X –RAY Diffraction

As x= (0.25, 0.5, 0.75) of ZnS, the XRD pattern of formed $Cd_{1-x}Zn_xS$ composite thin films have been shown in Figure (1). As shown in the figure, the films of polycrystalline and hexagonal structure of three notable peaks identical to diffraction of the (100), (002), and (101) planes due to (JCPDS Card No: 40-835), [14]. It can be obviously seen that the preferred peak has been orientated at (002) plane. The intensities of the preferred peak of all films have been became more sharp and increased as ZnS ratio increasing. Table (1) shows the confirmed data of XRD pattern of $Cd_{1-x}Zn_xS$ composite thin films of (900 mJ).

Table (1): The confirmed data of XRD pattern of $Cd_{1-x}Zn_xS$

900 mJ	2θ (deg.)	θ (deg.)	Θ (rad)	B (deg.)	B (rad)	d Å	(hkl)
$Cd_{0.75}Zn_{0.25}S$	25.161	12.584	0.219	1.02	0.0177	3.536	(100)
	26.768	13.384	0.233	1	0.0174	3.327	(002)
	28.335	14.167	0.247	1.06	0.0184	3.147	(101)
$Cd_{0.5}Zn_{0.5}S$	25.46	12.73	0.222	1.04	0.0182	3.49	(100)
	27.06	13.53	0.236	0.84	0.0146	3.29	(002)
	28.54	14.27	0.248	1.29	0.0225	3.12	(101)
$Cd_{0.25}Zn_{0.75}S$	26.6	13.3	0.232	1.066	0.018	3.34	(100)
	28.38	14.19	0.247	1.07	0.018	3.15	(002)
	29.8	14.9	0.259	1.44	0.019	3.03	(101)

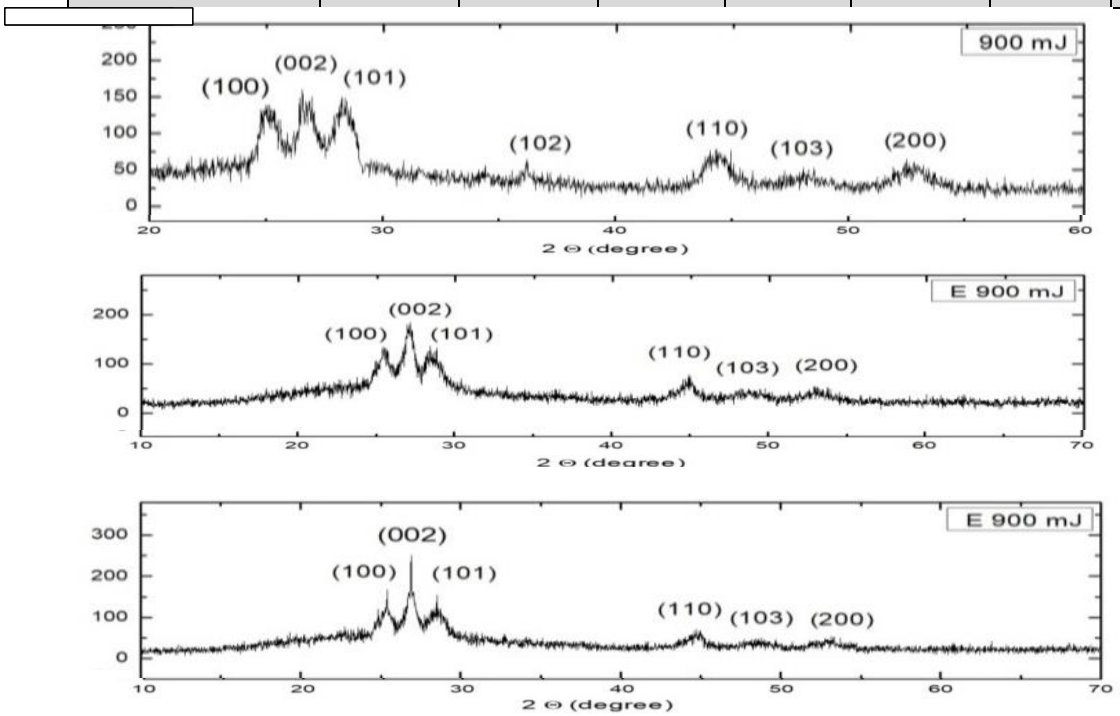

Figure 1: The X-ray diffraction (XRD) patterns of the prepared thin films $Cd_{1-x}Zn_xS$

For further information about the film's structure as well as the vital structural parameters of the preferred plane (002) of high energy (900 mJ) have been calculated from the confirmed XRD data, such as lattice parameters (**a**) Eq. (1), and (**c**) Eq. (2), crystallite size (**D**) Eq. (3), the strain (**ε**) Eq.

(4), and density of dislocations (**δ**) Eq. (5). [15-20]. The calculated values have been tabulated in Table (2).

$$a = \sqrt{1/3}\,\lambda/\sin\theta \quad (1)$$

$$c = \lambda/\sin\theta \quad (2)$$

$$D = \frac{k\lambda}{\beta\cos\theta} \quad (3)$$

$$\varepsilon = \frac{\beta\cos\theta}{4} \quad (4)$$

$$\delta = 1/D^2 \quad (5)$$

Table (2): The significant structural parameters of preferred plane (002) of $Cd_{1-x}Zn_xS$ thin films

(002) plane of (900 mJ)	D (nm)	$\delta\times10^{-3}$ ($1/nm^2$)	a (Å)	c (Å)	$\varepsilon\times10^{-3}$
$Cd_{0.75}Zn_{0.25}S$	8.17	14.982	3.84	6.65	4.243
$Cd_{0.5}Zn_{0.5}S$	8.10	15.237	3.79	6.58	4.278
$Cd_{0.25}Zn_{0.75}S$	7.66	17.051	3.65	6.33	4.526

From Table (2), the structure of $Cd_{1-x}Zn_xS$, x= (0.25, 0.5, 0.75), composites films within nanoscale and the calculated values of crystallite size of the composite have been slightly decreased due to the addition of ZnS with different ratio. Hence the dislocations (δ) and the strain (ε) values show the composites of high crystalline quality and low imperfections. The lattice constants values (a) and (c) of the composites films are extremely near to the standard values (a= 4.06 **Å**, c= 6.62 **Å**) of standard data card of $Cd_{1-x}Zn_xS$ (JCPDS Card No: 040-835) [14] indicating that films are in a low lattice distsortion.

Morphological Properties

AFM images of the prepared $Cd_{1-x}Zn_xS$, x= (0.25, 0.5, 0.75), composite thin films are presented in Figure (2). Figure (2) images denote that the microstructure of the films surface consists of spherical shaped grains. In this figure the formation of agglomerated grains one on the top of the other represent The white regions. Hence the large clusters forming from the neighboring grains come together. Therefore, grains in the white regions are greater in size in the comparison to others. The homogeneity of the films is thought to be formed initially layer by layer and then island growth type as reported W.D. Callister, [21]. From the figure, films demonstrate a rougher surface of cluster structures and accumulates with different heights. The average diameter (D), surface roughness (R_a), and root mean square surface roughness (R_q) values that evaluated from AFM analysis have been listed in Table (3). As clearly from the figure and the table, the (D), (R_a) and (R_q) values of the composite films have been slightly decreased as ZnS content increasing, which may be due to the good crystalline quality as given in XRD results.

Table (3): The roughness (Ra), root mean square (Rq), and grain size (D)

Sample	Ra (nm)	Rq (nm)	D(nm)
$Cd_{0.75}Zn_{0.25}S$	3.59	3.62	48.35
$Cd_{0.5}Zn_{0.5}S$	3.51	3.56	45.27
$Cd_{0.25}Zn_{0.75}S$	3.45	3.32	42.02

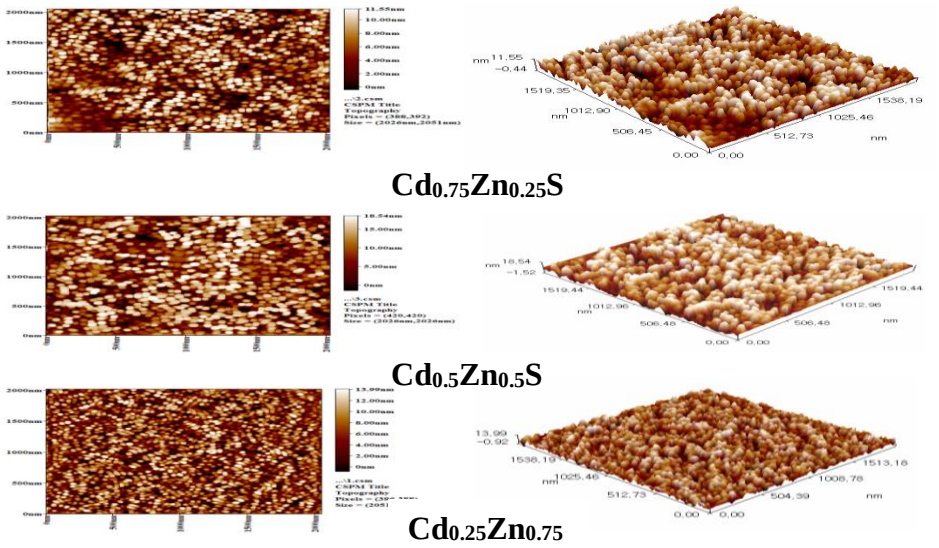

Figure 2: AFM images of the prepared $Cd_{1-x}Zn_xS$ thin films

To examine the effects of ZnS content on the surface morphology of the prepared $Cd_{1-x}Zn_xS$ thin film, the selected films have been scanned using Scanning Electron Microscopy, as shown in Figure (3)**.** The composites films are formed from spherically shaped grains without creaks or pinholes, homogeneous structure, and well covered to the substrates which that notice from the figures. The relative size and number of the smaller sized grains of mixed composite thin film decreased with increasing the ratio of ZnS. The SEM study confirms that even at low ratio of ZnS content has been effectively changed the microstructure $Cd_{1-x}Zn_xS$ thin films as reported by L. S. Ravangave, and *et. al.*[22]. the microstructure images of $Cd_{1-x}Zn_xS$ composites films corporate the AFM and XRD analysis.

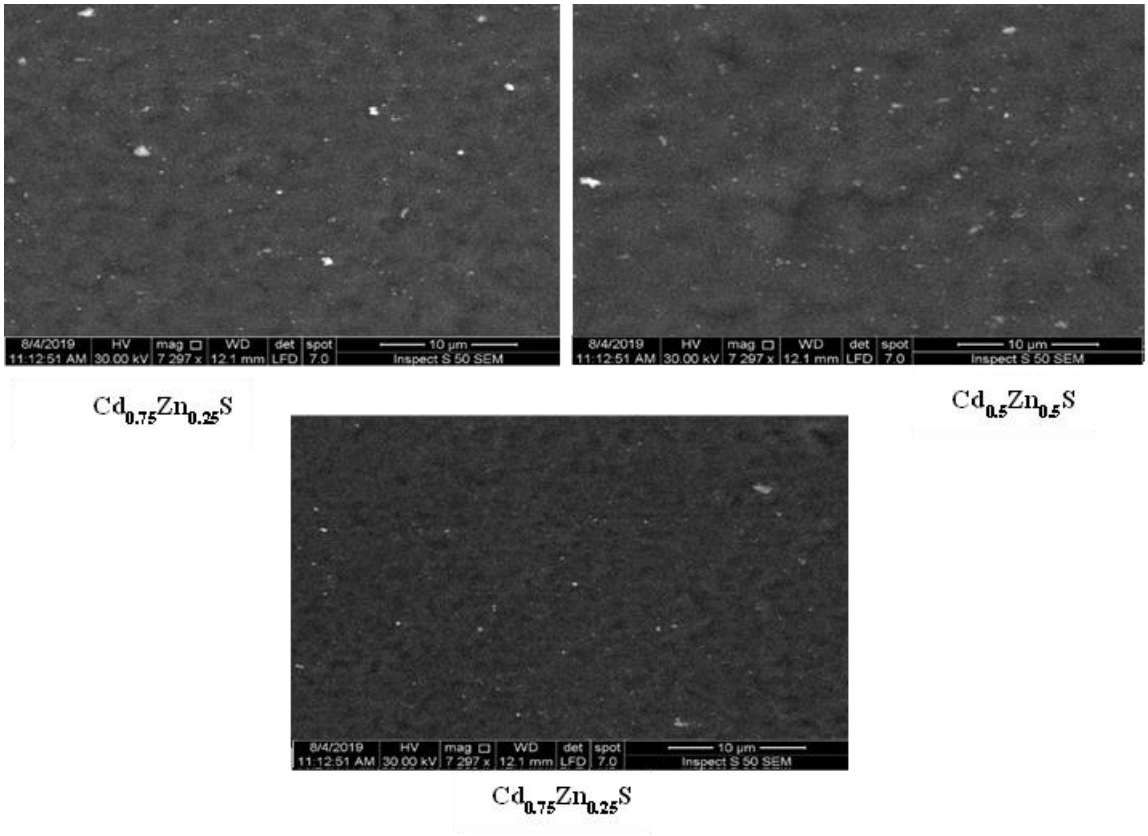

Figure 3: SEM images of the prepared $Cd_{1-x}Zn_xS$ thin films

Optical Properties

The Figure (4) shows the absorption spectra of $Cd_{1-x}Zn_xS$ deposited thin films (x=0.25, 0.5, 0.75) at (900 mJ). The figure show that absorbance edge of the composite films lies in the visible region and have been shifted towards the shorter wavelengths with respect increasing of ZnS concentration as reported by G. Jia, and *et.al.*, [23]. This behavior is due to increase the ZnS content in the composite corresponding to the absorption edge of ZnS which is about 340 nm. The studies of the absorption publicized that the deposited thin films are very low absorptive and is more suitable for the fabrication of solar cells, as reported by S. M. Thahab, and *et. al.*, [24].

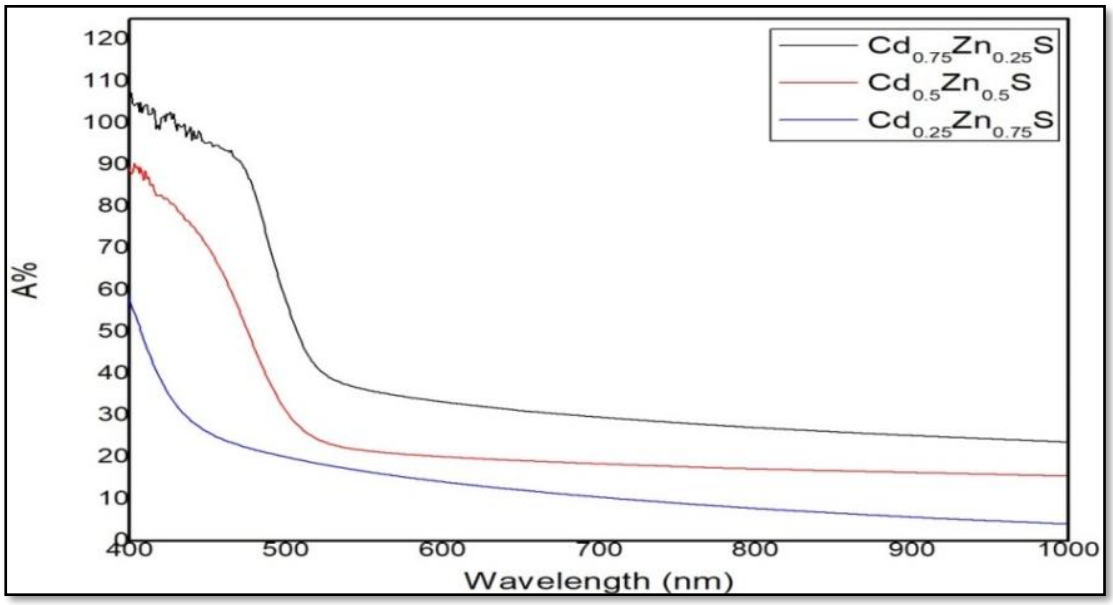

Figure 4: The absorption spectrum of $Cd_{1-x}Zn_xS$ thin films of (900 mJ)

Optical transmittance spectra of $Cd_{1-x}Zn_xS$ films in the range of (400-1000 nm) are showed in Figure (5). The $Cd_{0.75}Zn_{0.25}S$ composite film shows a transmittance of (63.4% at 800 nm) and the transmittance increases up to (70.42 at 800 nm) and (78.41% at 800 nm) as the ZnS content increasing to 0.5 and 0.75 respectively. The increasing of ZnS ratio in the composite effects on the thin films transmission may be due to the effects of surface and structure. These affects such as better crystallinity, defect density and less surface irregularity can increase the transmission, as reported by M. Zakriaa, and et. al., [25].. Good transparency indicates low surface roughness, which is certificated by the roughness analysis of AFM studies.

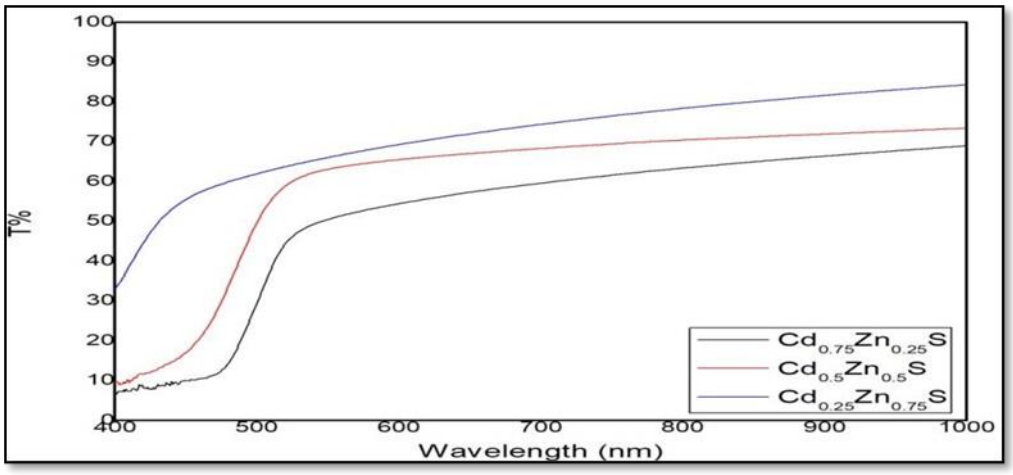

Figure 5: The transmittance spectrum of $Cd_{1-x}Zn_xS$ thin films of (900 mJ)

The absorption coefficients (α) ,eq.(6) [26], of $Cd_{1-x}Zn_xS$ composite thin films of energy of (900 mJ) have been presented in Figure (6). It is obviously that the absorbance coefficient value has been decreased as the ZnS ratio increasing. The absorption edges of the composite films in the visible region and the absorbance of value ($\alpha > 10^4$ cm^{-1})). The absorption coefficient of composite have been decreased as ZnS content increasing and this led to give a shifting towards UV region of high energy. As reported by S. M. Thahab, and *et.al*., [27].

$$\alpha = \frac{2.303\ A}{t} \qquad (6)$$

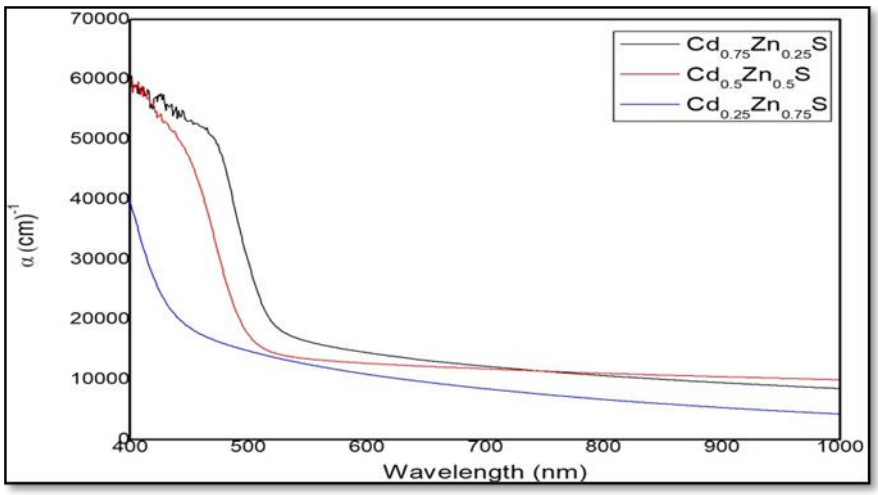

Figure 6: Absorption coefficient (α) of $Cd_{1-x}Zn_xS$ thin films of (900 mJ)

The optical energy gap for allowed direct transition is calculated by drawing a graphical relationship between $(\alpha h\nu)^2$ and photon energy ($h\upsilon$). The value of optical energy gap can be found

by protraction the straight part of the relationship curve to cut the x-axis at photon energy values. It represents the intersection point of the value of the direct optical energy gap of the composite . The calculated energy gaps values of $Cd_{1-x}Zn_xS$ composite films have been shown in Figure (7). The obtained direct band gap values have been increased as ZnS content increasing as shown in Table (4). The substitution of CdS by ZnS of higher ratio led to rise the energy gap as the ZnS of higher energy gap. This linear relation is almost due to the homogenous structure of $Cd_{1-x}Zn_xS$ composite thin films. This increment of E_g is in good agreement with the reduction of crystallite size of XRD and AFM analysis. The values of the table indicate good agreement results with the results by S. M. Thahab, and *et.al.*, [27].

Table (4): The energy gap and wavelength of $Cd_{1-x}Zn_xS$ thin films.

Sample	E_g (eV)	(λ nm)
$Cd_{0.75}Zn_{0.25}S$	2.35	526
$Cd_{0.5}Zn_{0.5}S$	2.5	495
$Cd_{0.25}Zn_{0.75}S$	2.78	445

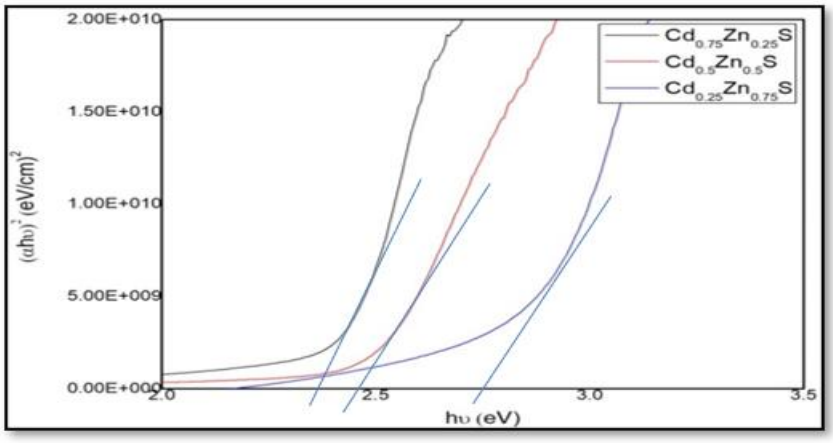

Figure 7: The band gap (E_g) of $Cd_{1-x}Zn_xS$ thin films of (900 mJ)

Conclusion

$Cd_{1-x}Zn_xS$ composites thin films, x= (0.25, 0.5, 0.75), have been synthesized by PLD technique with different ratio of (ZnS). Crystalline structure, morphology and the optical characteristics of the films have been studied. Rustles showed that: XRD patterns denote that all the films have a hexagonal and polycrystalline structure with highest three peaks along (100), (002), and (101) planes. The values of average diameter, surface roughness, and root mean square that evaluated from AFM analysis have been slightly decreased as ZnS content increasing, which may be due to the good crystalline quality as given in XRD results. The SEM study confirms that the relative size and number of the smaller sized grains of mixed composite thin film decreased with increasing the ratio of ZnS. $Cd_{1-x}Zn_xS$ films have good transparency which is indicated low surface roughness, and certificated by the roughness analysis of AFM studies. The optical band gap expands with ZnS ratio increasing to be 2.78 eV at $Cd_{0.25}Zn_{0.75}S$ composite film.

References

1. S. M. Thahab, A. H. O. Alkhayat, and S. M. Saleh, 'The optical properties of CdxZn1− xS thin films on glass substrate prepared by spray pyrolysis method', *Optik (Stuttg).*, vol. 125, no. 18, pp. 5112–5115, 2014.
2. A.Le Donne, D.Cavalcoli, R.A.Mereu , M.Perani ,L .Pagani, M.Acciarri, S.Binetti Materials Science in Semiconductor Processing Volume 71, 15 November 2017, Pages 7-11.
3. Vishwakarma, R. , J Theor Appl Phys 9, 185–192 (2015).
4. Zainab J. Shanan, Jinan A. Abd and kadhim A. Adem 2014 Australian Journal of Basic and Applied Sciences 8(817):311-316
5. Ettlinger, R. B., Cazzaniga, A. C., Canulescu, S., Pryds, N., AND Schou, J. (2015). Applied Surface Science , 336, 385-390.
6. Ashith V K, Gowrish Rao K. IOP Conf. Series: Materials Science and Engineering 360 (2018) 012058.
7. M.A. Hernandez-Fenollosa, M.C. Lopez, V. Donderis, M. Gonzalez, B. Mari, and J.R. Ramos-Barrado, J.Thin Solid Films, 516, (2008), 1622.
8. Burhan R. N. Al-Shafaay Journal o Kufa – Physics Vol.2 No.1 (2010)
9. Sachin V. Mukhamale and N. B. Chaure 2013 *AIP Conf. Proc.* 1512, 388.

10. Nanasaheb P. Huse, Avinash S. Dive, Deepak S. Upadhye, Sagar B. Bagul, Ketan P. Gattu & Ramphal Sharma 2017 *Ferroelectrics*, 519:1, 170-177
11. J Fang, P H Holloway, J E Yu, K S Jones, B Pathangey, E Brettschneider, T J Anderson, Applied Surface Science, 70, 701, 1993.
12. P. Kumar, A. Kumar, P.N. Dixit, and T.P. Sharma, Indian J. Pure Appl. Phys., 44, (2006), 690–693.
13. K. N. Chopra and A. K. Maini, Thin films and their applications in military and civil sectors. Defence Research and Development Organisation, Ministry of Defence, 2010.
14. W. G. Huckle, G. F. Swigert, and S. E. Wiberley, 'Cadmium Pigments. Structure and Composition', *Ind. Eng. Chem. Prod. Res. Dev.*, vol. 5, no. 4, pp. 362–366, 1966, doi: 10.1021/i360020a016.
15. M. Ohering, 'Materials science of thin films deposition and structure'. Academic Press, San Diego, 2002.
16. Z. J. Shanan and J. Ali, 'Structural, Morphological and Optical Properties of ZnS Thin Film Deposited by Pulsed Laser Deposition Technique', *Aust. J. Basic Appl. Sci.*, no. October 2016, pp. 311–316, 2014.
17. E. Lifshin, *X-ray Characterization of Materials*. John Wiley & Sons, 2008.
18. J. Mietz, 'Materials science and engineering - An introduction. VonW. D. Callister, Jr., 3. Auflage, XX, 811 S., zahlreiche Abb. und Tab., John Wiley & Sons. Inc. New York, 1994, paper back $37.95, handback $79.50, ISBN 0-471-30568-5', *Mater. Corros. und Korrosion*, vol. 45, no. 11, pp. 632–633, 1994, doi: 10.1002/maco.19940451110.
19. A. S. Z. Lahewil[a], Y. Al-Douri[a], U. Hashima, and N. M. Ahmedb, 'Structural, analysis and optical studies of cadmium sulfide nanostructured', *Procedia Eng.*, vol. 53, pp. 217–224, 2013.
20. M. A. Yıldırım, 'The effect of copper concentration on structural, optical and dielectric properties of CuxZn1− xS thin films', *Opt. Commun.*, vol. 285, no. 6, pp. 1215–1220, 2012.
21. W. D. Callister and D. G. Rethwisch, 'Characteristics, applications, and processing of polymers', *Mater. Sci. Eng. An Introd. 4th ed., John Wiley Sons, Inc., New York*, pp. 465–505, 1997.
22. R. L. S. Ravangave L. S, 'Study of structural, Morphological and Electrical Properties of

$Cd_xZn_{1-x}S$ Thin Films', *IOSR J. Appl. Phys.*, vol. 3, no. 3, pp. 41–47, 2013, doi: 10.9790/4861-0334147.

23. G. Jia, N. Wang, L. Gong, and X. Fei, 'Optical properties and forming mechanism of CdZnS Thin Film grown by chemical bath deposition', *Chalcogenide Lett.*, vol. 7, no. 5, pp. 377–383, 2010.
24. S. M. Thahab, A. H. O. Alkhayat, and S. M. Saleh, 'Influence of substrate type on the structural, optical and electrical properties of CdxZn1− xS MSM thin films prepared by Spray Pyrolysis method', *Mater. Sci. Semicond. Process.*, vol. 26, pp. 49–54, 2014.
25. M. Zakria, A. Mahmood, A. Shah, Q. Raza, and E. Ahmed, 'Tunability of physical properties of (Cd: Zn) S thin film by Close Space Sublimation Process (CSSP)', *Prog. Nat. Sci. Mater. Int.*, vol. 22, no. 4, pp. 281–287, 2012.
26. W. B. Salih, 'The Study of Optical Properties of Thin filmsPrepared by Chemical Spry Pyrolysis Technique', *J. Univ. Anbar pure Sci.*, vol. 4, no. 2, pp. 41–49, 2010.
27. M. S. Hossain *et al.*, 'Effect of annealing on the properties of ZnxCd1-xS thin film growth by RF magnetron co-sputtering', *Energy Procedia*, vol. 33, pp. 214–222, 2013.

A study of The orientations of liquid crystal SDS by NMR method

Dr.Abdul Alrazak Al-soufi

Abstract

In this article I had studied the physical properties of liquid crystal which called SDS by nuclear magnetic resonance NMR.I had to find the relationship between splitting energy levels and orientation crystals in solution by different temperatures in strong magnetic e ld (9.4 Tesla). This had been found by two ways: theorec ally and experimentally. A - Theoretically: I had found all values of the possible energy levels when the angle & changed from 0 to 120°. We notice that the strong magnetic field leads to the splitting energy levels. By the value of this splitting we can calculate frequency Δv theo and soup parameter S in each angle. B- Experimentally : I had found value Δv exp and S exp by die rent temperatures from 278K to 333K. I find great accordance with the theoretical results according of these results, the value of soup parameter is decreased

side by side with the increasing temperatures. In this case, the liquid crystal is gradually changed to the anisotropy.

دراسة توجيهات البلورات السائلة لمركب SDS

بواسطة التجاوب المغناطيسي النووي NMR

د. عبد الرزاق الصوفي

كلية العلوم – قسم الفيزياء – جامعة البعث

الملخص:

تم في هذا البحث إيجاد العلاقة التي تربط بين الأنقسام في سويات الطاقة و توجهات بلورات SDS في المحلول بوجود شوارد Na^+ بتغير درجات الحرارة و بوجود الحقل المغنطيسي القوي نظرياً و تجريبياً . أما نظرياً فقد تم إيجاد جميع قيم السويات الطاقية الممكنة عند تغير الزاوية θ (ما بين الناظم على كل بلورة و المحور الرئيسي للحقل المغناطيسي) من الصفر حتى 120^0 و لاحظنا أنه بوجود الحقل المغناطيسي القوي يحدث إنشطار للسويات الطاقية بالتالي يحدث توجهات مفضلة للبلورات ومن مقدار هذا الانشطار تمكنا من حساب التواتر $\Delta V\ theo$ ورتبة التوجه s عند كل زاوية θ بالإعتماد على التابع الهملتوني والميكانيك الكوانتي. أما تجريبياً فتم إيجاد قيم ΔV و s

بتغير درجات الحرارة من الدرجة 278k حتى الدرجة 333k وتم مقارنتها مع النتائج النظرية وحصلنا على توافق كبير بينهما . وهذا يدل على أن درجة توجه البلورات الكلية s تنخفض بازدياد درجة الحرارة وهذا يؤدي إلى أن تتحول البلورات السائلة تدريجياً إلى حالة anisotropy و عند الدرجة 333k تكون البلورات قد انحلت كلياً.

مقدمة:

من أبرز خواص البلورات السائلة هي أنها تشابه الحالة الصلبة للمادة من حيث التموضع على شكل صفوف طويلة وفي نظام التوجهات وهي بنفس الوقت تشابه الحالة السائلة للمادة من حيث اللزوجة و الحركية وغيرها . على الرغم من حداثة هذا العلم إلا أننا نجد أن الأبحاث العلمية التي تفسر الخواص الفيزيائية للبلورات السائلة قد أصبحت كثيرة ومتنوعة وذات استخدامات تقنية هامة جداً. فكان أول ظهور لها في ساعة المعصم و الآلة الحاسبة الجيبية وهي الآن تنافس بشكل كبير تقنيات أخرى لأنها ملفتة للنظر و طويلة البقاء و سعرها معتدل . وخاصة في مجال البصريات فمثلاً أحدث الصناعة لشاشات الكمبيوتر تعتمد على البلورات السائلة المرجع [*2-1*] . وللحصول على البلورات السائلة لهذا المركب SDS (sodium dodecyl sulfate) الذي له الصيغة الموجودة في الشكل [1] نضيف مقدار ضئيل من هذا المركب إلى الماء نجد أ، هذا المركب يتشرد ويتشكل له رأس قطبي مؤلف من شاردة الصوديوم والسولفات وذيل لا قطبي مؤلف من السلاسل الكربونية .

$$C\text{-}(CH_2)_3 - O - SO_3^- Na^+ H_3$$

7.11% صوديوم ديسيل سولفيت و 13.05% بنتانول و 0.2% بروم الصوديوم و 97.84 ماء.ونلاحظ تحت المجهر أن الجزيئات تتجمع على شكل مكورات ثم بزيادة التركيز تأخذ هذه المكورات شكلاً اسطواناً ثم تتجمع فوق بعضها البعض وتنبسط لتأخذ شكلاً صفائحياً طبقياً عندما يصل تركيز جزيئات هذا المركب إلى 5% من الوزن الكلي لا بد من التنويه إلى أنني قد أجريت الجزء العلمي من هذا البحث في مختبر NMR في جامعة تريستا – إيطاليا. NMR Labaratory – Trieste University – Italy

المؤتمر العلمي الدولي الرابع عشر
لجمعية الرياضيات العراقية والمنعقد تحت شعار
الإبداع يلتقي بالتحديات من اجل التقدم العلمي والتكنولوجي
للمدة 4 - 5 اب 2024
دمشق - سورية

هدف البحث وطريقته :

يهدف البحث الدراسة توزع السويات الطاقية الحزينات البلورات السائلة المركب SDS للطيف الناتج عن هذا المركب عند وضع المركب ضمن حفل مغناطيسي قوي (Tesls 9.4) بواسطة جهاز الرنين المغناطيسي النووي NMR وذلك بتغيير درجات الحرارة (278-323k) لأن البلورات تنحل عند درجات حرارة أكبر من هذه الدرجة . وبذلك يمكن أن نحدد طريقة ارتباط الانقسام في السويات الطاقية وتوجهات الجزيئات في المحلول نتيجة وجود الحقل المغناطيسى القوي الذي يؤثر على رباعيات الأقطاب للمركب المدروس الشكل رقم [١] وذلك بالاعتماد على التابع الهاملتوني والميكانيك الكوانتي المرجع [٤] . وذلك عند دراسة هذا المركب بدرجة حرارة الغرفة ومن ثم دراسة هذا المركب بواسطة جهاز الرنين المغناطيسي النووي بتغيير درجات الحرارة السويات الطاقية للمركب SDS[ذي العزم الزاوي النووي (I=3/2)] الناتجة عن التأثير المتبادل بين رباعيات الأقطاب والحقل المغناطيسي الخارجي الشديد:

أ- الحقل المغناطيسي الخارجي الشديد والمركب SDS

عند وضع نواة المركب فى حقل مغناطيسي قوي وثابت (Tesls 9.4) فإن السوبات سوف تنشطر نتيجة عزم مغناطيسي نووي وتتحدد قيمة الفرق في السويات الطاقية ΔE بقيمة تواتر الرنين (الطنين) الناتج كما في الشكل [1] حيث ΔE =hv وهي تعبر عن مطيافية NMR . وبما أن العزم الزاوي (وبالتالي العزم المغناطيسي) لكل نواة يختلف عن الآخر وبالتالي فإن الفجوة الطاقية ΔE الهيدروجين مثلا تختلف عن الديتريوم نتيجة اختلاف تواتر الرنين لكل منهما المرجع رقم [5] . أما إذا كان العزم المغناطيسي معدوماً نجد أنه لا يوجد أي انشطار بالسويات الطاقية وبالتالي لا يوجد أي طيف NMR للمادة المرجع [٦].

بشكل عام تملك كافة النوى لجميع المركبات عزما زاوياً | يأخذ القيم

-3/2 , -1/2 , 1/2 , 3/2- يرافق هذا العزم عزماً مغناطيسياً يعطى بالعلاقة $\mu = \gamma I$ حيث γ الجيرومغناطيسية إذا خضعت النوى التي تملك عزماً زاوياً لا يساوي الصفر إلى حقل مغناطيسي خارجي يحدث تأثير متبادل وتمتلك طاقة إضافية تعطى بالعلاقة $E = -\mu B$ وهذه العلاقة تؤول إلى $E = -\mu_Z B$ ولكن $\mu_Z = \gamma\, m_1 \hbar$ ومنه $E = -\gamma m_1 \hbar B$ وهذا يعني أن طاقة النواة ستعاني انزياحاً مقداره متناسب مع شدة الحقل المغناطيسي الخارجي ومع نسبة الجير ومغناطيسية ومع مسقط I على المحور z وبما أن العزم I له $(2I + 1)$ مسقط فإنها تتباعد (تنتشر) بالمقدار نفسه $\hbar\gamma B$ الذي يدعى الفجوة الطاقية . أما حالتنا المدروسة لجزيئات البلورات السائلة المركب SDS نجد أن:

I=3/2 ,$m=0,\pm 1/2,\pm 3/2$ في يملك فقط ثلاث سويات طاقية فرعية مختلفة والانتقالات المتاحة

ومنه: $\Delta E = h\nu = \hbar\gamma B$ V=$\gamma B/2\pi$

في تقنية NMR وكما ذكرنا سابقاً يستخدم حقل مغناطيسي قوي حوالي (Tesls 9.4) وهو أكبر بخمس مرات من الحقل المغناطيسي الأرضي . كذلك نلاحظ أن مجال تواترات مطيافية NMR من المرتبة الثامنة (مقدرة بالهرتز) وهي تميزه عن غيره من المطيافيات الأخرى المرجع[7]

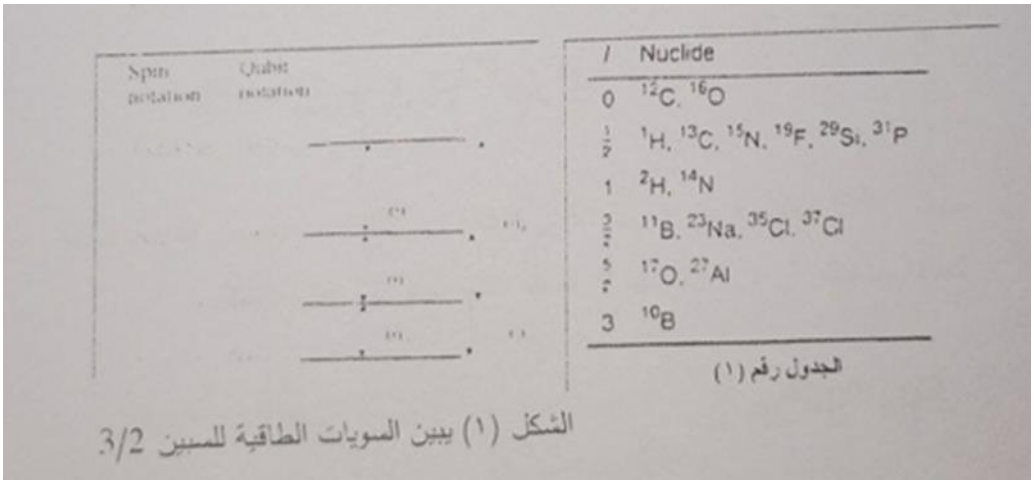

يبين الجدول (١) قيم العزم الزاوي لنوى بعض العناصر الهامة التي من ضمنها نوى الصوديوم بوجود الحقل المغناطيسي القوي للمركب SDS.

أخيرا" يمكن أن نبين أن نوع الجهاز الذي تم العمل عليه هو : NMR spectra were

measured on a Bruker AMX600 spectrometer

ب - وصف السويات الطاقية النووية لجزيئات المركب SDS :

يمكن وصف سويات الطاقة للطيف الناتج عن الرنين المغناطيسي بوجود حقل مغناطيسي قوي (Tesls 9.4) للتأثيرات المتبادلة لرباعي الأقطاب في المركب SDS على الشكل التالي يمكن أن نعبر عن الطاقة الكلية للطيف الناتج عن الرنين المغناطيسي بالتابع الهاملتوني H بواسطة معادلة شرود نغر : $H\psi = E\psi$ عندما تمتلك النواة عزوماً مختلفة كما في حالة المركب SDS يؤخذ تأثير هذه الأقطاب على أنه اضطراب ويكتب التابع الهملتوني على النحو :

$$H = H^{(0)} + \lambda H^{(1)} + \lambda^2 H^{(2)}$$

حيث يشير λ إلى رتبة الاضطراب

$$\psi = \psi^{(0)} + \lambda\psi^{(1)} + \lambda^2\psi^{(2)}$$

ويكون التابع الخاص لهذا الهملتوني هو :

الذي تقابله القيمة الخاصة :

$$E = E_0 + \lambda E^{(1)} + \lambda^2 E^{(2)}$$

حيث : $E^{(1)}$ التصحيح من المرتبة الأولى للطاقة و $E^{(2)}$ التصحيح من المرتبة الثانية للطاقة وباعتبار أن : $\lambda 1$= نجد أن الطاقة الكلية يمكن تكتب بالشكل :

$$H = H^{(0)} + H^{(1)} + H^{(2)} \quad \text{و}$$
$$E = E_0 + E^{(1)} + E^{(2)} + \cdots$$

سوف استخدم لاحقاً علاقة الطاقة الكلية هذه عند إيجاد درجة التوجه الكلية S لجزيئات البلورات السائلة للمركب SDS وبالتالي التابع الهاملتوني الكلي للسبين النووي لعزم رباعي الأقطاب والعزم المغناطيسي للمركب SDS يعطى بالشكل التالي :

$$H = H_Q + H_Z$$

$$H_Z = -\gamma\hbar H I_z$$

$$H_Q = \frac{e^2qQ}{4I(2I-1)}\left[\frac{1}{2}(3\cos^2\theta - 1)(3I_z^2 - I(I+1)) - \frac{3}{2}\sin\theta\cos\theta\{I_z(I_+ + I_-) + (I_+ + I_-)I_z\} + \frac{3}{4}\sin^2\theta(I_+^2 + I_-^2)\right]$$

حيث $I_+ = I_x + iI_y$ تسمى معامل التسلق (المرجع رقم ٨)

3 النتائج والمناقشة : يمكن تقسيم العمل إلى قسمين : 1 – قسم نظري 2- قسم تجريبي.

القسم النظري : المعطيات النظرية تمكننا من إيجاد جميع قيم السويات الطاقية الممكنة عندما تتغير الزاوية θ من الصفر إلى 90^0 ومنها يمكن حساب (Δv theo) لكل زاوية من الصفر حتى 120^0 أيضاً بعد ذلك يمكن إيجاد درجة توجه البلورات S (نظرياً) وذلك عندما تتغير الزاوية من الصفر حتى 120^0 (من أجل قيم θ الأكبر من 120^0 نجد أن النتائج تتكرر لذلك لا داع لكتابتها) عندها يمكن أن ترسم علاقة Δv theo بدلالة درجة التوجه S . علاقة الطاقة E_m^n توضح مقدار مساهمة الطاقة للاضطراب ذي الرتبة المرجع [٨] كما يلي:

$$E_m = E_m^{(0)} + E_m^{(1)} + E_m^{(2)} + \cdots\cdots \quad \ldots\ldots\ldots\ldots(1)$$

$$E_m^{(0)} = -\gamma\hbar H_m = -h\nu_L m \quad \ldots\ldots\ldots\ldots(2)$$

$$E_m^{(1)} = \frac{1}{4}h\nu_Q(3\mu^2 - 1)(m^2 - \frac{1}{3}\alpha). \quad \ldots\ldots\ldots\ldots(3)$$

$$E_m^{(2)} = -h\left(\frac{\nu_Q^2}{12\nu_L}\right)m\left[\frac{3}{2}\mu^2(1-\mu^2)(8m^2 - 4a + 1) + \frac{3}{8}(1-\mu^2)^2(-2m^2 + 2a - 1)\right] \ldots\ldots\ldots\ldots(4)$$

$$\nu_L = \frac{\gamma H}{2\pi}, \quad \mu = \cos\theta, \quad a = I(I+1), \quad \nu_Q = \frac{3e^2qQ}{h2I(2I-1)}$$

نتيجة لذلك تمكنا من حساب قيمة الثوابت الثلاثة السابقة بوجود الحقل المغناطيسي (Tesls 9.4) للمركب SDS فوجدنا أنها ثوابت تساوي :

$$a = 15/4 = 3.75 \qquad \nu_Q = 10.5\ MHz \qquad \nu_L = 105.749$$

بالاعتماد على ذلك يمكن حساب جميع قيم الطاقة كالتالي :

أ - إن السوية الطاقية الصفرية تملك قيم للطاقة $m=\pm 1/2, \pm 3/2$ لإيجاد هذه القيم نعوض في العلاقة رقم (٢) فنجد أن

$$E^{(0)}_{-3/2=+1046,925.10} - 28 \qquad E^{(0)}_{-\frac{1}{2}=+348,975.10} - 28$$

$$E^{(0)}_{+\frac{3}{2}=-1046,925.10} - 28 \qquad E^{(0)}_{+\frac{1}{2}=-348,975.10} - 28$$

ب - إن السوية الطاقية الأولى E^1_m تقسم حسب قيم m حيث يمكن إيجاد جميع هذه القيم (كلاً على حدا) من أجل جميع الزوايا θ من

الصفر حتى 120^0 وذلك بتعويض قيمة هذه الزاوية في المعادلة رقم [٣] ثم ندون النتائج في الجدول رقم [٢]

$\boldsymbol{\theta}$	$\boldsymbol{E^{(1)}_{+\frac{1}{2}}}$, $\boldsymbol{E^{(1)}_{-\frac{1}{2}}}$
$\theta = 0$	$\mathbf{-34,65.10^{-28}}$
$\theta = 10$	$\mathbf{-33,080355.10^{-28}}$
$\theta = 20$	$\mathbf{-28,568925.10^{-28}}$
$\theta = 30$	$\mathbf{-21,65625.10^{-28}}$
$\theta = 40$	$\mathbf{-13,17393.10^{-28}}$
$\theta = 50$	$\mathbf{-4,14951075.10^{-28}}$
$\theta = 60$	$\mathbf{+4.33125.10^{-28}}$
$\theta = 70$	$\mathbf{+16,974066.10^{-28}}$
$\theta = 80$	$\mathbf{+17,234538.10^{-28}}$
$\theta = 90$	$\mathbf{+17,325.10^{-28}}$
$\theta = 100$	$\mathbf{+17,234538.10^{-28}}$
$\theta = 110$	$\mathbf{+16,974066.10^{-28}}$
$\theta = 120$	$\mathbf{+4,33125.10^{-28}}$

الجدول رقم (٢) يبين قيم و $E^{(1)}_{-\frac{1}{2}}$ وقيم $E^{(1)}_{+\frac{1}{2}}$ من أجل زوايا مختلفة حتى 1200 هي كالتالي :

$\boldsymbol{\theta}$	$\boldsymbol{E^{(1)}_{+\frac{3}{2}}}$, $\boldsymbol{E^{(1)}_{-\frac{3}{2}}}$
$\theta = 0$	$\mathbf{-34,65.10^{-28}}$

$\theta = 10$	$\mathbf{-33{,}080355.10^{-28}}$
$\theta = 20$	$\mathbf{-28{,}27012.10^{-28}}$
$\theta = 30$	$\mathbf{-21{,}65625.10^{-28}}$
$\theta = 40$	$\mathbf{-13{,}17512.10^{-28}}$
$\theta = 50$	$\mathbf{-4{,}1498235.10^{-28}}$
$\theta = 60$	$\mathbf{+4.33125.10^{-28}}$
$\theta = 70$	$\mathbf{+16{,}974066.10^{-28}}$
$\theta = 80$	$\mathbf{+17{,}234538.10^{-28}}$
$\theta = 90$	$\mathbf{+17{,}325.10^{-28}}$
$\theta = 100$	$\mathbf{+17{,}234538.10^{-28}}$
$\theta = 110$	$\mathbf{+16{,}974066.10^{-28}}$
$\theta = 120$	$\mathbf{+4{,}33125.10^{-28}}$

الجدول رقم (3) يبين قيم و $E^{(1)}_{-\frac{3}{2}}$ وقيم $E^{(1)}_{+\frac{3}{2}}$ من أجل زوايا مختلفة من الصفر حتى 120

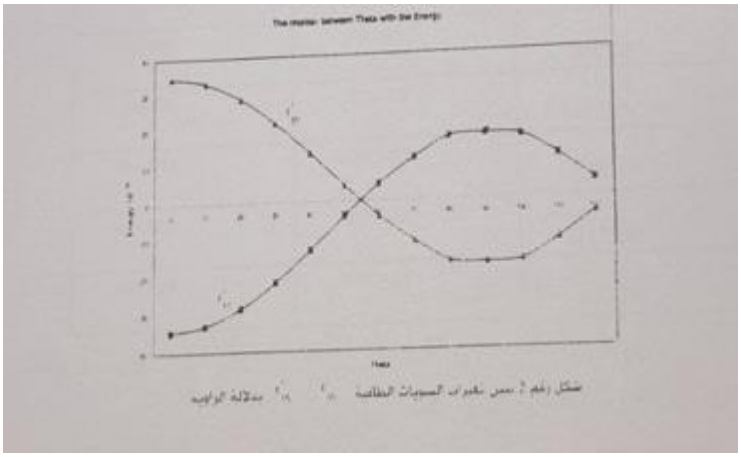

لحساب قيمة التواتر V لتوجد قيمة الفرق في السويات الطاقية كالتالي :

نحسب أولا السوية $\Delta E_{\frac{3}{2},-\frac{3}{2}}$ كالتالي:

$$\Delta E_{\frac{3}{2},-\frac{3}{2}} = \left(E^{(0)}_{\frac{3}{2}} + E^{(1)}_{\frac{3}{2}}\right) - \left(E^{(0)}_{-\frac{3}{2}} + E^{(1)}_{-\frac{3}{2}}\right)$$

جدول رقم (4) يبين قيم $\Delta E_{\frac{3}{2},-\frac{3}{2}}$

θ	$\Delta E_{\frac{3}{2},-\frac{3}{2}}$	$V_{\frac{3}{2},-3/2} * 10^6$
$\theta = 0$	-2093.85	-317.25
$\theta = 10$	-2093.85	-317.25
$\theta = 20$	-2093.85	-317.25
$\theta = 30$	-2093.85	-317.25
$\theta = 40$	-2093.85	-317.25
$\theta = 50$	-2093.85	-317.25
$\theta = 60$	-2093.85	-317.25
$\theta = 70$	-2093.85	-317.25
$\theta = 80$	-2093.85	-317.25
$\theta = 90$	-2093.85	-317.25
$\theta = 100$	-2093.85	-317.25
$\theta = 110$	-2093.85	-317.25
$\theta = 120$	-2093.85	-317.25

$$\Delta E_{\frac{3}{2},-\frac{1}{2}} = \left(E^{(0)}_{\frac{3}{2}} + E^{(1)}_{\frac{3}{2}}\right) - \left(E^{(0)}_{-\frac{1}{2}} + E^{(1)}_{-\frac{1}{2}}\right)$$

جدول رقم (5) يبين قيم $\Delta E_{\frac{3}{2},-\frac{1}{2}}$

θ	$\Delta E_{\frac{3}{2},-\frac{1}{2}}$	$V_{\frac{3}{2},-1/2} * 10^6$
$\theta = 0$	-1325.675	-200.859
$\theta = 10$	-1329.73	-202.842

$\theta = 20$	-1338.76	-201.475
$\theta = 30$	-1352.587	-204.937
$\theta = 40$	-1369.55	-207.507
$\theta = 50$	-137.600	-210.242
$\theta = 60$	-1404.6125	-212.820
$\theta = 70$	-1419.848	-215.128
$\theta = 80$	-1430.369	-216.722
$\theta = 90$	-1430.55	-216.75
$\theta = 100$	-1430.369	-216.722
$\theta = 110$	-1419.848	-215.128
$\theta = 120$	-1404.612	-212.820

السلاسل الأربعة في الشكل رقم (٣) عبارة عن فرق المتواتر بين السويات الطاقية الأربعة نتيجة انشطار السويات الطاقية عند تعرضها لحقل مغنطيسي خارجي كما هو مبين في الجداول السابقة:

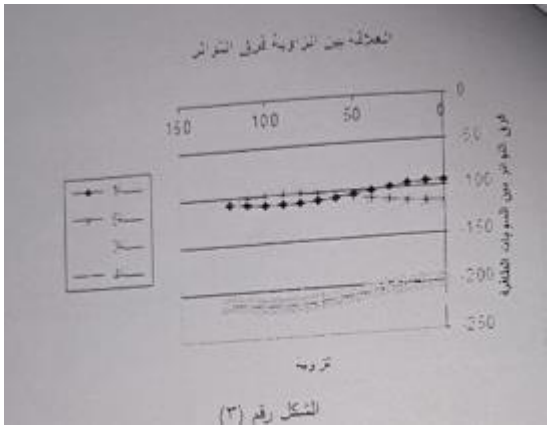

الشكل رقم (٣)

$$\Delta E_{\frac{3}{2}\frac{1}{2}} = \left(E_{\frac{3}{2}}^{(0)} + E_{\frac{3}{2}}^{(1)}\right) - \left(E_{\frac{1}{2}}^{(0)} + E_{\frac{1}{2}}^{(1)}\right)$$

جدول رقم (6) يبين قيم $\Delta E_{\frac{3}{2}\frac{1}{2}}$

θ	$\Delta E_{\frac{3}{2},\frac{1}{2}}$	$V_{\frac{3}{2},1/2} * 10^6$
$\theta = 0$	-627.725	-95.109
$\theta = 10$	-631.788	-95.725
$\theta = 20$	-640.810	-97.092
$\theta = 30$	-654.637	-99.187
$\theta = 40$	-671.6	-101.757
$\theta = 50$	-689.65	-104.492
$\theta = 60$	-706.662	-107.07
$\theta = 70$	-721.898	-109.378
$\theta = 80$	-732.419	-110.972
$\theta = 90$	-732.6	-111
$\theta = 100$	-732.419	-110.972
$\theta = 110$	-721.898	-109.378
$\theta = 120$	-706.662	-107.07

$\Delta V_{01} = V_{\frac{3}{2},1/2} - V_{\frac{3}{2},3/2}$ و $\Delta E_{01} = E_{\frac{3}{2},1/2} - E_{\frac{3}{2},3/2}$

جدول رقم(7) يبين قيم ΔV_{01}

θ	$\Delta V_{01} * 10^6$
$\theta = 0$	-95.109
$\theta = 10$	-95.725
$\theta = 20$	-97.092
$\theta = 30$	-99.187
$\theta = 40$	-101.757
$\theta = 50$	-104.492

$\theta = 60$	-107.07
$\theta = 70$	-109.378
$\theta = 80$	-110.972
$\theta = 90$	-111
$\theta = 100$	-110.972
$\theta = 110$	-109.378
$\theta = 120$	-107.07

$$\Delta V_{12} = V_2 - V_1 = V_{\frac{3}{2},-\frac{1}{2}} - V_{\frac{3}{2},\frac{1}{2}}$$

جدول رقم [8] يبين قيم Δv_{12}

θ	$*10^6\Delta v_{12}$
θ=0	-105.75
θ=10	-105.75
θ=20	-105.75
θ=30	-105.75
θ=40	-105.75
θ=50	-105.75
θ=60	-105.75
θ=70	-105.75
θ=80	-105.75
θ=90	-105.75
θ=100	-105.75
θ=110	-105.75

θ=120	-105.75

Δv_{23} يبين قيم [9] جدول رقم $\Delta v_{23} = v_3 - v_2 = v_{\frac{3}{2}-3/2} - v_{\frac{3}{2}-1/2}$

θ	$*10^6 \Delta v_{23}$
θ=0	-116.39
θ=10	-115.774
θ=20	-114.407
θ=30	-112.312
θ=40	-109.742
θ=50	-107.007
θ=60	-104.429
θ=70	-102.121
θ=80	-100.527
θ=90	-100.5
θ=100	-100.527
θ=110	-102.121
θ=120	-104.429

Δv_{13} يبين قيم [10] جدول رقم $\Delta v_{13} = v_3 - v_1 = v_{\frac{3}{2}-3/2} - v_{\frac{3}{2}-1/2}$

θ	$*10^6 \Delta v_{13}$
θ=0	-222.14

θ=10	-221.524
θ=20	-220.157
θ=30	-218.062
θ=40	-215.492
θ=50	-212.575
θ=60	-210.179
θ=70	-207.871
θ=80	-206.277
θ=90	-206.25
θ=100	-206.277
θ=110	-207.871
θ=120	-210.179

جدول رقم [11] يبين قيم $\Delta v_{02} = v_2 - v_0 = v_{\frac{3}{2}-1/2} - v_{\frac{3}{2}-3/2}$

θ	$*10^6 \Delta v_{02}$
θ=0	-200.859
θ=10	-201.475
θ=20	-202.842
θ=30	-204.937
θ=40	-207.507
θ=50	-210.242

θ=60	-212.82
θ=70	-215.128
θ=80	-216.722
θ=90	-216.75
θ=100	-216.722
θ=110	-215.128
θ=120	-212.82

جدول رقم [12] يبين قيم $\Delta v_{12} - \Delta v_{01}$

θ	$*10^6\ \Delta v_{12} - \Delta v_{01}$	s
θ=0	10.641	1.013
θ=10	10.024	0.954
θ=20	8.657	0.824
θ=30	6.562	0.624
θ=40	3.992	0.38
θ=50	1.257	0.1197
θ=60	-1.32	-0.125
θ=70	-3.629	-0.345
θ=80	-5.223	-0.497
θ=90	-5.25	-0.5
θ=100	-5.223	-0.497
θ=110	-3.629	-0.345

θ=120	-1.32	-0.125

جدول رقم [13] يبين قيم $\Delta v_{23} - \Delta v_{12}$

θ	$*10^6\ \Delta v_{23} - \Delta v_{12}$	s
θ=0	-10.641	-1.013
θ=10	-10.024	-0.954
θ=20	-8.657	-0.824
θ=30	-6.562	-0.624
θ=40	-3.992	-0.38
θ=50	-1.257	-0.1197
θ=60	1.32	0.125
θ=70	3.629	0.345
θ=80	5.223	0.497
θ=90	5.25	0.5
θ=100	5.223	0.497
θ=110	3.629	0.345
θ=120	1.32	0.125

جدول رقم [14] يبين قيم $\Delta v_{02} - \Delta v_{13}$

θ	$*10^6\ \Delta v_{23} - \Delta v_{12}$	s
θ=0	21.281	2.0267
θ=10	20.049	1.909
θ=20	17.315	1.649

θ=30	13.125	1.25
θ=40	7.985	0.76
θ=50	2.515	0.239
θ=60	-2.64	-0.251
θ=70	-7.257	-0.691
θ=80	-10.445	-0.994
θ=90	-10.5	-1
θ=100	-10.445	-0.994
θ=110	-7.257	-0.691
θ=120	-2.64	-0.251

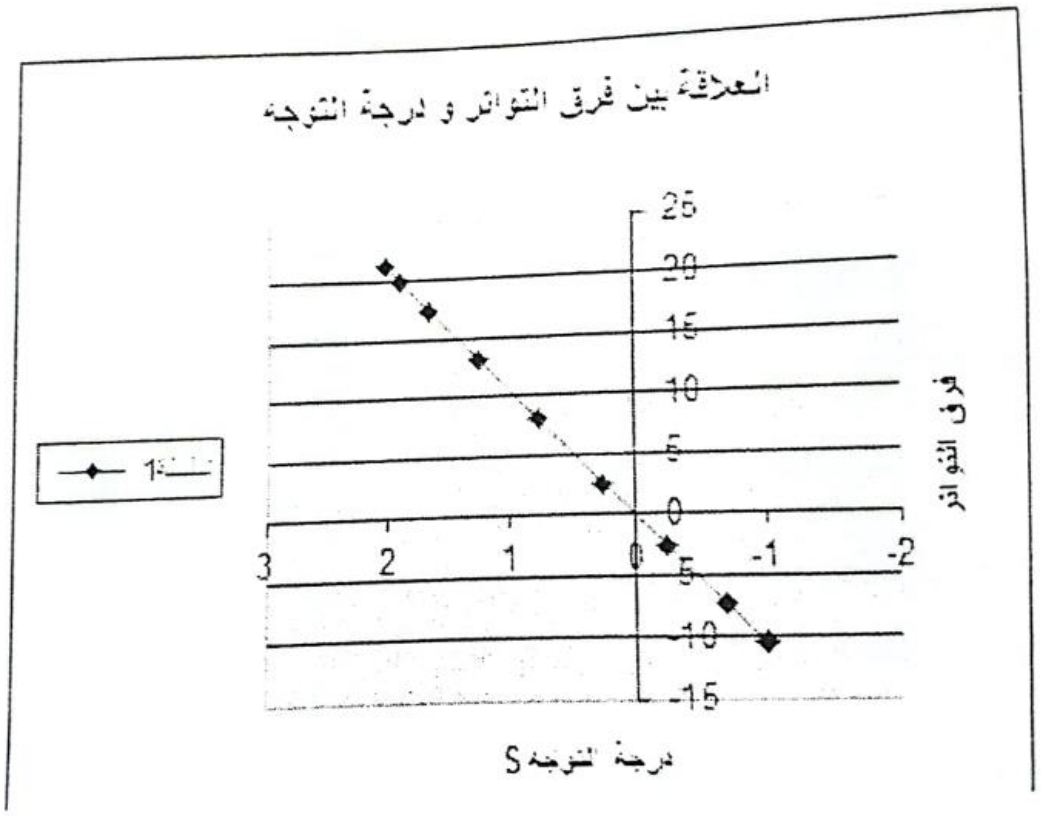

الشكل رقم [٤]

وبذلك تمكنا من إيجاد العلاقة بين فرق التواتر للسويات الطاقية ودرجة التوجه الكلية للبلورات نظرياً والآن سنقوم بإيجاد هذه العلاقة تجريبياً ونقارن النتائج النظرية مع التجريبية لمعرفة مدى تطابقها :

٢ - القسم التجريبي:

تم استخدام نوى ^{23}Na ذات السبين l=3/2 للبلورات السائلة للمركب SDS من نوع ليوتروبك تحتوي على 7.11% صوديوم دوسيل سولفات و 13.05% بنتانول و 0.2% مولNaBr و 79.84% ماء. إذا وضعنا البلورات السائلة لمركب SDS تحت المجهر الإلكتروني نلاحظ أن البلورات الصفائحية تسبح في المحلول بشكل حر و عشوائي عند غياب الحقل المغناطيسي. وعندما نعرض هذا المركب (بدرجة حرارة الغرفة إلى حقل مغناطيسي قوي 9.4Tesla بحيث ينطبق اتجاه هذا الحقل على الاحداثي Z العمودي على سطح التكدس) و يخترق الأنبوب الذي يحوي المركب من الأسفل إلى الأعلى نلاحظ أن جميع التكدسات (البلورات الصفائحية) تتوقف عن الحركة و تثبت في مكانها بحيث يصنع الناظم على كل بلورة من هذه البلورات (و الذي ينطبق على المحورZ) زاوية θ مع المحور الرئيسي للحقل المغناطيسي مختلفة عن الأخرى و يقيس الجهاز التواتر الكلي الإجمالي Δv لهذه البلورات . ويظهر على الشاشة منحنيان بيانيان يعبران عن الانشطار الذي تم للسويات الطاقية نتيجة تعرض المركب للحقل المغناطيسي كما في الشكل [٥] . ومن معرفة Δv الكلية يمكن معرفة درجة التوجه الكلية للبلورات المتعرضة لهذا الحقل S (عند درجة حرارة معينة) . ويمكن إعادة نفس الخطوات السابقة وفي كل مرة نزيد درجة حرارة المركب بمقدار درجتين أو خمس درجات حتى نصل إلى الدرجة 333K ونراقب الطيف الناتج ونقرأ قيمة التواتر الكلي Δv ومنها يمكن

حساب درجة التوجه S فتحصل على الجدول [١٥] . وعندها يمكن رسم العلاقة بين التواتر الكلي الإجمالي Δv ودرجة التوجه الكلية S التي حصلنا عليها بتغير درجات الحرارة الشكل رقم [٦].

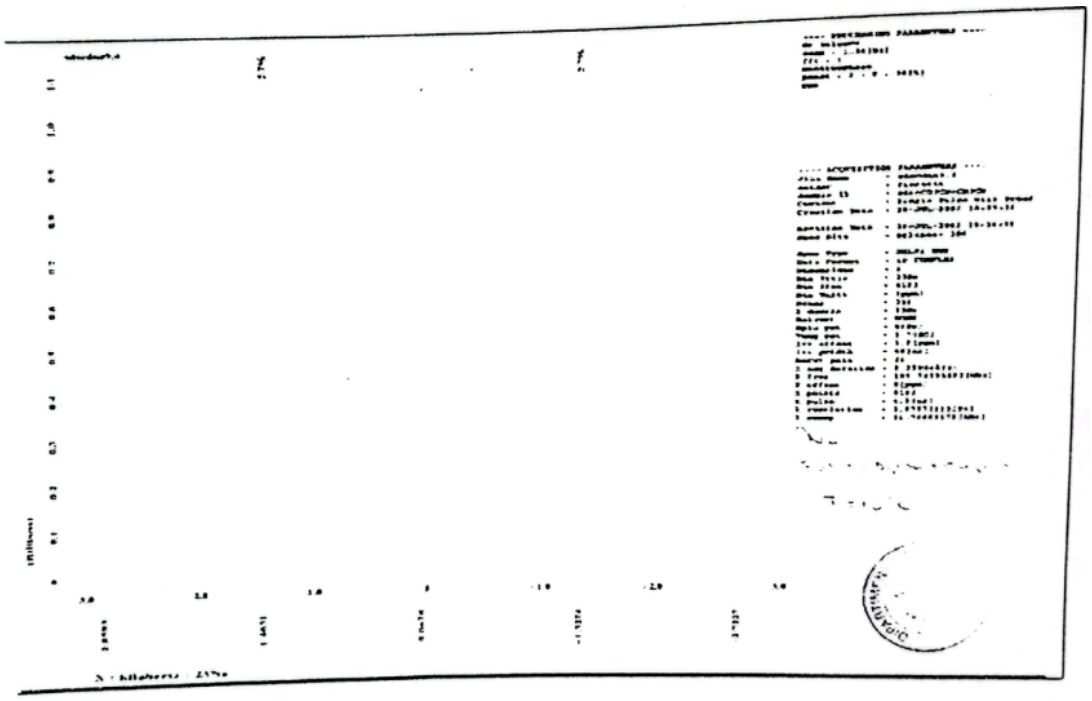

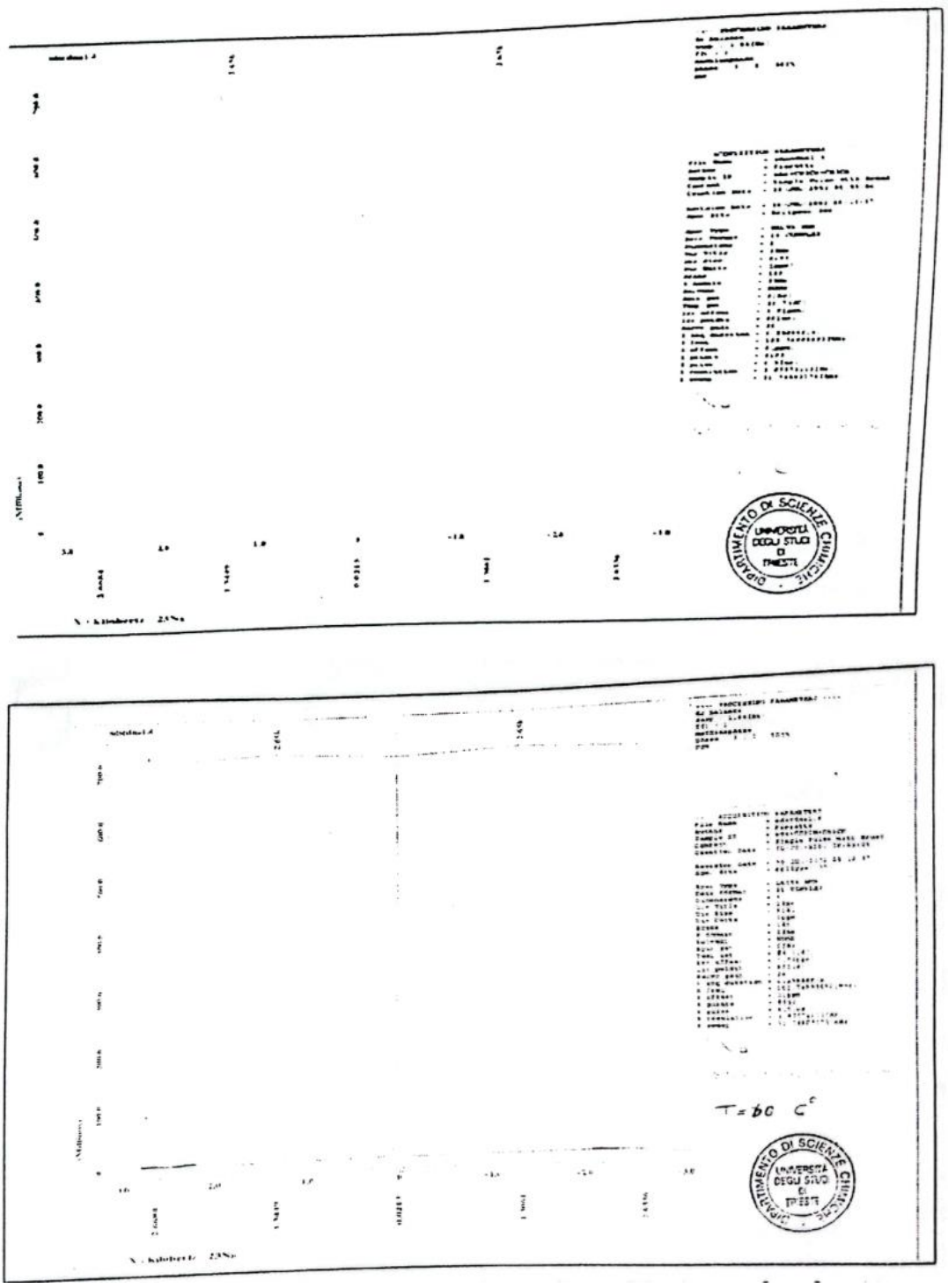

شكل [5] يبين العلاقة بين تواتر الشدة الطيفية للخطوط كما ظهرت على شاشة الجهاز NMR تجريبياً بدرجات حرارة مختلفة [10-30-60] .

جدول رقم 15 يبين قيم Δv تجريبياً

T(°C)	$*10^6\Delta v$	$S=\Delta v/v_Q$
5	5.615	0.534
7	5.604	0.533
10	5.581	0.540
15	5.538	0.527
20	5.481	0.522
22	5.453	0.519
25	5.426	0.516
27	5.387	0.513
30	5.301	0.505
40	4.4	0.419
47	3.1	0.295
50	2.2	0.209
55	1.2	0.114
60	0	0

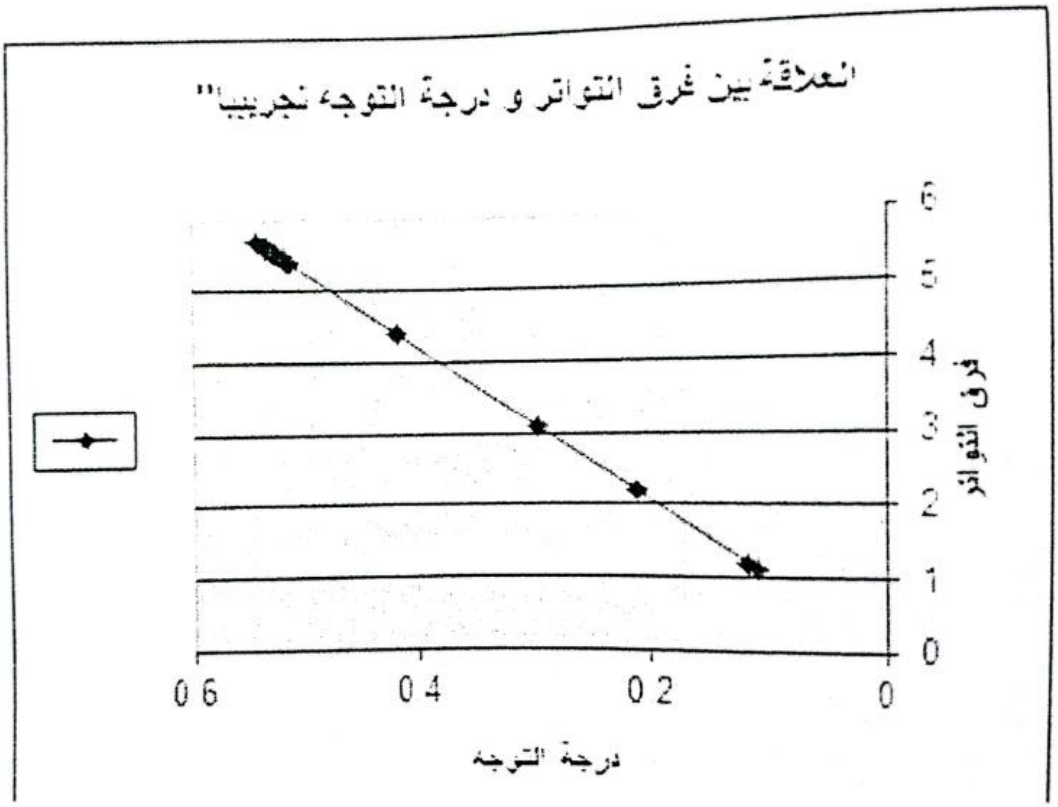

يمكن أن تتلاشى سويات الطاقة المنشطرة بفعل رباعيات الأقطاب في البلورات السائلة للمركب SDS وذلك عند انحلال البلورات بدرجات حرارة مرتفعة 333K . من مقارنة الخط البياني للنتائج التجريبية التي حصلنا عليها مع الخط البياني للنتائج النظرية نرى توافق كبير بينهما و هذا يدل على أن درجة توجه البلورات S للمركب SDS تنخفض بازدياد درجة الحرارة.

4- الخلاصة :

يمكن أن نخلص إلى القول بأننا تمكنا من تحديد طريقة ارتباط الانقسام في السويات الطاقية وتوجهات الجزيئات في المحلول بتغير درجات الحرارة وبوجود الحقل المغناطيسي القوي وذلك نظرياً وتجريبياً فنظرياً تم إيجاد جميع قيم السويات الطاقية الممكنة عندما تتغير الزاوية θ من الصفر حتى 120^5 ، ولا حظنا أنه بوجود الحقل المغناطيسي القوي يحدث انشطار للسويات الطاقية للمركب المدروس وبالتالي يحدث توجهات مفضلة للبلورات ومن مقدار الانشطار في السويات الطاقية تمكنا من حساب التواتر Δv theo ورتبة التوجه S عند كل زاوية θ . بعدها تم إيجاد قيم $\exp\Delta v$ و S تجريبياً بتغير درجة الحرارة وتم مقارنتها مع النتائج النظرية فوجد توافق كبير بينهما . ويمكن أن نستدل من ذلك بأن درجة توجه البلورات الكلية S تنخفض بازدياد درجة الحرارة بحيث تبدأ البلورات السائلة تدريجياً بالتحول إلى الحالة Anisotropy و بعد هذه الدرجة وتحديدا عند الدرجة 333K تكون البلورات قد انحلت كلياً في المحلول عندها لا يلاحظ أي انشطار يذكر للسويات الطاقية حتى بوجود الحقل المغناطيسي القوي وبالتالي يكون المركب قد تحول بالكامل إلى الحالة السائلة .

المؤتمر العلمي الدولي الرابع عشر
لجمعية الرياضيات العراقية والمنعقد تحت شعار
الإبداع يلتقي بالتحديات من اجل التقدم العلمي والتكنولوجي
للمدة 4 - 5 اب 2024
دمشق - سورية

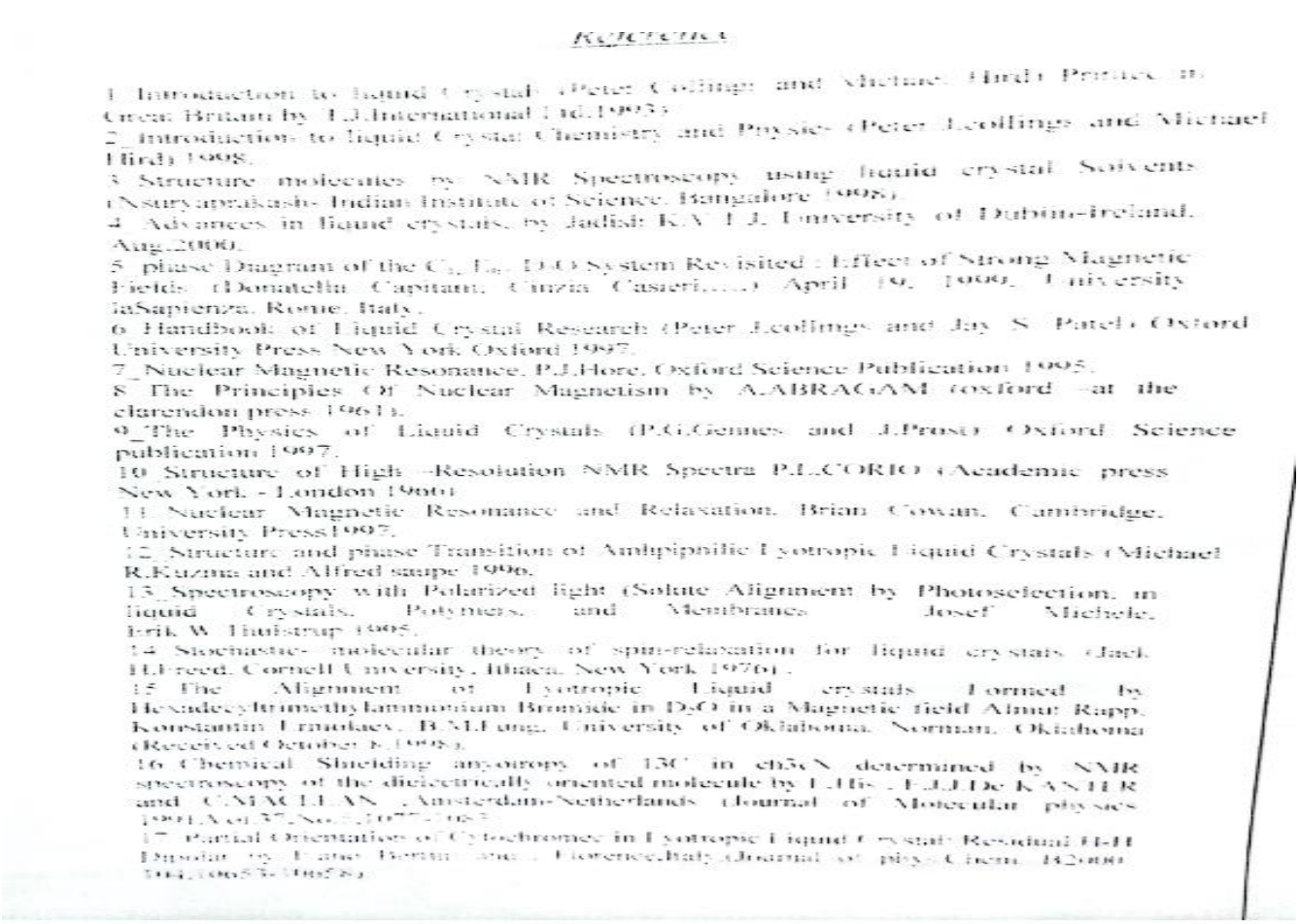

References

1_Introduction to liquid Crystal (Peter Collings and Michael Hird) Printed in Great Britain by T.J.International Ltd.1993.
2_Introduction to liquid Crystal Chemistry and Physics (Peter J.collings and Michael Hird) 1998.
3_Structure molecules by NMR Spectroscopy using liquid crystal Solvents (Nityanandakashi- Indian Institute of Science, Bangalore 1998).
4_Advances in liquid crystals, by Jadish K.V. I.I. University of Dublin-Ireland. Aug.2000.
5_phase Diagram of the $C_{12}E_6$ H2O System Revisited : Effect of Strong Magnetic Fields (Donatella Capitani, Cinzia Casieri,.....) April 16, 1999, University laSapienza, Rome, Italy.
6_Handbook of Liquid Crystal Research (Peter J.collings and Jay S. Patel) Oxford University Press New York Oxford 1997.
7_Nuclear Magnetic Resonance, P.J.Hore, Oxford Science Publication 1995.
8_The Principles Of Nuclear Magnetism by A.ABRAGAM (oxford -at the clarendon press 1961).
9_The Physics of Liquid Crystals (P.G.Gennes and J.Prost) Oxford Science publication 1997.
10_Structure of High -Resolution NMR Spectra P.L.CORIO (Academic press New York. - London 1966)
11_Nuclear Magnetic Resonance and Relaxation, Brian Cowan, Cambridge, University Press1997.
12_Structure and phase Transition of Amphiphilic Lyotropic Liquid Crystals (Michael R.Kuzma and Alfred saupe 1996.
13_Spectroscopy with Polarized light (Solute Alignment by Photoselection, in liquid Crystals, Polymers, and Membranes Josef Michele, Erik W. Thulstrup 1995.
14_Stochastic- molecular theory of spin-relaxation for liquid crystals (Jack H.Freed, Cornell University, Ithaca, New York 1976).
15_The Alignment of Lyotropic Liquid crystals Formed by Hexadecyltrimethylammonium Bromide in D2O in a Magnetic field Almut Rapp, Konstantin Tiraokes, B.M.Fung, University of Oklahoma, Norman, Oklahoma (Received October 8, 1998).
16_Chemical Shielding anysotropy of 13C in ch3cN determined by NMR spectroscopy of the dielectrically oriented molecule by E.E.Burnell, J.J.De KANTER and C.A.M.E.LAN, Amsterdam-Netherlands (Journal of Molecular physics 1991,Vol.37,No.6,1977-1983)
17_Partial Orientation of Cytochromes in Lyotropic Liquid Crystal: Residual H-H Dipolar (by Dante Bertini, Anna ... Florence,Italy (Journal of phys. Chem. 142000 104,10853-10858)

Computer Scope
Computer, Intelligent Application

Automated medicinal and aromatic plants using GIS (with a preconceived knowledge)

Dr. Mahmoud Diaf AL-Mohamed
Department of Environment and Forestry – Faculty of Agricultural Engineering – AL-Furat University –Syria
mahmoud.dayyaf@gmail.com

المؤتمر العلمي الدولي الرابع عشر
لجمعية الرياضيات العراقية والمنعقد تحت شعار
الإبداع يلتقي بالتحديات من اجل التقدم العلمي والتكنولوجي
للمدة 4 - 5 اب 2024
دمشق - سورية

Abstract

This research aims to redirect the functionality of ArcMap, is a software from the group of Geographic Information Systems (GIS), for automating medicinal and aromatic plants. This application gives the ability to identify a plant, directly in the field with a preconceived knowledge. Of course, this knowledge will be done after the completion of the automating of the plants in this application. If a researcher or interested in medicinal and aromatic plants wants to know some information about a plant, suggested system should enter plant specific "keywords" within it. These keywords will eventually lead him to know the scientific name of the plant and, all its medicinal and aromatic properties that have been previously programmed within the application tables. In addition, he can know the location and coordinates of this plant in the region or even at the level of the country. In the future, this application can be generalized to include the biodiversity in general, such as *flora* and *fauna*. It is a qualitative achievement, as this product will provide a great service to all interested amateurs, researchers, universities and institutes students in the fields of pharmacy, natural sciences, agricultural and wildlife, and even for ordinary people.

Keywords: Medicinal, Aromatic Plants, Electronic Guide of Medicinal, Aromatic Plants, Biodiversity.

Introduction

To date, the total estimated number of species on Earth is about 8.7 million (more or less 1.3 million)—the most accurate calculation ever made—with 6.5 million species on land and 2.2 million in the oceans [1]. Scientists have counted the currently known, described, and accepted number of plant species at 374,000, of which approximately 308,312 are vascular plants,[2] with 295,383 flowering plants (angiosperms; monocots: 74,273; dicots: 210,008) [3]. Scientists estimate that there are about 3,227 species of medicinal and aromatic plants belonging to 235 different plant families [4]. The most commonly recognized forms of agriculture were agroforestry, intensive agriculture, and controlled agriculture, followed to a much lesser extent by intensive agriculture and natural care. Of the species recognized, 954 have an International Union for Conservation of Nature (IUCN) genus name. As for us as ordinary people or even as researchers, how many types of these medicinal and aromatic plants do we know? The desire to learn and know the nature of living organisms around us is an innate instinct in humans, especially with regard to plants of all types and forms found on our planet Earth. Whenever we walk in a garden or go on a trip to a forest, we always have a feeling of knowing the name of this or that plant, especially those plants with beautiful flowers and fragrant smell, and what are their medical or nutritional benefits in our daily lives. We may know the names and benefits of some of these plants, but we certainly do not know the names and benefits of many of them due to the huge diversity of their types and varieties. Although these plants are sources of most of the vitamins our bodies need, they are also excellent food sources in addition to being the primary producer of medical and pharmaceutical drugs and extracting the finest types of natural perfumes, or to avoid poison

from them. However, humans still do not know the names and properties of most of these plants. Historically, it is known that the method of identifying plant names in general and medicinal and aromatic plants in particular has gone through many stages, starting from the use of medical dictionaries and various classification books, to the use of computers and up to the present day where artificial intelligence techniques are used through smart digital cameras. Despite the technological progress in artificial intelligence methods, there are still difficulties to this day in quickly and directly identifying the name of the plant and its characteristics. In this research, we present a method and a tool for every ordinary person, amateur or researcher who can take this application with him on his outings in the forests or while walking in the fields, where he can use this application to quickly identify the name of the plant and its characteristics when this application is completed and accomplished in a way, noting that this application does not cancel the benefits of previous methods, but rather it is complementary and complementary and provides a new and innovative scientific and technical benefit.

Reference study

If we go back in time to see the evolution of the methods used to identify medicinal and aromatic plants throughout history, we find that they have gone through different stages. We can show this through the following narration: Traditional methods (papers): such as botanical classification books or dictionaries of medicinal and aromatic plants [5] and [6]. Using the computer: Researchers currently use the computer to link as many traits as possible associated with the plant, whether qualitative or quantitative traits, according to [7] and [8]. Then they calculate the taxonomic (or genetic) distance that separates each pair of taxonomic groups treated based on the evaluation of the common traits between these taxonomic groups studied. They concluded that there are morphological characteristics of plants that are always taken into account during plant identification by computer. Google search engine (https://lens.google.com): It requires two important things: First, it requires knowing the real scientific name of the target plant to enter its name in the search engine, and second, you must be lucky enough to know whether this or that plant is present in a reliable scientific encyclopedia, due to the large number of pages and sites where information is mixed and often contradictory, within websites. Image search engine (https://images.google.com): In fact, using it, we do not reach a result, unless there is a near-perfect match between the image of the plant taken by the camera, and another image of the same type that was previously archived on the Internet. This is difficult because the search engine gives you many possibilities, and you must search for the name of the target plant among many different images of plants. This is not a practical and tedious method and is not completely reliable. Artificial intelligence: Many universities and research centers in the world, such as America, Canada, Britain, Germany and other countries, are currently creating smart applications via mobile phones to achieve the best results in identifying plants, as indicated by [9], [10], and [11]. They have provided these applications with a huge number of digital images of plants,

which have been captured and stored within this application. Collecting the stored data will help to automatically identify the target plant. These images may be of the entire plant, as indicated by [12], or of parts of it, such as flowers, [13] or together for flowers and leaves. Thus, to achieve the greatest possible accuracy in terms of plant recognition. There are currently more than 10 applications that adopt this method, such as: *Flora Incognita - Pl@ntNet - PictureThis - Plant.id iNaturalist - Plantnet - Plant Spot - Planta - Plant Identifier - Plant Identification - Smart Identifier - PlantDetect Lite....* etc. In fact, most of these applications are still in the establishment phase, and the accuracy varies according to many conditions during the process of capturing the digital image. We can summarize that the process of identifying plants through applications that rely on artificial intelligence has become a focus of major global universities, institutes and research centers. We can also conclude that this is a great achievement in identifying the plant by simply capturing the image of this plant. However, it would be so if plant recognition in this way were 100% guaranteed. However, most authors of these applications point out that there is still a percentage of errors that are possible, according to Waldchen, director of research based on the Flora Incognita application at the Max Planck Institute for Biochemistry in Germany. In addition,[14] he pointed out the same criticisms about the *Leafsnap* application in the proceedings of the 12th Conference on Computer Vision (ECCV) held in Florence, Italy in 2012. If we go back a little to the scientific literature on how to distinguish between plant species, we find that there are certain parameters that can be relied upon to distinguish one plant from another or one plant group from another according to [7]. Any of these parameters is called a taxonomic characteristic, which means: any characteristic of an organism that can be measured, described or counted, whether visible or invisible, and is characterized by its presence in two distinct forms that can be distinguished from one another, and must be exclusively genetic. These visual characteristics will be the focus of our attention in this research for a simple reason, which is that all scientific references have confirmed that all characteristics are worthy of study during the process of identifying or distinguishing between plants, whether they are visible or invisible, and there is no reason to point out the neglect of any characteristics. In this research, we are not in a classification process as much as we need to benefit from using the most important morphological characteristics approved by the approved international classification books. In addition to what we can observe from the external morphological characteristics during the different stages of plant growth and then automate them within this application in the form of keywords. In fact, we can say that if this application is relied upon, people who will use it will be able to identify the desired plant quickly, easily and in an enjoyable way.

Goal of research

The research aims to redirect the function of the ArcMap, which is a software, specialized in Geographic Information System (GIS), so that, anyone interested in medicinal and aromatic plants can learn about the name of the plant and its medicinal uses or other

advantages, using this application, wherever he is. Through it, we can quickly identify this or that plant without resorting to paper references from various books and references, simply by placing the "keywords" about the visible morphological characteristics of the entire plant or one of visible organs as: stems, branches, leaves, flowers, fruits and seeds, etc., within the tables of ArcMap software.

Problematic of research

In fact, although rapid progress in modern technology uses to identify plants directly in the fields such as using smartphones to identify plants, these applications still have many criticisms such as:

- Lack of accuracy and many applications are still based on probability theory.
- Paying money because most of them are not free.
- Specialized in the countries where this technology is made despite the tremendous progress in modern technology.

We in this research are trying to provide a new application that differs from the mechanism of the work of smartphones related to manufacturing intelligence. The application that we accomplished depends on the researcher himself on the one hand, and the software used on the other hand.

Significance and justification the research

In fact, the process of identifying plant species and determining its therapeutic, nutritional and ecological properties is a prerequisite for many disciplines such as pharmacology, agriculture, science, wildlife etc.

In the field of pharmacology for example:

- If a pharmaceutical company indicated that, there is a beneficial, effective compound, and it would like to know what kinds of plants contains it. Through this application, we can find out all the plants that contains this compound very quickly.
- As, if the same company wanted to know where to find those plants, are found in nature, through this application, it is possible to access the locations of dispersed plant within the territory of country, and it can be generalized to include anther regions and countries wider.
- If someone wants to be acquainted with the largest possible numbers of medicinal and aromatic plants in his country, he must obtain this application after completing. We confirm again after completing this application.

Means of research

We used the following means:

- ArcMap is a software developed by Environmental Studies and Research (ESRI) at the National Aeronautics and Space Administration (NASA) in the United States of America. It is a geographic information system (GIS), which deals with maps and satellite and aerial imagery. ArcMap is the former main component of the ArcGIS suite of geospatial data

processing software from *Esri* (https://en.wikipedia.org/wiki/ArcMap). It is primarily used to view, edit, create, and analyze geospatial data. ArcMap allows the user to explore the data within a dataset, symbolize features accordingly, and create maps. This is done through two distinct sections of the program, the table of contents and the data frame. ArcMap users can create and manipulate datasets to include a variety of information. For example, maps produced in ArcMap generally include features such as north arrows, scale bars, titles, legends, stylized lines, and so on. The software package includes a set of styles for these features. In addition, there is the ability to load many other reference styles to apply to any mapping or function.

- A laptop equipped with an automatic charging battery for easy carrying while looking for identifying medicinal and aromatic plants.
- A metric ruler
- A mobile phone with a digital camera, preferably of high accuracy, loaded with the Global Positioning System.
- References about medicinal and aromatic plants.

Steps and method of research

Now, if we are faced with a plant located somewhere, in a garden, a field, a forest, a desert, the banks of a river or the sea, etc., we want to identify it. In this case, we will face two hypotheses:

First, we have a preconceived knowledge about this plant

Since we know the local and scientific name of the plant and its medicinal and therapeutic properties, and we have the desire to automate this plant within the relevant application, so that it is easy for anyone who comes after us to recognize it directly without any effort. In addition, we do not forget to photograph all the visible parts of this plant digitally as much as possible, such as stems, branches, leaves, flowers, fruits, seeds, etc. Then we enter these images into the application. However, the most important condition in this work is that we put "keywords" in simple and easy metaphorical terms for any part of the plant or even the general appearance of the plant, as we will explain later.

7.1. Second, we have no a preconceived knowledge about this plant

Results and discussion

We will discuss the results of the first hypothesis through the following application:

Practical example _1 (the first hypothesis)

We have a preconceived knowledge about the name of the plant and its medicinal and aromatic properties:

During our wandering on 7/4/2021 in the Ecological Garden at the Faculty of Science (Damascus University- Syria), we saw an herbaceous plant, in an advanced stage of growth, called *"Rosmarinus oficinales*". We stood a distance (about 2 meters) from this plant, and noticed the following features:

- **Leaves:** The plant appears to give the viewer more of the underside of the leaves than the upper side. The underside of the leaves also appeared paler than the upper side. The plant cover seemed so dense that we could not see the stems. When we touched the leaves with our fingers, we found that the pale white color of the underside of the leaves was due to the presence of very small white fluff, which gave them this pale color. We smelled our fingers after touching the leaves, and our attention was drawn to the presence of an aromatic smell similar to the smell of camphor (note that previous smart applications that use smart cameras do not capture or smell the smell of plants, and this is the most important feature that distinguishes the application we are dealing with in this research from those smart cameras). The leaves also appear to be seated, opposite, thread-like, with a leathery texture, and downward-curving edges that are 2-3 cm long and 1-2 mm wide. In fact, these external characteristics are the same as those mentioned in the scientific reference [15]. However, it is possible to add an important remark that the sessile leaves always form a very acute angle with the stem to the point that the leaf partially accompanies it and then moves away as we approach the leaf apex, as in Figure 1. At least, we can see this morphological phenomenon before the flowers appear. At this stage of growth, we did not see the flowers because it seems that it was not time for them to appear. Finally, we recorded the most important keywords related to the leaves in the program table (Table 1) in addition to the medicinal and therapeutic properties of the leaves because we have prior knowledge about them.

Table 1- The most important of "key words", effective compounds, and other information about the leaves.

Branches

	Branches	Key_words	Date(photos+Notes)
▶	Rosmarinus oficinales	The branches holding the leav	7/4/2021

- **Branches:** holding the leaves were tender, and after we removed the leaves from them, they looked pale, tending to the same color of the underside of the leaves. After that, we noted the most important keywords related to the branches in the software table (table 2).

- **Stalk:** we could not see it until after removing the upper parts manually due to its density. The stem appeared to be much branched and of varying and small diameters, its color tending to burnt gray covered with numerous

Table 2: Keywords, date of photos and notes about the branches.

Leaves

	Leaf	Key words	Effective Compounds	Preparation Method	Date(photos + notes)
▶	Rosemary leaf	hite color of the underside of the heir is due to the presence of white micro-fluff. The leaf has a sessile needle that n	Rosemary leaves contain vol	Rosemary leaves are used inte	14/4/2021

peels that were easy to fall, and this is evidence of plant aging, because we do not see such scales in young plants. After that, we record the most important keywords related to the stem in the software table (table 3).

Stalk

	Stalk	Key words	Date(Photos+Notes)
▶	Rosmarinus oficinales	The stalk, we could not see it until after removing the upper shoots manual	7/4/2021

Table 3- Keywords, date of photos and notes about the stem.

Finally, we open the software and recorded the following apparent information that we saw about the plant in Table 4 within the software for the whole plant, in addition to the previous information related to the therapeutic, medicinal and aromatic properties that we know. Here, we also added additional information that is very important for those interested in collecting samples of medicinal and aromatic plants, which is the location and spread of this plant. This was on by determining the address of the location of this plant through satellite images, including the spatial coordinates, by means of a GPS device (table 5).

Table 4 - Information about the location and coordinates of plant.

Location (Rosmarinus oficinales)

	Location_1	GPS
▶	Rosemary (Rosmarinus oficinales) - Location_1 - East of the canteen of the Faculty of Architecture - Da	【33】 ^0 【30】 ^' 【39.1】 ^" N, 【36】 ^0 【16】 ^' 【53.1】 ^" E

We also adopted reliable scientific reference about this plant (Rosmarinus oficinales), whether university books or from research published in international refereed journals as [16], and other references within the software tables (table 5), to note general information as, taxonomic properties, effective compounds, medicals benefits, damages, preparation methods, location, scientific references, etc.

Table 5 - Information about taxonomic, therapeutic properties, location, etc., for *"Rosmarinus oficinales"*.

General Information

	Local Name	Scientific Name	Family	Genus	Order	Class	Division	Kingdom	General Description	Effective Compound	Medicinal Benefits	Use Damages	Preparation Metho	Location	GPS	Date(Photos+N	Scientific Reference
▶	Rosemary	Rosmarinus offcin	Lamiace	Rosmari	Lamiales	Angiop	Mangolioph	Plant	A herbaceous plant of t	It contains a volatile oil,	It is used medicinally b	A small amount of it	"It can be used as a ri	Damascus -	【33】	14/4/2021	Calabrese, V., Scapag

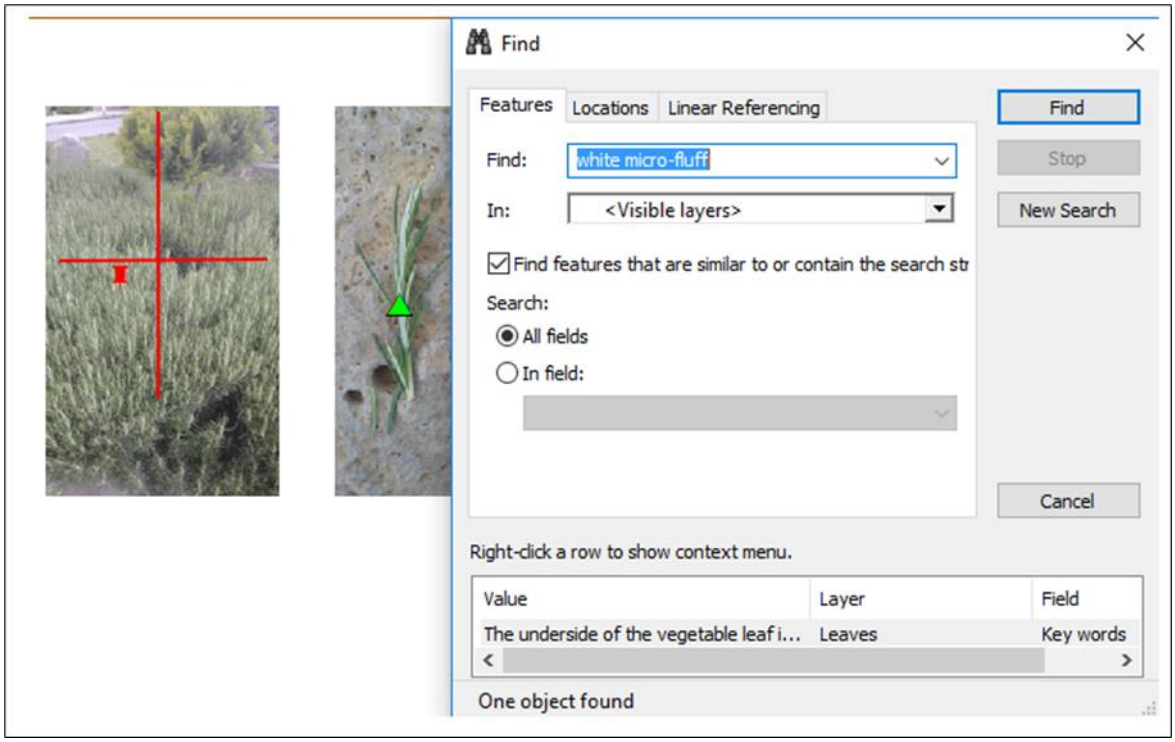

Now, someone somewhere, interested in medicinal and aromatic plants, saw this plant somewhere, and wants to know about this plant, what should he do? Firstly, he should have a laptop with this application installed, moreover, all the information, especially the "keywords" about this plant, should be archived in the application previously. The application opens to the main page of the Medicinal Plants Project. Inside the next search icon, as in Figure 1, he writes any noticeable note that caught his attention about any member of this plant, for example: he writes "white fluff" as "keyword". Immediately, two vertical and crossed arrows will appear above the plant with this property. By clicking on this intersection point, the name of the plant will appear with the scientific name, all its taxonomic characteristics, medicinal and aromatic properties, and even its location in nature with its spatial coordinates. If this person thinks that this plant is "rosemary" and wants to make sure of that without the need to put keywords, he can write the scientific name of this plant inside the previous search icon. The plant will appear directly to him as an image, and the intersecting arrows will point to it in the same way. Within

Fig. 1- Tool for identifying the location of Rosemary on a satellite image (Landsat, r: 30 m, 2021) (A), and an accurate image from Google Earth in high resolution (Bing, r: 0.5 m, 2021), (B).

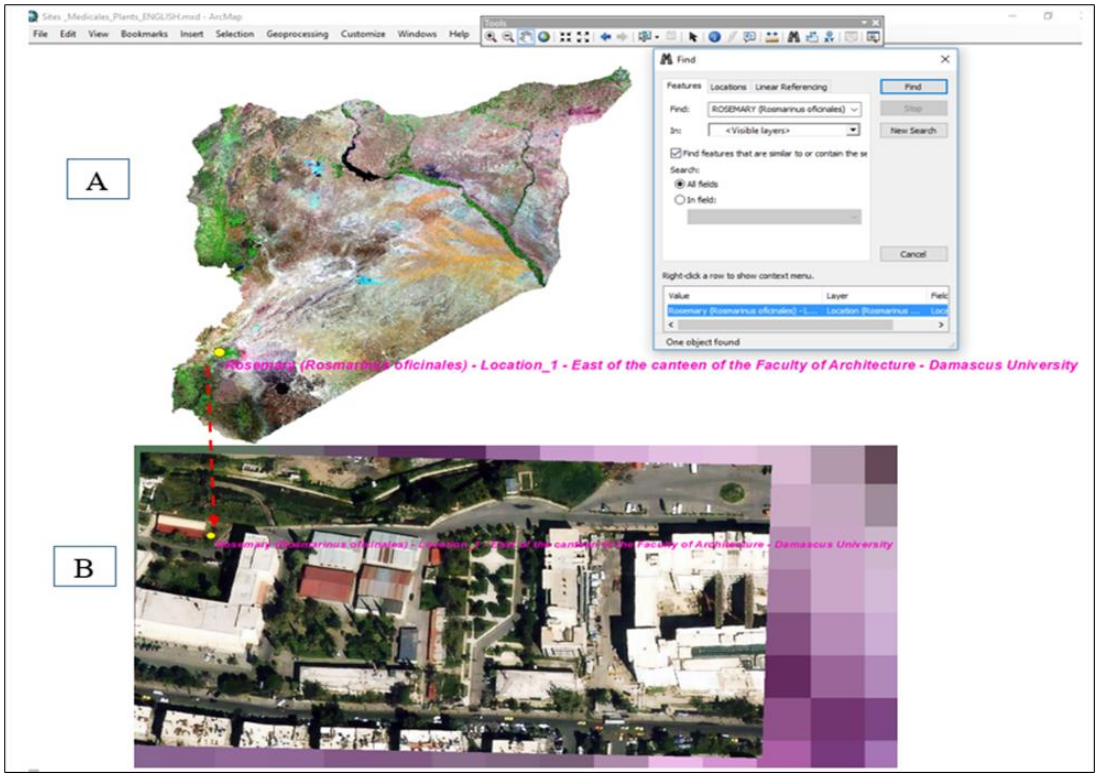

electronic tables, the application will display all the images related to this plant in addition to tables of its various medicinal and aromatic properties.

The same person wanted to tell a friend about a place, looking for the location of this plant, he can send him the address without asking anyone else, he just has to go to the second part of this search and open the next page as in Figure 2 within the application and type the keyword "rosemary", (Figure: 2) two crossed arrows will appear indicating the geographical location of the plant, and he will get the following result with the most accurate details about the address of the plant's location with the help of satellite images (from Google Earth), which we have archived within the program. However, the questioner may ask us, maybe there is another plant other than “Rosemary”, or that many plants have "microscopic white fluff" on the underside of the leaf! The answer is yes, and this exists in nature, there are many plants that have this property, but we will not limit ourselves to this property only, but we will add the length and width of the leaf, for example. Do all plants within different species have the same length and width of leaves? In fact, after the application is completed and all the information is collected on as many plants as possible, of course, just typing “fine white fuzz” as a “keyword” will give us all the plants that have fine white fuzz on the underside of the leaf, and we can see it visually through the digital images archived within the program. However, we can reach the intended plant simply by adding another characteristic of the leaf within the same previous “keyword”, such as leaf length and width. Let us say there is

another plant, or several other species that have the same leaf length and width, and then we move on to another keyword for another characteristic we recorded, such as “leaves have an aromatic smell”. If not, we move on to another organ such as the stem, flowers or fruits, so there must be a real difference because science says, especially genetics with regard to plants and any living organism, that no two plants are exactly alike, even if they are of the same species, genus, order, class and section [10]. On the contrary, we find that this application, once completed, will help researchers and those interested in knowing the extent of the relationship between plant species that share the same "keywords" and thus the same external and sensory characteristics. However, the questioner may ask us, using the search tool; we can search for any keyword within any other computer such as *Excel* and *Word* programs, and easily access the information looking for! To answer such a question: Yes, but the *Excel* and *Word* program interfaces are not sufficient to accommodate millions of digital images of plants, and do not contain pre-programmed digital tables to record the required information. In addition, their dynamism does not suit the input materials, i.e. images or satellite images, as they are office or statistical software. Moreover, we cannot link plants to their geographical locations spatially on maps or satellite images.

The benefits and advantages of this application

It does not need the Internet to work. The most important thing that distinguishes this application from the application of artificial intelligence is that we can reach to identify of the name of the plant by simply using “*keywords*” for apparent formal characteristics related to the appearance of the plant in general, or any organ. If, we are not successful to identify the plant from key words related to the flower, we may use another keyword for the leaf for example, and so in the end we will definitely come to know the name of the plant.

This is better than the imaging adopted in artificial intelligence applications because digital imaging requires many conditions. The process can succeed and may not succeed, and it can give several possibilities, i.e. several images of several different plants, and so on. Even if the plant name is given directly without any other possibilities, this needs to be checked and referred to the references to make sure of that as long as there is no application that gives a 100% match. In other words, doubt is always present and the possibility of error is possible and always present. We also emphasize that, the keywords will not be complicated, but rather they are expressed in common linguistic terms close to the mind. So that the cultural heritage in naming plants in many countries took its name from distinctive outward features, and the examples are many. There is also a very great possibility to unify these terms in order to be universal as long as they express the characteristics of a clear formal phenomenon related to plants to the eyes of any person present in any area and in any country of the world.

Notes: Of course, this application requires sufficient time due to the need for accuracy in obtaining information to reach the desired results. It is required for those who want to use this application to be familiar with some linguistic terms about the phenotype of the different

organs of the plant when entering keywords to search for the name of the plant if they do not know it beforehand. Finally, through the following diagram (1), we can summarize the method of automating the previous medicinal plant or any medicinal or aromatic plant in general, whether we encounter it in nature (in agricultural fields or in forests) or even if we encounter a picture of it on different pages and sites on the Internet. To access the medicinal or aromatic properties, it is sufficient to put either the scientific name of the plant, if we have a preconceived knowledge of the name of this plant, and if we do not have prior knowledge, it is sufficient to enter any distinctive characteristic that distinguishes this plant, such as keywords, until we reach its scientific name and then know its various characteristics through the tables and views that make up the software in addition to the places where it is spread in nature after entering different satellite images into the program files. At the end of the automation process, we get an electronic extension (*.mxd*) with a name such as (*Sites_Medicales_Plants.mxd*) which is the name of the project through which we save all the automation steps and all the information entered into it. The fun thing about this program is that we can modify, add and delete information whenever we want.

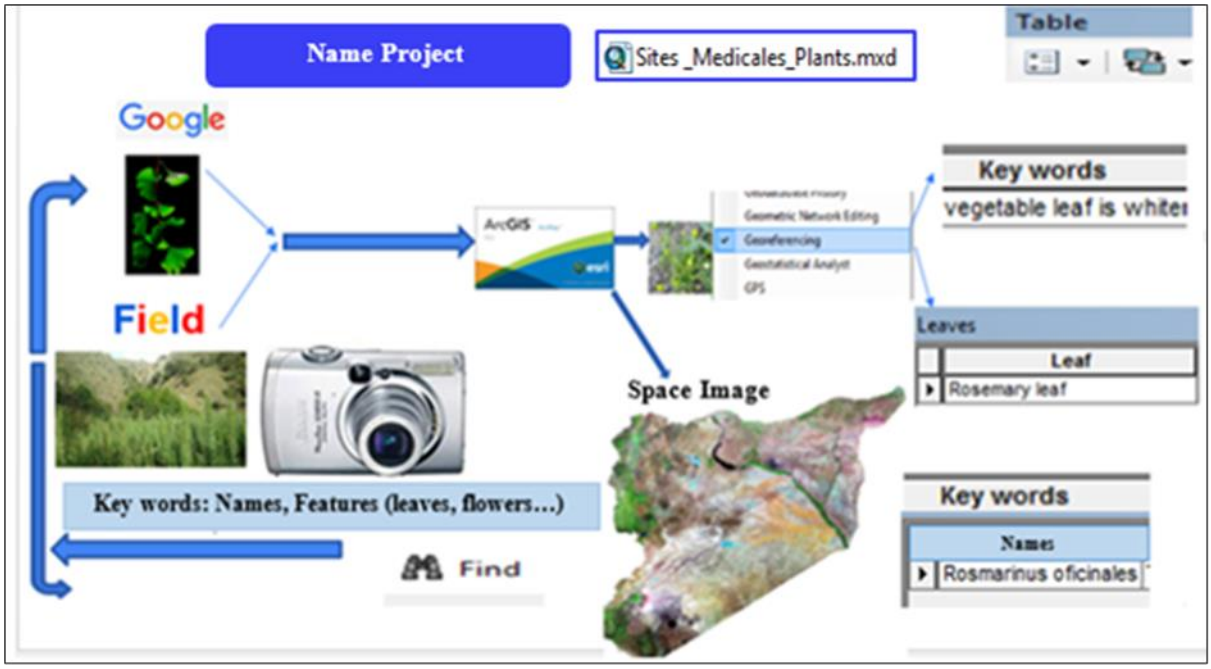

Schema 1 - Steps of automated medical and aromatic plants using GIS (ArcMap) (with a preconceived knowledge).

Conclusion and recommendations

Based on the many benefits mentioned above, we can say that this application is an effective means that supports modern means that rely on artificial intelligence using photographs. This application is characterized by being free and does not require an internet connection. This application does not accept many possibilities to reach the target plant, as we have noticed in other artificial intelligence applications that rely on digital cameras. The interesting thing

is that this application can be modified, added or deleted any information at any time we want, in addition to the spatial linking of plant locations in their natural distribution sites and locations. The use of keywords in this application increases our knowledge of the extent of kinship and similarity between plants in these characteristics, which will increase the knowledge stock to distinguish between the many and varied plants. Even the issue of repeating the same keywords for a member of the plant will certainly not be repeated for the rest of the members due to the innate and genetic nature of plants. In order for this application to be available and practically effective in our daily lives, it requires recording all medicinal and aromatic plants in a region or country, and this requires moving around and taking information about plants throughout the seasons because plants are in a state of gradual development, whether for annual or seasonal plants or even evergreens. We recommend through this research to continue recording any information about any plant that we may encounter in our daily lives or that we know in advance and know where it is spread because our ignorance and lack of knowledge of the benefits of many plants may eventually lead to their extinction, especially in sensitive areas that witness fires, uprooting and environmental degradation. Developing this application on a local or global level requires that this topic be adopted by one of the scientific institutions, similar to similar projects in other countries that seek to protect medicinal and aromatic plants in particular and biodiversity by identifying their medicinal and aromatic value in general and thus protecting them from deterioration and extinction.

References

[1] Mora C, Tittensor DP, Adl S, Simpson AG, Worm B. How many species are there on Earth and in the ocean? PLoS biology. 2011;9:e1001127.

[2] Christenhusz MJ, Byng JW. The number of known plants species in the world and its annual increase. Phytotaxa. 2016;261:201–17-–17.

[3] Joppa LN, Roberts DL, Pimm SL. How many species of flowering plants are there? Proceedings of the Royal Society B: Biological Sciences. 2011;278:554-9.

[4] Brinckmann JA, Kathe W, Berkhoudt K, Harter DE, Schippmann U. A new global estimation of medicinal and aromatic plant species in commercial cultivation and their conservation status. Economic Botany. 2022;76:319-33.

[5] Al-Ghazal SK. The valuable contributions of Al-Razi (Rhazes) in the history of pharmacy during the middle ages. JISHIM. 2003;2:9-11.

[6] Levey M. Early Arabic pharmacology: an introduction based on ancient and medieval sources: Brill Archive; 1973.

[7] Reddy S. University Botany III:(Plant Taxonomy, Plant Embroyology, Plant Physiology): New Age International; 2007.

[8] Babujian G, Al-Gadi I. Basic of Botanical Classification: Damascus Uuniversity; 2010 (in Arabic).

[9] Rzanny M, Mäder P, Deggelmann A, Chen M, Wäldchen J. Flowers, leaves or both? How to obtain suitable images for automated plant identification. Plant methods. 2019;15:1-11.
[10] Maxted N, Hunter D, Ríos RO. Plant genetic conservation: Cambridge University Press; 2020.
[11] Veitch NC, Elliott PC, Kite GC, Lewis GP. Flavonoid glycosides of the black locust tree, Robinia pseudoacacia (Leguminosae). Phytochemistry. 2010;71:479-86.
[12] Wäldchen J, Mäder P. Plant species identification using computer vision techniques: A systematic literature review, in archives of computational methods in engineering. ISSN: 1134-3060 (Print) 1886-1784. 2017.
[13] Seeland M, Rzanny M, Alaqraa N, Thuille A, Boho D, Wäldchen J, et al. Description of flower colors for image based plant species classification. 2016.
[14] Kumar N, Belhumeur PN, Biswas A, Jacobs DW, Kress WJ, Lopez IC, et al. Leafsnap: A computer vision system for automatic plant species identification. Computer Vision–ECCV 2012: 12th European Conference on Computer Vision, Florence, Italy, October 7-13, 2012, Proceedings, Part II 12: Springer; 2012. p. 502-16.
[15] Shihab H, Al-Nouri AS, Hawassli H. Pharmaacology (2) practical part: Damascus University; 1997 (in Arabic).
[16] Calabrese V, Scapagnini G, Catalano C, Dinotta F, Geraci D, Morganti P. Biochemical studies of a natural antioxidant isolated from rosemary and its application in cosmetic dermatology. International journal of tissue reactions. 2000;22:5-13.
https://en.wikipedia.org/wiki/ArcMap)
(https://images.google.com)
(https://lens.google.com)

Computerized Numerical Modeling Using Computational Fluid Dynamics Methodology to Study Inclined Plates in a Sedimentation Basin for Water Treatment

Dr. Tasnim Mkresh
University of Aleppo
tsnimmkresh@gmail.com

المؤتمر العلمي الدولي الرابع عشر
لجمعية الرياضيات العراقية والمنعقد تحت شعار
الإبداع يلتقي بالتحديات من اجل التقدم العلمي والتكنولوجي
للمدة 4 - 5 اب 2024
دمشق - سورية

Abstract

with the development of computer technologies and software, we have turned to numerical modeling programs in all fields, such as structural, thermal, fluid flow, electrical, and mechanical fields, in addition to other fields. In order to achieve optimal benefit and design with regard to economic feasibility and effectiveness, reliance has been placed on the Finite Element Method (FEM)and methodology Computational Fluid Dynamics(CFD) is the science of predicting the flow of fluids and comparing analytical results with laboratory results. These programs are distinguished by their high ability to solve the problem regardless of the number of variables and the ability to conduct the optimal design process. Thus, through it, laboratory experiments can be replaced, which leads to reducing the material cost of laboratory experiments. To reach the best design and operational condition in the fastest time, least effort, lowest cost, and most variables, in this research a series of experiments were conducted to compare the sedimentation efficiency in the presence of inclined plates with the efficiency of the traditional precipitator, laboratory-based and modeled using the ANSYS FLUENT program. It was concluded that the sedimentation efficiency by providing the basin with inclined plates leads to due to the decrease in the area of land occupied by traditional sedimentation basins by 10 times, with a water residence time of 15 minutes, an angle of inclination of the plate of 55° with the horizon, and a decrease in water turbidity to 14 NTU, which is a value consistent with the national standards for discharging treated water into the open aquatic environment, this would save the area of land allocated for basins. Sedimentation, time and cost of treatment.

Keywords: Numerical Modeling, Computational fluid dynamics, Finite Element Method, ANSYS FLUENT Program, Inclined Plates.

1.Introduction to numerical analysis

The principle of numerical analysis lies in creating, analyzing, and implementing a set of algorithms to arrive at numerical solutions to mathematical problems in various branches of mathematical sciences, medicine, and engineering. As a result of the development of digital computers, there has become an urgent need to analyze mathematical models in science and engineering in order to solve the complexities present in them. A system was adopted that combines numerical analysis, computer graphics, and symbolic mathematical calculations, in order to facilitate the creation, solution, and interpretation of mathematical models. Numerical analysis studies all aspects of the problem in numerical terms. This was achieved by understanding numerical methods and implementing them in the form of computerized programs that are distinguished by their reliability and effectiveness [1].

1.1. Mathematical methods for numerical analysis

- The first method: In the event of facing a difficult problem that cannot be solved directly, this problem can be replaced with another close one that can be solved quickly and

easily. An example of this method is the use of interpolation in developing digital merging methods and root exploration methods.

- The second method: using linear algebra and real and functional analysis.
- The third method: It depends on understanding the nature of the error and the problem before approximating it. This contributes to establishing extrapolation processes to improve the level of the convergence method for the numerical method.
- The fourth method: It depends on the use of a polynomial, which is an algebraic expression of a certain degree that contains a group of numbers and variables coordinated according to a specific pattern, and it generally belongs to the group of real numbers [2].

2. A theoretical overview of fluid dynamics

Fluid motion science is concerned with studying the relationship between space and time of moving fluids. The Lagrangian method for describing the flow of a fluid in kinetic terms depends on defining the velocity vector at every moment and at every position in the flow field. From a kinematic perspective, it is also necessary to know the value of the local pressure at every point and for all moments, even if friction is neglected.

In the Lagrangian method, the coordinates of the particle A (x, y, z) at any instant of time t are expressed as a function of its initial coordinates (a, b, c) at instant t_0, and it can be written as a function of a, b, c,t We express it as velocity components The molecule with the following equation (1)

$$\frac{dx}{dt} \quad \frac{dy}{dt} \quad \frac{dz}{dt} \qquad (1)$$

We express the components of acceleration in equation (2) Considering that (a, b, c) are constant

$$\frac{d^2x}{dt^2} \quad \frac{d^2y}{dt^2} \quad \frac{d^2z}{dt^2} \qquad (2)$$

As a result of the presence of the phenomenon of diffusion in the flow of fluids, it is difficult to determine the movement of individual molecules in the flow field over time. Therefore, in order to describe the movement of the fluid, it is appropriate to know the transformations of the flow characteristics with time, such as the speed and pressure of a molecule or group of molecules (a specific mass of fluid) at a point. A certain flow field. This method of describing fluid movement is called Euler's method.

In other words, it can be said that the Lagrange method looks at the transformations of the properties of a specific mass of fluid with time, while the Euler method looks at the transformations of the properties of flow with time at a specific point in the flow field and not with respect to a specific mass of the fluid.

Flow velocity is considered the most important property that must be determined at any point in the flow field. It is known that the velocity vector at any point in the flow field is a function of the spatial interval and time, we can decompose the velocity vector into components u, v, w with respect to the coordinates x, y, z, respectively. Thus, we can define

the velocity vector in vacuum at any instant t.
u = f1 (x,y,z,t) ,v = f2 (x,y,z,t), w = f3 (x,y,z,t)
The geometric location of the positions of the molecule as it moves from one place to another, i.e. the curve that the molecule draws during its movement within the fluid is known as the path, and the curve that touches the velocity ray at any point in the flow field is known as the stream line [3].

3. Steps of numerical modeling using the Computational Fluid Dynamics methodology

3.1. Building a mathematical model which is a set of mathematical relationships that achieve the physical properties of a particular system that we want to simulate using the CFD methodology. This set of mathematical relationships is called the term Solvers, which determine the physical properties of an issue, and the term Boundary Conditions to understand the mathematical model system and the surrounding conditions (such as the type of fluid: compressible / incompressible) and (the type of flow: turbulent or laminar).

3.2. The process of converting a mathematical model into a language or form that a computer can understand and work on. The Discretization Method, that is, converting differential equations into a set of algebraic equations that the computer can calculate using specific algebraic operations. To accomplish this step, there are several methods, including

- Finite Difference Method (FDM): It is a mathematical method for converting differential equations into finite differences at the center of the cell to obtain a series of equations for the values of the variable at points in space or time.
- Finite Volume Method (FVM): The basic idea of the finite volume method is to divide the integral shape into many control volumes that cover the area of interest. The shape of the control volume depends on the nature of the geometric shape of the studied problem.
- Finite Element Method (FEM): This method is considered relatively modern and has crystallized in the field of structural engineering and has been circulated to many other fields until it has become the most important method for numerical analysis using computers in all physical and mathematical applications. It is considered one of the most important methods through which we can transform mathematical equations that describe a specific physical state and are subject to terminal conditions. The appropriate elementary equations are divided into a set of algebraic equations that the computer can calculate and understand. This method divides the model into a mesh/grid that connects a group of points, and we obtain the solution at each point of the grid [4].

3.3. Analyze the Numerical Scheme a term to verify the validity of the method used to convert a mathematical model to a numerical one in order to fulfill the following conditions (Consistency, Stability, Convergence , Accuracy).

3.4. Solve the computer takes this step after determining all the terminal conditions, and the solution method is determined by the student (permanent flow or variable with time).

3.5. Post – Processing show the solution results in different ways with contour colors, arrows, or lines, depending on the design goal.

4. Navier-Stokes method in studying fluid flow

The principle of conservation of mass: that is, mass is constant with respect to time, considering M as the mass of the fluid, the equation is (3)

$$\frac{\partial}{\partial t} M = 0 \qquad (3)$$

equation (4) represents the change in mass within the studied space, where the mass of the liquid equals the density multiplied by the volume, where (c.v) is the abbreviation for control volume and represents a small volume in a CFD simulation

$$\frac{\partial}{\partial t}\int_{C.V} \rho . dV = 0 \qquad (4)$$

equation (5) expresses mass flow across control surfaces, where n is the normal radius, A: area, and

V: volume

$$\frac{\partial}{\partial t}\int_{C.s} \rho . dV . n . dA = 0 \qquad (5)$$

To achieve the mass conservation relationship, the equation (6) must be met

$$\frac{\partial}{\partial t}\int_{C.V} \rho . dv + \frac{\partial}{\partial t}\int_{C.s} \rho . dv . n . dA = 0 \qquad (6)$$

That is, the flow of mass across the specified surfaces, in addition to the change in mass that occurs within a certain volume, must equal zero.

The integration process represents the collection of all simulation space and all simulation surfaces so that we can represent all shapes and fluids within this simulation. When divided into mesh or grid, we have small cubes with three axes in the x, y, z direction.

equation (7) based on the law of momentum: force = speed × mass

$$\frac{\partial}{\partial t}\int_{sys} v . dm = F \qquad (7)$$

equation (8) expresses the sum of the moments applied to the body = the sum of the flow of moments + the sum of the moments

$$\sum F_{C.V} = \frac{\partial}{\partial t}\int_{C.V} V . \rho . dV + \frac{\partial}{\partial t}\int_{C.s} V . \rho . dV . n . dA \qquad (8)$$

equation (9) by substitution, we have three equations of motion and one equation of continuity, four equations with unknowns u, v, w (velocity components on the x, y, z axes)

$$\frac{du}{dx} + \frac{dv}{dy} + \frac{dw}{dz} = 0 \qquad (9)$$

We have unknown values for the stresses on all surfaces and in all directions, so we will adopt the Navier-Stokes equations, considering that the fluid that we will study is water, as it is incompressible, meaning the density is constant, we note that as a result of the difficulty of using traditional methods in solving the deduced differential equations, we resorted to the digital solution using the CFD method. Thus, it is possible to replace conducting very expensive practical laboratory experiments, so we design many experiments with less time and effort [5].

5. Analysis using Ansys Fluent software

The ANSYS program initially appeared as a program specialized in solving problems and engineering applications in computational fluid dynamics using the finite element method. It is a program used to simulate these problems and stabilize their results using the computer. The program contains analytical tools for pre-processing of engineering problems, solving these problems, and processing them to produce the results in the most appropriate manner with practical reality.

The program's tools are most often used in its analysis: numerical analysis of finite element problems that are difficult to solve using traditional methods, whether for dynamic, static, linear or non-linear analysis, fluid flow problems (air and water) and heat transfer, as well as problems of structural, mechanical, electrical and medical applications.

The program can be handled in several ways:

- Reciprocal interaction method: This method is called reciprocal interaction between the user and the program.
- The programming method: In this method, the program is dealt with by giving commands to the program by writing them on an input file or by entering them in text form in the input window, so that these commands are written using the variable-based design language.
- The binary method: In this method, the two previous methods are combined, as data can be entered using the second method and the results can be viewed using the first method [6].

6. Stages of modeling a sedimentation basin using the ANSYS FLUENT program using the CFD methodology

(Figure 1) shows the main interface of the ANSYS FLUENT program and the stages followed to reach the results

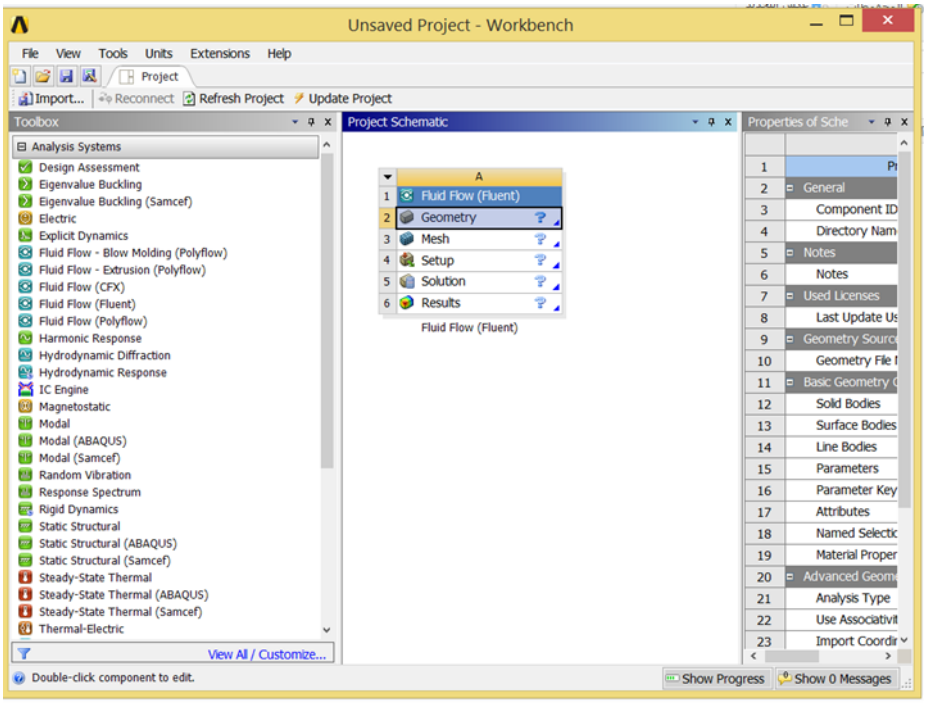

Fig. 1- FLUID FLOW (Fluent) interface

6.1. Geometry: In which the engineering model is drawn and designed with the dimensions studied, which is a basin with a length of 25 m and a width of 6 m. The distance of the exit weir from the entrance is 19 m and the height of the basin is 3 m. All inputs related to the issue are defined, such as taking Earth's gravity into consideration, determining the component parts of the model and determining the system of units used SI (kg, m, s, k, A, N, V) as shown in (Figure 2).

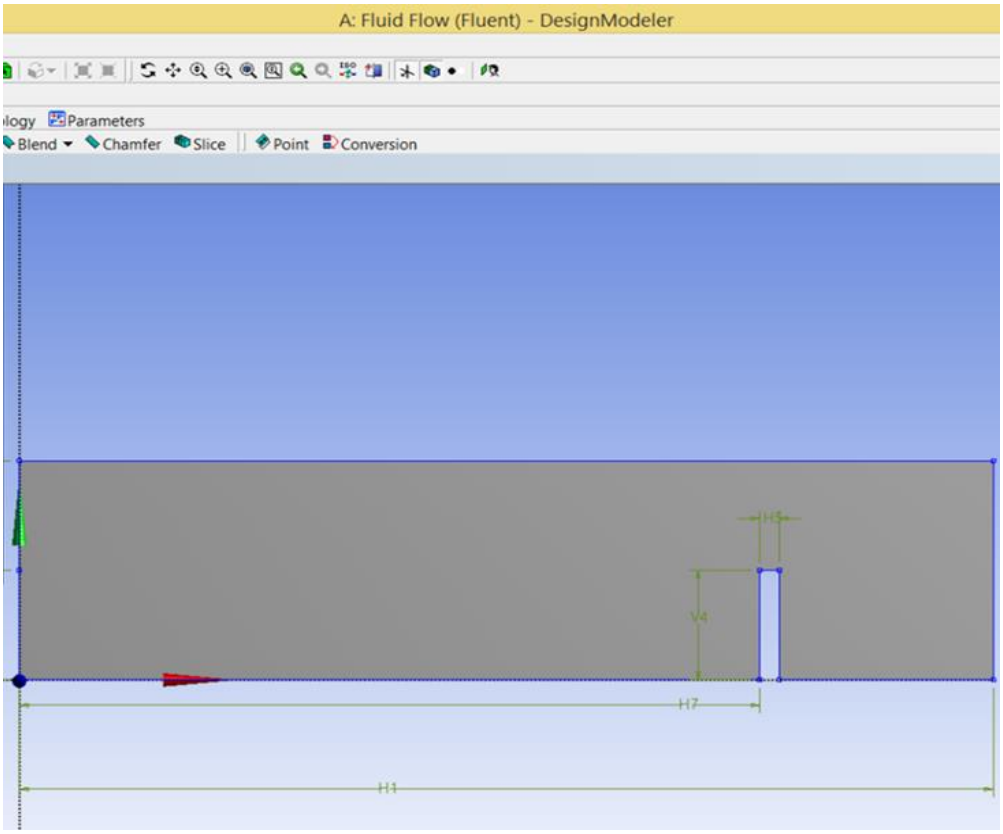

Fig. 2 -Geometry stage in sedimentation basin modeling

6.2. Dividing the Meshing model: in which the entry area (Figure 3) is named and identified, and the barriers are divided and the field is divided into points. Each point is represented by an algebraic equation that is solved at the designated point according to the type of mesh (either a fine or rough mesh). When the size of the elements is fine, the model requires a large number of calculations, thus increasing the solution time and the space needed for the computer processor. When the desired results of the experiment are of high importance, it is preferable to divide the elements precisely (fine), but when the accuracy of the results is not very important, it is preferable to choose a medium size of divisions to reduce the calculations in the analysis stage (solution). In modeling, we have relied on the type of square grid. The shape is smooth and the number of nodes = 15189 nodes and elements = 14848 (Figure 4).

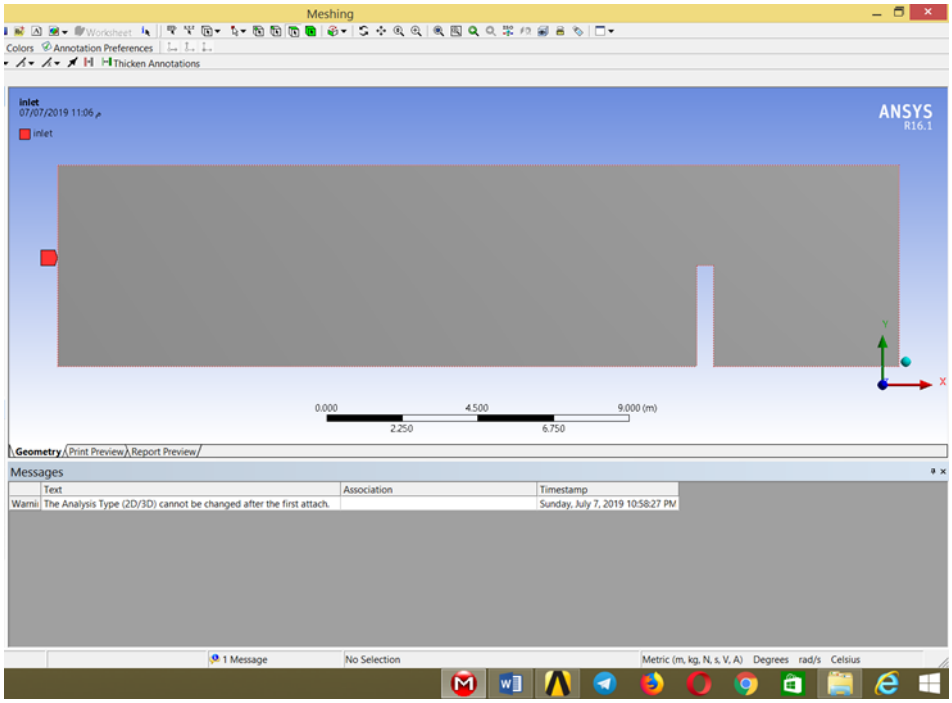

Fig. 3- Determine the inlet of the basin in the Mesh stage

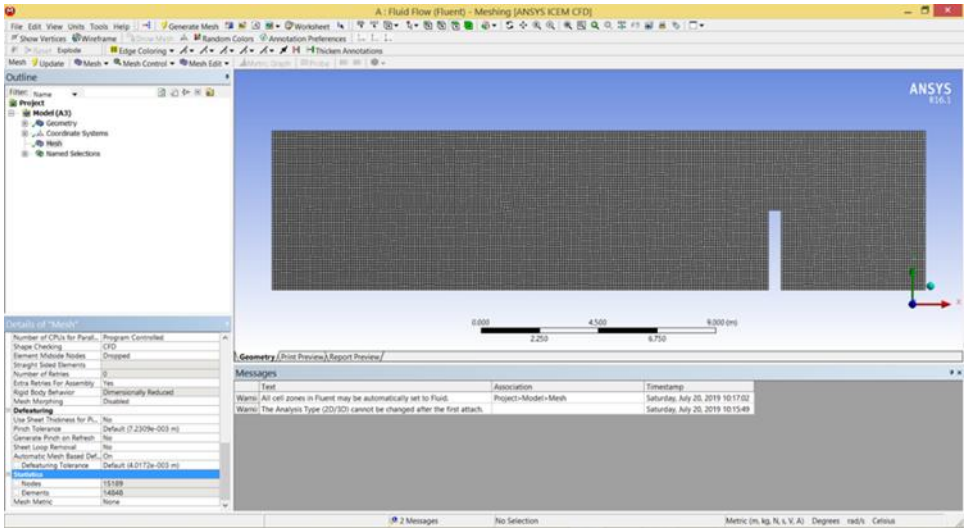

Fig. 4- Determine the mesh type (square) and (smooth) in the Mesh stage

6.3. setup: It is considered the most important stage because it determines the materials that make up the model, from which we determine the type from solid to fluid. (Figure 5) also shows how to define the properties of the material from the material list, where the properties

of the materials included in the experiment were downloaded from the fluent database. We chose water-liquid and carbonate. Calcium used as a suspending material.

Definition of the oceanic and initial conditions (velocity 0.3 m/sec, temperature 20ºC, pressure at the water surface 0 pascal, intensity of turbulence and viscosity, where the flow is laminar, Reynolds number Re < 2000, and determining the type of exit weir, which is thin-edged).

At this stage, the equations governing flow and heat transfer are converted into a system of algebraic equations for one of the numerical analysis methods, and the finite element method was used.

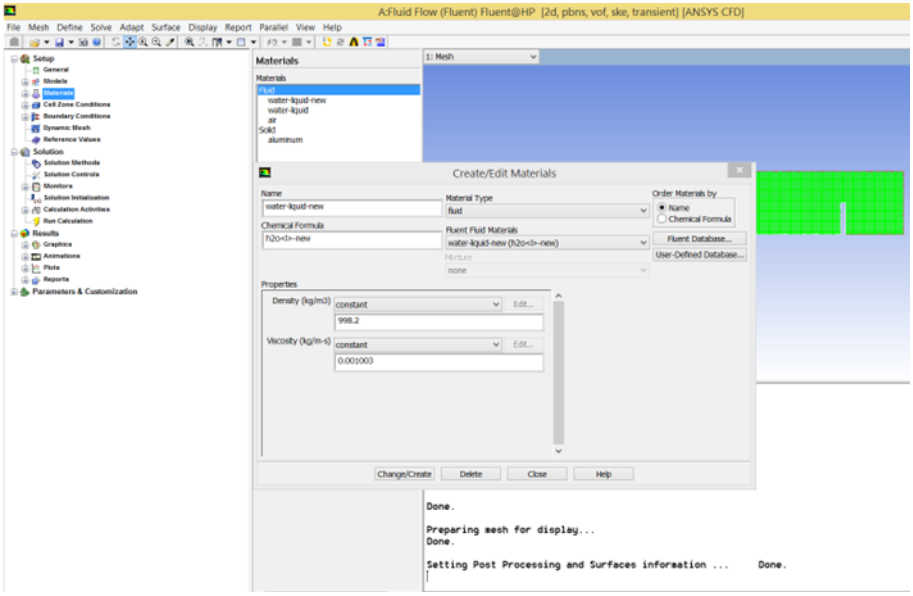

Fig. 5- Determine the type of materials used and parameter values during the setup stage

6.4. The solution stage: is where the solution is completed by successive approximation after determining the number of approximation steps necessary to perform the solution, where the processor stops when reaching it, as shown in (Figure 6), where the number of attempts (Iteration) is entered from the number of time steps field and we press the calculate button and the number of times the solution is shown. With the amount of error in a chart, and with each iteration, values are calculated for the properties of the fluid at each point and know whether the solution is the expected result or not. The percentage of error is determined between each iteration and the next, and reaching this percentage is the sign of reaching the expected solution, and this is what is known as the convergence of the solution.

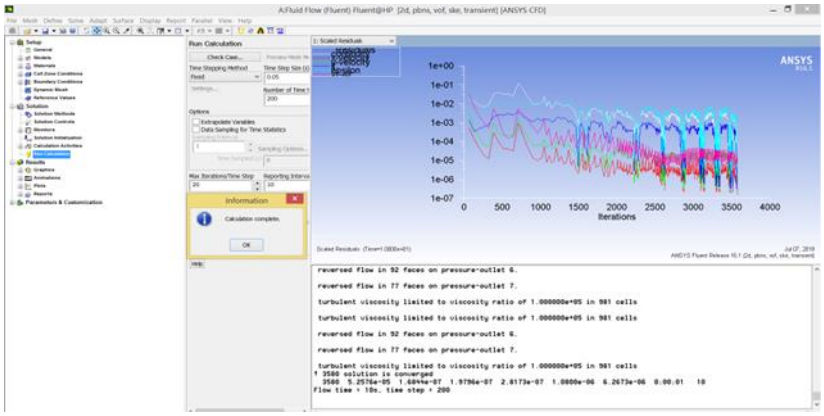

Fig. 6- Finish the number of successive approximation steps specified in the solution phase

6.5. Results stage: After completing the solution, the results can be displayed and analyzed interactively in several different forms (contour drawings, charts, graphs, arrows), and the colors can be controlled. The program is also equipped with a special window for displaying the results, which is CFD-Post.

7. Inclined plate sedimentation

Lamella inclined plate clarifier is composed of multiple sets of inclined plates. The inclined plate sedimentation tank is a kind of solid-liquid separation equipment commonly used in the sewage treatment process. It is characterized by high treatment capacity and stable operation, but it can achieve a small footprint. The inclined plate sedimentation tank uses the principle of "shallow sedimentation" to shorten the sedimentation distance of particles, thereby shortening the sedimentation time, and increasing the sedimentation area, thereby improving the treatment efficiency and greatly improving the burial capacity of the sedimentation tank. The processing capacity of the sedimentation tank is seven to ten times higher. [7]

As (Figure 7) shows, the suspended solids to be disposed of are deposited on the bottom face of the plate.

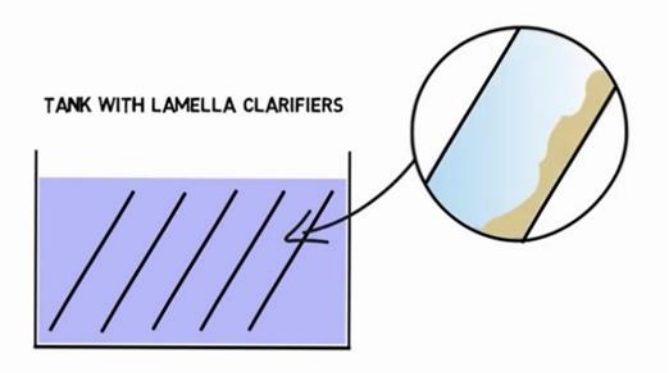

Fig. 7- Providing the sedimentation basin with inclined plates

(Figure 8) shows laboratory work by supplying glass sedimentation basins with inclined glass plates at an angle of 55 degrees with the horizon in the hydraulics laboratory of the Faculty of Civil Engineering at the University of Aleppo.

Fig. 8 - Preparing and supplying laboratory inclined plates

Samples were also drawn to measure turbidity with a spectrophotometer. The initial turbidity value of the raw water before treatment = 400 NTU, and after the end of the water's residence time in the sedimentation basin equipped with inclined plates, it reached 14 NTU, meaning the turbidity removal efficiency reached 96.5%, while the efficiency was 70% in the case of Conventional sedimentation basin without plate supply.

(Figure 9) shows the modeled results with contours, where the red color reflects the maximum values of distributed turbidity, and the blue color reflects the minimum values of turbidity distributed between two parallel plates inclined at 55 degrees to the horizon.

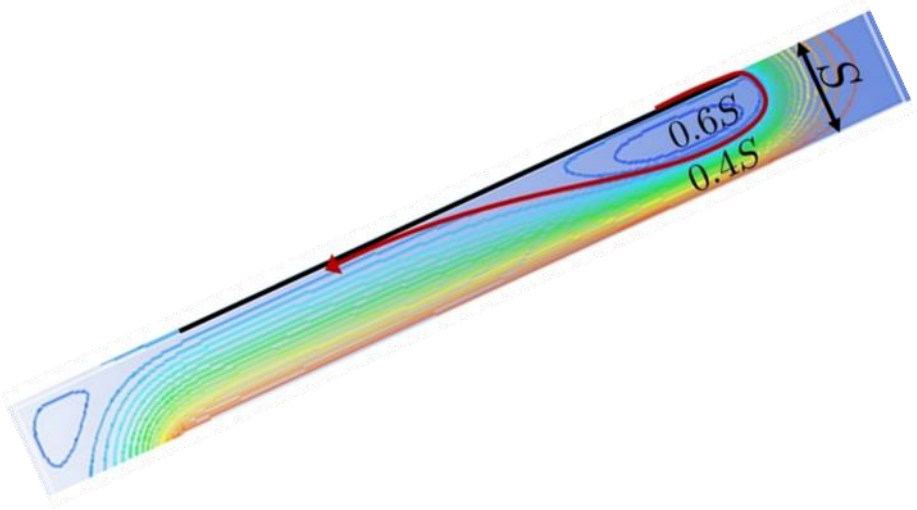

Fig. 9 - shows typical results for turbidity distributed between two parallel plates inclined at 55º to the horizon

8. Discussion of results

The results were presented and analyzed laboratory and model using the CFD methodology using the finite element method for flow in a sedimentation basin equipped with inclined plates with specific dimensions and initial and circumferential conditions. (Table 1) shows the efficiency of turbidity removal as a percentage with laboratory work and comparing it with the efficiency of turbidity removal with software work according to the change in the angle of inclination of the plates with the horizon.

Table 1 - Laboratory and computer turbidity efficiency by changing the degree of inclination of the plate

Angle of inclined plates (º)	Laboratory turbidity (NTU)	computationally turbidity (NTU)
40	17	17.5
45	15	16
55	13.5	14
60	14.5	15

9. conclusions

Compatibility with laboratory and model values has been reached, as the sedimentation efficiency by providing the basin with inclined plates leads to a 10-fold reduction in the area of land occupied by traditional sedimentation basins, with a water residence time of 15 minutes, for an optimum inclination angle of the plate with the horizon of 55°, and a lower The turbidity of the water reached 14 NTU after its value in untreated water was 400 NTU. Thus, the costs of laboratory experiments were reduced by relying on numerical modeling, which is the product of mathematical equations and integrations included in modern computer programs.

References

[1] Groetsch, C. W., & Nashed, M. Z. (2006). Kendall Eugene Atkinson: An Appreciation.

[2] Abramowitz, M., & Stegun, I. A. (2021). Numerical Differentiation.

[3] Wesseling, P. (2001). Elements of computational fluid dynamics. Lecture Notes WI, 4011.

[4] Hirsch, C. (2007). Numerical computation of internal and external flows: The fundamentals of computational fluid dynamics. Elsevier.

[5] Bhatti, M. M., Marin, M., Zeeshan, A., & Abdelsalam, S. I. (2020). Recent trends in computational fluid dynamics. Frontiers in Physics, 8, 593111.

[6] Matsson, J. E. (2023). An introduction to ansys fluent 2023. Sdc Publications.

[7] Dao, N. T. M., Liu, B., Terashima, M., & Yasui, H. (2019). Computational fluid dynamics study on attainable flow rate in a lamella settler by increasing inclined plates. Journal of water and environment technology, 17(2), 76-88.

المؤتمر العلمي الدولي الرابع عشر
لجمعية الرياضيات العراقية والمنعقد تحت شعار
الإبداع يلتقي بالتحديات من اجل التقدم العلمي والتكنولوجي
للمدة 4 - 5 اب 2024
دمشق - سورية

Exploring The Engagement of Students with Artificial Intelligence Shock : A Case Study At Junior High School In Jakarta,Indonesia

Maram Taher, Dr. Rini Triastuti, Dr.Mohammad Muchtarom

Sebelas Maret University

maramtaher731@gmail.com

Abstract

This study investigates the application of an e-learning platform that supports artificial ,intelligence and STEM technology, while clarifying the role of teachers, parental interest and learning motivation in students' achievement in civic education in a junior high school in Jakarta, Indonesia. A proportional random selection was used to generate a sample of 50 ,students at SMP Jakarta. The research instrument used was in the form of a questionnaire interviews, and observations.The results of this research show that students at SMP are able 'to adapt to the AI-based learning environment, and AI significantly improves students learning motivation, especially in critical thinking and problem solving. The study concludes that integrating AI into the curriculum can increase student engagement and learning outcomes in collaboration with teachers and parental interest at home, emphasizing the need for AI training before academic endeavors in new contexts**.**

Keywords: artificial intelligence(AI), learning motivation, learning outcomes.

1. Introduction

A technological revolution in education has started with the emergence of the artificial intelligence era, and Education changes in accordance with the times giving moral education new life. Civic education is still in its infancy in Indonesia, but it is currently expanding quickly in many other nations[1][2].For instance, The "New Generation of Artificial Intelligence Development Plan," released by the State Council in July 2017, explicitly identifies intelligent education as a key task: "using intelligent technology to accelerate the reform of talent training mode and teaching methods and build a new education system that includes intelligent learning and interactive learning[3].However, improvements in technology have a Shock and come with hazards connected to essential, technical, and value aspects that make them less effective in civic education[4].

The phenomenon of AI shock is a common thing experienced by the per-university level-students in Indonesia, especially Jakarta city. Jakarta is an urban area that captures the strong Javanese culture. Teachers are also afraid that artificial intelligence, which is known as the "Fourth Industrial Revolution",will replace their work in the civic classroom Instead of

helping to facilitate the educational process[5]. An e-learning platform that supports AI and STEM technology is regarded in this study is (https://www.iCivics.org/) in the classroom.

2. Background

Definition 2.1.

Artificial intelligence (AI) is, in general, a science that mimics the intelligence held by living organisms and applies it to machines in order to solve problems. Several professional viewpoints corroborate this understanding [6].

(1)John McCarthy (1960): Artificial Intelligence (AI) is the creation of machines that can think like humans and are designed to do so by modeling human cognitive processes.

(2)Rolston (1988): Artificial intelligence (AI) is the application of computers to solve real-world issues, including human mental processes.

(3)Teahan (2010): Artificial Intelligence is the science of creating computer systems that exhibit multiple forms of intelligence.

John McCarthy, who is widely regarded as the father of artificial intelligence, first used the phrase artificial intelligence (AI) in 1955 when he and his associates prepared a proposal for the 1956 Dartmouth Summer Research Project on Artificial Intelligence.[7] AI was defined as computers that "... use language, form abstractions and concepts, solve kinds of problems now reserved for humans, and improve themselves" in the proposal.[8]. Since then, computer science's artificial intelligence field has grown. Throughout its history, computer scientists as well as experts from anthropology, biology, philosophy, psychology, and linguistics have contributed to and debated many aspects of artificial intelligence (AI), leading to a divergence in the field's studies and advancements[9]. Because numerous writers have presented multiple definitions of artificial intelligence, it is challenging to come up with a consensus on one. Creating intelligent machines is the general focus of AI research [10]. As stated in numerous other definitions[11].[12].[13] of artificial intelligence in this context refers to human intelligence. Creating intelligent machines is the general goal of AI research, and as indicated by numerous other definitions, intelligence in this context refers to human intelligence.[7].

Defition2.2.

The term "artificial intelligence shock" refers to the Industrial 4.0 era, which used cloud computing, artificial intelligence, and the Internet of Things in a variety of human endeavors[14].[15].[16]. Furthermore, modern society has advanced into Society 5.0, where intelligent technology supports every aspect of human endeavor [17].An industrial revolution known as the "AI Shock Revolution" is built on intelligent technology that can link digital, biological, and physical devices that are linked and able to communicate via online media. Academic difficulties equip graduates to use technologies that haven't been discovered yet, solve problems that haven't been identified yet, and enter the workforce that hasn't been developed yet [18].The secret to dominating industry is education.4.0. Through

improving and fairly distributing high-quality education, increasing access to it, and emphasizing the value of using technology to deliver a world-class education, Education 4.0 supports the realization of intelligent education and produces students with at least five 21st century skills: collaboration, communication, critical thinking, creativity, and caring. The 21st century offers multiple paradigms for education, including Information that is constantly accessible, machine calculation that is faster, automation that facilitates daily tasks, and communication that is always and everywhere available. However, a new paradigm known as STEAM—Science, Technology, Engineering, Art, and Mathematics—has emerged as a result of the industrial 4.0 age [20].The Education 4.0 paradigm states that: educational institutions must prepare students to meet the challenges of Industry 4.0 or the 21st century in order to produce output that can be ready for work; educational programs need to adopt technology and also the STEAM paradigm (Science, Technology, Engineering, Art, and Mathematics); education can make students intelligent but also have good character. The social life that students participate in can be fostered by schools.

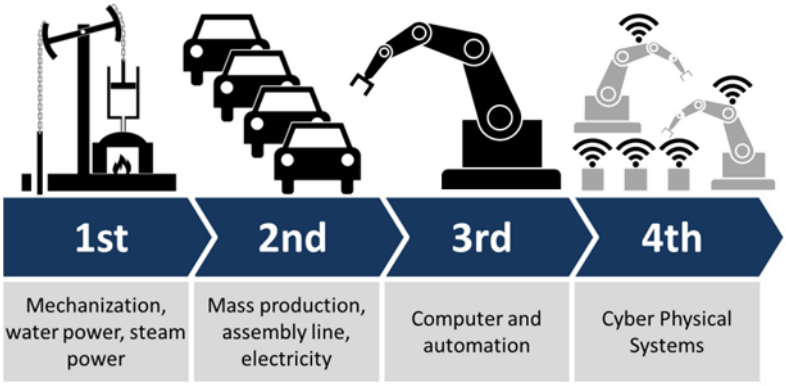

Figure 1 illustrates the stages of change start from Industry 1.0 to Industry 4.0.

Figure 1 Development of Industria Technolog

(Source:https://id.wikipedia.org/wiki/Industri_4.0).

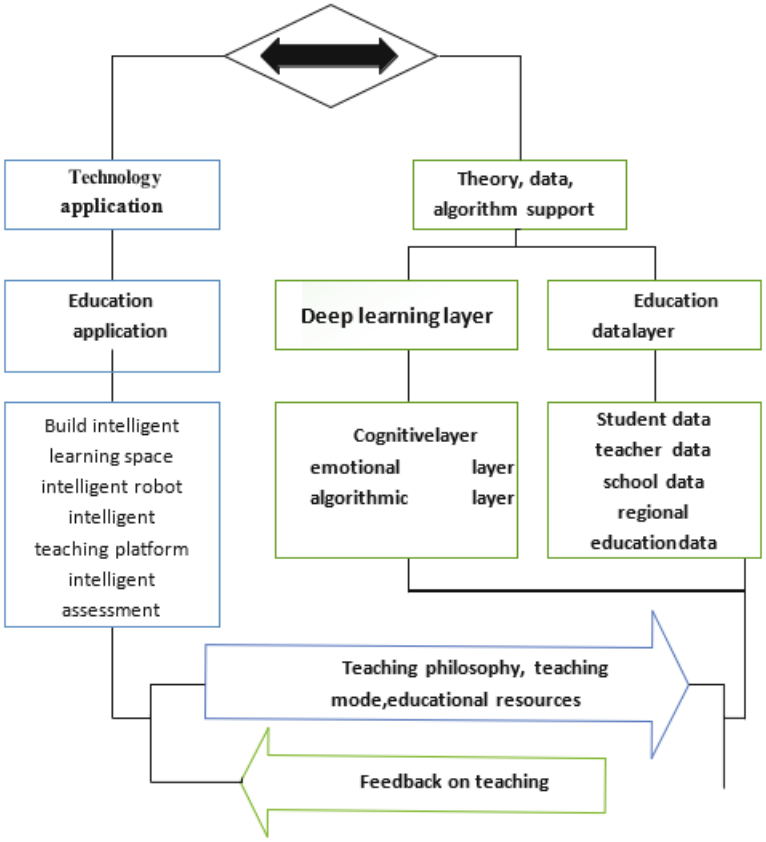

Figure 2: Educational AI technology

Civic education

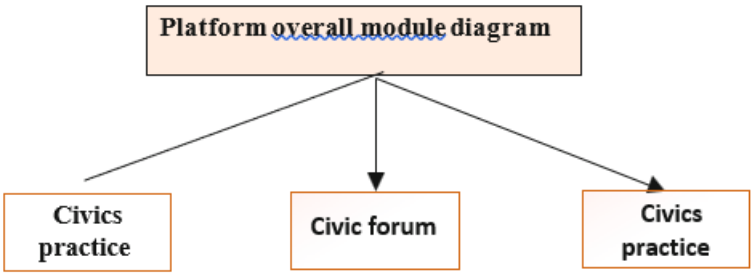

Figure: Overall Module of intelligence paltform

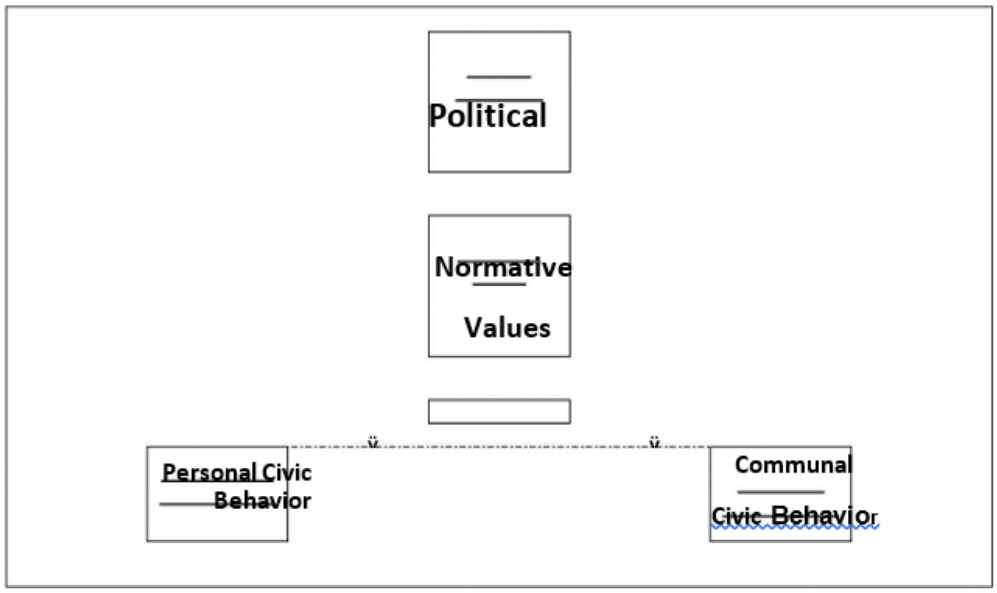

Chart1: Four Concepts of Civic Education

3. Methods

This study uses a descriptive qualitative research design, where data are collected through one-on-one interviews,in-depth observations and survey. The study participants were fifty students from SMP Jakarta who were randomly selected proportionally based on their willingness to participate in the study.Data collection was conducted over a period of months the results were analyzed thematically.

3.1.Data Collection Techniques: The interview techniques are used directly (face-to-face) and in-depth interview, according to the Interview Guide is a semi-structured interview guide.[21]. It's supported by a recording tool in the form of a "special recorder" to record the results of the interviews. A survey is using a distributed questionnaire.The questionnaire technique is used by answering on google drive form sheet.The respondents **3.1.Data Collection Techniques:** The interview techniques are used directly (face-to-face) and in-depth interview, according to the Interview Guide is a semi-structured interview guide.[21]. It's supported by a recording tool in the form of a "special recorder" to record the results of the interviews. A survey is using a distributed questionnaire.The questionnaire technique is used by answering on google drive form sheet. ,The respondents included boys and girls with the majority in the age group of 13-15 years. The remaining respondents were older than 15 years.All participants were students enrolled injunior high schoolat SMP Jakarta,Indonesia.

The statuses of the pupils who continue to attend the junior high schools are collected in many photo documents that taken in order to gathering data and different records from archives and collections of local customary laws, Indonesia's Cybersquatting Law for the document.

3.2.Data Collection Validity: Since this study is descriptive qualitative, the data collected will be qualitatively examined with the triangulation techniques are done in this paper to compare data collected using different ways with data inspected from the same source[22]. Because data can be considered legitimate if it is collected appropriately [23]and presented descriptively.

3.3. Data Analysis Techniques:

Figure 3: Flow chart of civic education big data platform application.

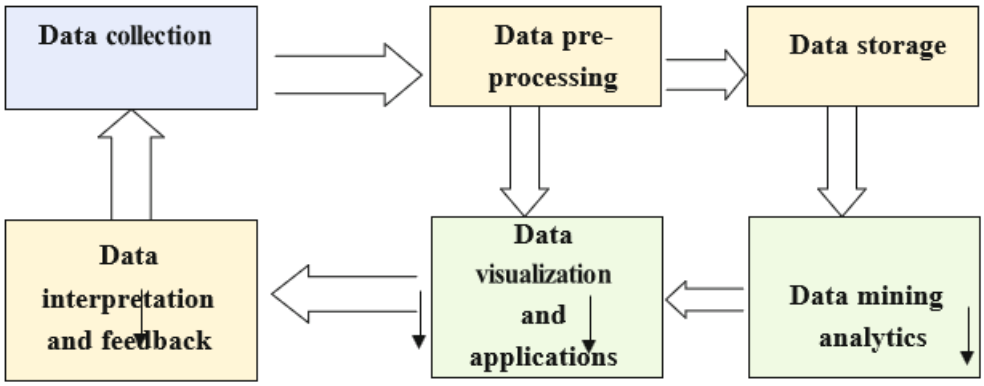

3.1. Data Analysis Validity: (Figure)

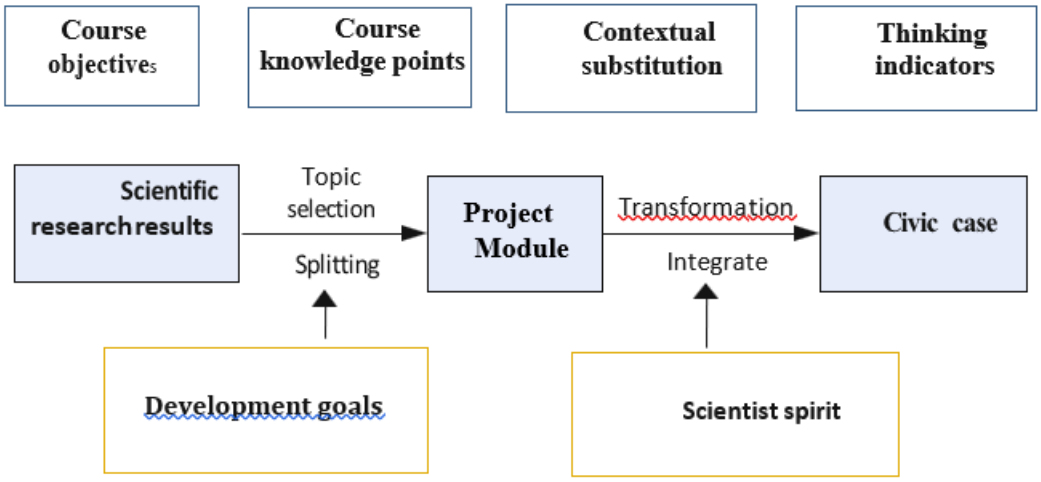

1. Result and Discussion

The degree of students' engagement and reactions to an iCivics website that supports artificial intelligence(AI) and STEM technology in the classrooms, were determined, as

shown in Table 1 below:

Table(1) Student's engagement of iCivics website.

	Engagement Frequency(%)			Mean	Std.Dev.
	AE	**PE**	**DE**		
D	0	0	3	4.73	0.452
A	27.3	24.2	24.2	4.76	0.435
SA	72.7	75.8	72.	4.70	0.529

D: Disagree.
A:Agree.
SA:Strongly Agree.
AE:Active Engagement.
PE:Passive Engagement
DE:Disengagement.
Std.Dev:Standard deviation value.

The terms actively engaged students, passive engaged students, and disengaged students were used to analyze the type of student engagement in the table above which shows the greatest increase in student engagement when using the educational website in the classroom. Also, all the questions have a high mean value greater than 4.0. When compared to other items, the four items have the largest standard deviation value (standard deviation = 0.609), indicating that the distribution of engagement scores is more dispersed than the mean score value.

The reason for the increased participation and interaction of students in addition to deep understanding is the teacher's assistance in the lesson and the parents' interest in two integrated directions, and because of maintaining the student's attention not being distracted inside the classroom and reviewing at home.

The interviews expanded the discussion to include questions about student needs regarding the additional role teachers should play as AI technology development.T9 shared, for instance, a new project my teacher is working on to figure out how to help me use websites with artificial intelligence as teaching materials. Put differently, the decision regarding the app's usefulness for their students and the manner in which they should utilize it falls on the shoulders of the teachers. Accordingly, T8's statement that "My subject teacher has a key role to play" in how to use AI services efficiently in the 1990s was an intriguing result from the interviews on the changing role of teachers. He declared, "I really want to pursue post-secondary education." I want to learn how to create learning applications in the future, not

just use them." As a result, it is clear from the above that teacher participation in the creation of civic education tools can be crucial to their effective use and can be bolstered by empirical intelligence, as instructors can offer a variety of viewpoints on how to teach the various components of these tools.

T8: the eighth student.

T9: the ninth student

Applications with artificial intelligence are only tools made to improve student learning and teacher effectiveness.Additionally, despite the fact that AI is altering many facets of education and self-learning, these developments shouldn't be seen negatively, according to the interviews. Rather, educators and school administrators need to understand the new roles that AI-integrated learning environments require of them and be ready to adjust accordingly[24]. On the other hand, , whose educators has talents in both development and adaptability, highlights that the most crucial phase of AI is the learning- giving phase.But on the other hand, some students, such as T13 and T12, told us that their parents noticed that T13 and T12, after using this technology, became more disciplined in studying, and now they pay more and better attention during the academic subject, which made them study more seriously and desire to achieve higher grades.Students T5, T10, and T4 added: The parents of each of them were punishing them because of their low grades. This puts pressure on them. Equally, some people are sounding the alarm about various aspects due to the huge trend that the country is witnessing towards artificial intelligence. They believe that these classrooms are laboratories for future generations. While these iron tools may help their children raise their grades, it is not yet clear how to achieve this until they become adult citizens, as is the case with parents of T1, T2, T3, T17, and others.Parents have an important role in forming an adolescent's personality at home before introducing them to new experiences at school, as their educational backgrounds are frequently the first informal institutions that children are exposed to before transitioning to official education institutions in schools.[25]

T1: the fist student**.**

T2: the second student.

T3: the third student.

T4: the fourth student.

T5:the fifth student**.**

T10:the tenth student.

T12:the twentieth student.

T13:the threaten student.

T17:the seventh student.

Learning motivation

After examining the results, it can be said that teaching civic education to students using the EAI-based methodologies enhances their learning processes. Children that are keen to study

about Pancasila and civics show a desire to do so using the AIS approach. Students also discuss the importance of civic education and Pancasila in their lives.The study also discusses the necessity of using technology—more especially, artificial intelligence in order to create educational activities that would hold students' attention. The methods that AI can affect student performance and learning environments are listed below.

EAI: Educational Artificial Intelligence.

For example, T18expressed interest in using AI website, saying that returning home would help him learn more. “The less you repeat in order to memorize the script, the happier you will be,” he insisted. In fact, T19 didn't seem too concerned about using the AI-powered learning method. Since my English is only at an intermediate or intermediate level, I have to admit that I feel a little nervous. But like my colleagues, I have to accept change and move forward. He knew that despite his fears, he had to expose them to technological advances. Accordingly, despite T20's expression of his teachers' concerns, T34 emphasized that in order for him to learn from technology effectively and quickly, his parents and school must provide guidance for its correct use. This message cannot be overstated.

Participants were also introduced to the idea of the possibility of replacing parents and teachers at home with educational centers based on artificial intelligence. All agreed that parents and teachers will continue to need guidance and supervision; Artificial intelligence will not replace them. T44, for example, said, “My teacher has to help me, and in my opinion my teacher is still an important person.” T45 added: “Now I think my school still needs teachers in the classroom.” Websites with educational AI are just tools, and I still need the support of my family and teachers because the primary responsibility of a teacher is to facilitate students' learning. This is the job that AI can help my teachers do.

AI: Artificial Intelligence.

T19:the nineteenth student.

T20:the twentieth student.

T34:the thirty fourth student.

T44:the forty fourth student.

T45:the forty fifth student.

4. Conclusion

We conclude from this research study that upgrading the engagement of the junior high school pupils by using EAI in civic classrooms that work to improve critical thinking and responsibility of the students in AI-era when the highest value of the learning upgrade was obtained in caring parent and trained teachers(By %).

References

[1]-Dewantara, J. A., Suhendar, I. F., Rosyid, R., & Atmaja, T. S. (2019). Pancasila as ideology and characteristics civic education in Indonesia. International Journal for Educational and Vocational Studies, 1(5), 400-405.

[2]-Campbell, D. E. (2019). What social scientists have learned about civic education: A review of the literature? Peabody Journal of Education, 94(1), 32-47.
[3]-Waluyandi, F., Trihastuti, R., & Muchtarom, M. (2020). Implementation of parental involvement in learning civic education. Budapest International Research and Critics in Linguistics and Education (BirLE) Journal, 3(4), 1686-1695
[4] -Aziz, S., & Dowling, M. (2019). Machine learning and AI for risk.management. Disrupting finance: FinTech and strategy in the 21st century, 33-50.

Selwyn, Neil. "What's the problem with learning analytics?." Journal of Learning Analytics 6, no. 3 (2019): 11-19.
Hastungkara, D. P., & Triastuti, E. (2019). Application of e-learning and artificial intelligence in education systems in Indonesia. ANGLO-SAXON: Journal of the English Language Education Study Program, 10(2), 117-133.
Sumakul, D. T. Y., Hamied, F. A., & Sukyadi, D. (2022). Artificial intelligence in EFL classrooms: Friend or foe?. LEARN Journal: Language Education and Acquisition Research Network, 15(1), 232-256.
[8]-McCarthy, J. (1960). Recursive functions of symbolic expressions and their computation by machine, part I. Communications of the ACM, 3(4), 184-195.
-McCarthy, J., Minsky, M. L., Rochester, N., & Shannon, C. E. (2006). A proposal for the dartmouth summer research project on artificial intelligence, august 31, 1955. AI magazine, 27(4), 12-12.
[9]Luckin, R., & Holmes, W. (2016). Intelligence unleashed: An argument for AI in education.
[10]-Nilsson, N. J. (2011). The Quest for Artificial Intelligence: A history of Ideas and Achievements, The Quest for Artificial Intelligence: A History of Ideas and Achievements.
[11]-Kusumadewi, S. (2003). Artificial Intelligence (Teknik dan Aplikasinya), Yogyakarta. Graha Ilmu.
[12]-Rich, E. (1983). Artificial intelligence.
[13]-Stone, P., Brooks, R., Brynjolfsson, E., Calo, R., Etzioni, O., Hager, G.& Teller, A. (2016).One hundred year study on artificial intelligence.
[14]-Muhammad Nizam, 2018; Office of Chief Economist Bank Mandiri, 2018.Muhammad Nizam, S. (2018). Revolusi industri 4.0: Suatu Pengenalan. Seranta FELDA Jabatan.
[15]-Sadiyoko, A. (2017). Industry 4.0: Ancaman, tantangan atau kesempatan? Sebuah introspeksi menyambut kemajuan teknologi saat ini.
[16]-Suwardana, H. (2018). Revolusi industri 4. 0 berbasis revolusi mental. JATI UNIK: Jurnal Ilmiah Teknik Dan Manajemen Industri, 1(2), 109-118.
[17]-Anggraheni, R., & Astuti, R. D. (2020). Revitalisasi nilai-nilai islami dalam edukasi guna mempersiapkan generasi menuju era Society 5.0 sebagai bagian dari strategi

rekonstruksi kejayaan peradaban Islam. Prosiding Konferensi Integrasi Interkoneksi Islam Dan Sains, 2, 31-34.
[18]-Pangestu, K., & Nuraini, N. L. S. (2020). Kesiapan Calon Guru Sekolah Dasar Dalam Menghadapi Era Revolusi Industri. ELEMENTARY SCHOOL JOURNAL PGSD FIP UNIMED, 10(2), 40-47.
[20]-Thompson, C. J., Barber, K., & Bourget, E. M. (2018). STEAM (Science, Technology, Engineering, Art, and Mathematics) Education and Teachers' Pedagogical Discontentment Levels. PEOPLE: International Journal of Social Sciences, 4(3), 496-518.
[21]-Moleong, l. (2014). Metodelogi penelitian kualitatif. Pt. Remaja rosdakarya. Journal of materials processing technology, 1(1), 1–8.
[22]-Sugianto, R., Darmayanti, R., & Humaidi, M. N. (2022). MUHAMMADIYAH EDUCATION'S READINESS IN THE SOCIETY 5.0 ERA. Al'Adalah, 25(1), 21-34.
[23]-Sugiyono. (2021). Metode Penelitian Kuantitatif, Kualitatif, dan R&D (2nd ed.). ALFABETA,cv. System, 38 (2010) 560-568.
[24]-Sharifuddin, N. S., & Hashim, H. (2024). Benefits and Challenges in Implementing Artificial Intelligence in Education (AIED) in ESL Classroom: A Systematic Review (2019-2022). International Journal of Academic Research in Business and Social Sciences, 14(1), 146-164.
-[25]Dini, E. S., Wardi, Y., & Sentosa, S. U. (2019, April). The Influence of Parent's Attention, Parents Education Background, Learning Facilities and Learning Motivation toward Student Learning Achievement. In 2nd Padang International Conference on Education, Economics, Business and Accounting (PICEEBA-2 2018) (pp. 819-827).

Congestion Control Mechanisms in Internet of Things: A Review of Current Techniques

Zaynab Saeed Hameed[1], Mohammed Arif Nadhom Obaid Al-agar[1] ,Zahraa Abbas Hassan[1]
Department of Computer Engineering, University of Technology, Baghdad, Iraq
Email : zaynab.s.hameed@uotechnology.edu.iq
MohammedArif.N.Alagar@uotechnology.edu.iq
Zahraa.A.Alzubydi@uotechnology.edu.iq

Abstract
In the network of Internet of Things, a substantial data volume is produced over a specific duration. Consequently, it becomes imperative to develop load balancing protocol to

optimize congestion control. This paper present an analysis of the existing mechanisms of IoT congestion control, categorized into pair of primary divisions known as performing offloading and protocol-dependent. These divisions are based on the methods employed to prevent congestion and balance load, accordingly. The protocol dependent technique is classified either a network layer protocol (RPL) or an application layer protocol (CoAP). That methods improve the functionality of CoAP and RPL protocols to effectively manage congestion. Conversely, the approach of offloading dependent encompasses various strategies to evenly distribute the network workload. Additionally, the analysis considers the main issues and objectives of different approaches in order to accomplish congestion control within an internet of thing network.

Keywords: Load Balancing Protocols, Offloading Techniques, Network Layer Protocol (RPL), Application Layer Protocol (CoAP)

1. Introduction

The "Internet of Things" is the network that enables users to access smart networks over the Internet. These gadgets are equipped with embedded capabilities to function both based on their internal states and the external environment. The IoT technology revolutionizes decision-making processes, as it enables these gadgets to sense and communicate, influencing how and where choices are made and by whom. It represents a significant advancement in wireless communication, with a diverse range of applications across various domains.[1, 2]. The primary idea of this concept is the widespread presence of various objects and devices, such as RFID tags, actuators, cell phones, sensors, etc., that can interact and collaborate to accomplish shared objectives through a unique and deliberate arrangement [3]. This is about a physical network device that is constantly creating and has an IP address connected to internet access and communication. It engages with additional internet-connected devices and systems that back applications in the sectors of healthcare monitoring, production line scheduling, and other decision-making procedures.

Internet of Things has a vast range of applications that greatly benefit human life, providing them with a simpler, more secure, and more exciting world. Some examples include smart urban communities, transportation systems, and homes. The incorporation of IoT technology has the potential to greatly enhance urban areas through infrastructure improvements, optimized public transportation, reduced traffic congestion, and the promotion of the health

and well-being of citizens who actively participate in the network [4]-[3]. The progress achieved by WiFi in the field of home automation has primarily been driven by the concept of networking electronic devices. Wi-Fi has become an integral part of the home Internet Protocol (IP) network, supporting various electronic gadgets such as mobile devices, TVs, and more. Additionally, with the rising popularity of mobile computing devices like tablets and smartphones, Wi-Fi has gained even more significance in this realm. [5]-[6]. IoT monitoring technology has a crucial function in continuously observing a psychological status of hospitalized patients. This advanced system employs sensors to collect a wide range of behavioural data, which is then analyzed and stored in the cloud and gateway. The encrypted information is then wirelessly transmitted to caregivers for further examination and evaluation. [7]-[8]. The deployment of Internet of Things (IoT) applications and scenarios mentioned previously presents promising advancements for intelligent technology. Nevertheless, there exist hurdles to surmount, including cost and execution. Furthermore, IoT encounters numerous other barriers such as self-organization, scalability, large amounts of data, power provision, data analysis, wireless connectivity, and compatibility [9]-[10]. In a specific scenario, a significant numbers of IoT devices are characterized by a restricted storage capacity and a slow processing rate causing congestion when numerous devices try to interact with one another. The packets of data exchanged via interconnected devices in IoT system have minimal data load, resulting in packet loss and expensive retransmissions required because of the congestion. This, in turn, leads to significant delays and substantial additional expenses. Moreover, IoT networks exhibit a notable level of mobility since they typically deal with dynamic nodes instead of static ones. The combination of small packet sizes, high retransmission rates, and mobility sets these compulsory networks are quite different from the current periodical networks that are being established. However, the current congestion control mechanisms created for conventional networks are not suitable for IoT networks. This highlights the need to design novel and effective congestion control mechanisms that are specifically customized for the distinct characteristics of IoT networks [11].

Loss of packets is a widely utilized signal for identifying congestion in the network. Certain components have been effectively or ineffectively coordinated and controlled by employing

alternate network sections to manage congestion.[12]. In the field of networking, when a source transmit a packet, it stays connected for certain duration, relying on an internal clock, to await confirmation of its delivery. If the confirmation is not received within this allotted time, the package is classified as lost because of network congestion [13]-[14]. This classification helps in triggering congestion control mechanisms to alleviate network traffic. In the domain of congestion control, the algorithms are responsible for managing network congestion when packet loss is detected. Nonetheless, within an IoT network, these algorithms prove to be ineffectual as they heavily depend on packet losses to discern congestion. This does not apply to lousy, lower power networks, where packet losses may arise from poor signal quality or link failures, among other causes. Furthermore, the congestion response is postponed until a packet loss happens [3]. Several congestion control techniques have been developed and put into use in Internet of Things networks to address these issues [15].

The structure of the paper is as below: Section (2) provides information regarding congestion control and covers it under many areas. In Section (3), several techniques are examined through an analysis of their key ideas and practical uses. Section (4) provides the future prognosis and concluding remarks.

1.1 Related works

An overview of existing techniques for preventing congestion issues in Internet of Things networks is provided by this study. Numerous surveys are carried out to evaluate network congestion in IoT devices. In [16] describes congestion detection, avoidance, and mitigation protocols; however, it ignores the usage of simulators and 6LoWPAN congestion control. In [15-16] authors described only congestion mitigation, whereas in [17] describes congestion detection and mitigation,[18] suggested only congestion mitigation,[19] provide details about IoT simulators,[20] explain congestion mitigation. In [17] suggested routing protocols and congestion control in 6LoWPAN [21]. describes congestion mitigation and avoidance. It present several types of routing protocols, congestion control in 6LoWPAN, congestion analysis and distinct categories of IoT simulators.

1.2. Purpose of research

This paper present an analysis of the existing mechanisms of IoT congestion control, categorized into pair of primary divisions known as performing offloading and protocol-dependent. It aims to provide an overview of congestion mitigation. The many approaches the authors used to alleviate application layer congestion are examined in this work, with a focus on improving and changing the restricted application protocol (CoAP). It also provides a brief assessment about the network level initiatives.

2. Definition of Congestion Control Mechanism

Understanding the intricacies of Internet of Things congestion control methods requires defining a specific description of a congestion control mechanism. Congestion control mechanisms are sets of algorithms and protocols that regulate the movement of data inside a network to prevent congestion and ensure efficient communication.

Various methods of congestion management have been developed for different phases of the IoT. Network congestion can result from high volumes of demand traffic and repeated transmissions within the network. In lousy, low power wireless networks, like the ones in the Internet of Things, retransmission is a persistent issue. The network and app levels have seen a great deal of congestion management thanks to protocol-based approaches. The many approaches the authors used to alleviate application layer congestion are examined in this work, with a focus on improving and changing the restricted application protocol (CoAP). It also provides a brief assessment about the network level initiatives.

There has been a discernible increase in data transfer. Over the previous few years due to the improved connectivity accessibility. However, in rare occasions, it has also led to congestion, which has resulted in packet loss. A solution to this issue is offloading, which involves dividing the load of a busier node among less busy nodes. This ensures that packets reach within the allocated time, hence reducing the need for retransmission.

The protocol-based congestion control technique places a strong emphasis on Round Trip Time (RTT) and Retransmission Timeout (RTO) in order to lessen network congestion and enhance traffic flow. On the other hand, during the offloading process, the nodes congestion load is evenly categorized throughout network to ensure traffic flows smoothly and lower network latency. Generally speaking, congestion control is classified as:

2.1 Congestion control that is dependent on protocols.

2.2 Network layer

Adopting a load-aware routing protocol design helps control network layer congestion. Congestion control is achieved through hop to hop communication, although this approach leads to increased overhead due to the sharing of control information between nodes [22]

An evaluation of 6LoWPAN in relation to congestion indicates that the occurrence of packet loss is relatively high as a result of buffer overload rather than loss experienced by the channel. To address that issue, author in [23] has put forth a formal proposition for a congestion control IPV6 with regards to routing protocol (known as RPL) that operates with low level of power consumption and lousy networks. This protocol intends to manage packet loss in congested networks that occur because of buffer overflow. Two unique measures have been introduced by the author to measure both occupancy of buffer and congestion awareness, leading to enhancements in efficiency and packet delivery rate. In contrast, the author in [24] suggests that the evaluation of congestion control should include the buffer's occupancy assessment. Additional overhead is needed with this method to communicate buffer occupancy data. The studies mentioned in references [25] and [26] show that during the parent selection phase in the routing process, high levels of traffic often lead to packet losses, primarily due to congestion and load balancing issues. The author in [27] proposed a technique known as (QU-RPL) simple queue utilization depending on the RPL protocol to solve this problem. To identify the parent node, QU-RPL considers both the hop distance from the RPL router and the utilization of nearby nodes. This method efficiently minimize loss in high queue and maximize packet shipping rate.

Controlling route topology and transmission power in wireless networks is beneficial for achieving optimal reliability and bandwidth within the networks [28].The power-controlled RPL protocol is suggested as a solution for managing variations in transmission power in order to prevent bandwidth loss caused the intention of improving the performance of routing for IoT networks. In order to achieve this objective, the routing topology design. Both the routing topology and transmission power are effectively managed by this protocol. In [29], The authors have presented a dense IoT network load balancing solution that uses less

energy. They have proposed the routing protocol known as Double Level Unequal Clustering. By employing that protocol, the traffic load has been divided among cluster members, while creating clusters of uneven sizes as well. Additionally, the number of cluster heads has been decreased. The NS2 network simulator was used to test the suggested strategy and the results demonstrated a throughput growth and energy usage decrease.

Table 1: Summery of Congestion control protocol in Network layer

Reference	Concept	Description
[22]	Load-aware Routing Protocol	Adopting a load-aware routing protocol design helps control network layer congestion. Congestion control is achieved through hop-to-hop communication, although this approach leads to increased overhead due to the sharing of control information between nodes.
[23]	Congestion Control IPV6 (RPL)	To address the issue of buffer overload, a formal proposition for a congestion control IPV6 routing protocol (known as RPL) has been put forth. This protocol operates with low power consumption and is intended to manage packet loss in congested networks due to buffer overflow. Two unique measures for buffer occupancy and congestion awareness are introduced, leading to enhancements in efficiency and packet delivery rate.
[24]	6LoWPAN Evaluation	An evaluation of 6LoWPAN in relation to congestion indicates that packet loss is relatively high as a result of buffer overload rather than loss experienced by the channel.
[25], [26]	High Traffic Packet Loss	Studies show that during the parent selection phase in the routing process, high levels of traffic often lead to packet losses, primarily due to congestion and load balancing issues.
[27]	QU-RPL Protocol	To solve high queue loss, the QU-RPL technique, which depends on the RPL protocol, is proposed. It considers both the hop distance from the RPL router and the utilization of nearby nodes to identify the parent node, efficiently minimizing loss in high queue and maximizing packet delivery rate.
[28]	Route Topology and Transmission Power Control	Controlling route topology and transmission power in wireless networks is beneficial for achieving optimal reliability and bandwidth. The power-controlled RPL protocol manages variations in transmission power to prevent bandwidth loss and improve the performance of routing for IoT networks.

Reference	Concept	Description
[29]	Dense IoT Network Load Balancing	A dense IoT network load balancing solution using the Double Level Unequal Clustering routing protocol is proposed. This protocol divides the traffic load among cluster members, creates clusters of uneven sizes, and decreases the number of cluster heads. The NS2 network simulator tests demonstrated throughput growth and energy usage decrease.

2.3 Application Layer

The Internet of Things (IoT) utilizes the common application protocol CoAP for limited applications. CoAP is primarily develop to operate over UDP. A large number of authors have expressed interest in creating CoAP congestion control techniques.

The author [30] presents a complete analysis of the congestion control system for CoAP . This survey focus predominantly on the alteration of the RTO (Retransmission Time Out) estimation process. This modification enhances the performance of CoAP/CoCoA; however, it fails to extract the signal of congestion from the round trip time (RTT) noisy sample. Numerous research studies have undertaken a comparison of CoAP/CoCoA.[30]-[31]. CoCoA is regarded as superior to CoAP in certain studies, although some have indicated that CoCoA causes an increase in retransmissions as the number of requests rises [32].

Within [33] The Eifel Re-transmissions timer is the basis to compute the RTO value, which was firstly researched for TCP [34]. In the aforementioned paper, The RFC6298 coefficients (Į, ù, K) have been modified by the author with an only one coefficient Û, in order to make it adaptive to deal with larger sender loads. This novel variable, Û, shows the proportion between the current RTT and RTO samples. However, the extracted signals of congestion from the RTT sample is not included. In [35] the author discussed four variants of CoCoA: CoCoA-S, CoCoA-F, & CoCoA-4 Strong. These adjustments mitigate the problem of lousy wireless networks and do away with the drawbacks of weak estimation. CoCoA-F improve competitiveness by decreasing the back off threshold, initial values, and RTO maximum. Additionally, it provides a cautious performance similar to CoCoA. The author focuses on distinguishing between wireless and congestion losses by utilizing estimators with a higher granularity of four states. This research improves the CoCoA's performance in wireless networks with loss. CoCoA-4-State-Strong adjusts to packet losses and increases throughput by 30–60%. However, there is a roughly 20% increase in the retransmission rate.

In [36] The author proposes a suggested adaptive method to deal with CoAP congestion.. Traffic priority and the packet loss rate have been considered with this mechanism. This mechanism include three main components: optimized RTO, Return timers, and congestion

prioritization. The type of equipment determines the traffic priorities. The amount of RTO back off is assigned with regards to both priority of the traffic as well as rate of packet loss. However, it should be emphasized that the author does not really use the suggested strategy, which raises doubt on its feasibility for advancement. [37] Reveals an alternative approach which consider an adaptive congestion control mechanism. This strategy works well for extremely congested networks, where more than one retransmission of a single packet is required. This particular approach effectively chooses the RTT value for the retransmitted packet. Although it does increase throughput and the number of completed transactions, it is not as efficient in cases where multiple retransmissions are unnecessary. the author of [38] suggested a precise version of CoCoA by addressing the limitations of the prior version (CoCoA+). These limitations included the close proximity of the values RTO and RTT, weak weights and updates for estimators, and the increase in RTO due to the decrease in RTT. The author conducted an analysis of CoCoA's performance in burst traffic patterns and found that the results were not satisfactory. To address these issues, CoCoA eliminates the causes of weak estimators and erroneous retransmission. Additionally, a new method is proposed to set the RTT measurement parameter initially. However, it is worth to indicate that the paper defines fixed amount that are not applicable to implement in significant (IoT) network issues. The author In [38], presents the address the network queuing delay , which is referred to as buffer bloat. Several congestion control mechanisms are ineffective in addressing buffer bloat concern and result in unrequired retransmission. Both CoAP and CoCoA are unable to deal with this issue and cause a wastage with network bandwidth. The author demonstrates the inaccurate RTO back off logic as the root cause of the issue and offers a novel back off logic as a fix for the buffer bloat issue...

[39] Tries to address the buffer bloat issue in network high congestion. They propose the use of Fast-Slow RTO to decide whether losses in packet are due to congestion or wireless channel loss. The approach includes three features: quick RTO computation and slow RTO, in addition to a self-adaptive timer for re-transmission. Fast RTO and TCP RTO are comparable, although fast RTO may have a lower maximum RTO value. The slow RTO function is comparable to the Karn algorithm. Compared to both CoCoA and CoAP, fast-slow RTO controls RTO in extremely crowded traffic efficiently and yields a quicker Flow Completion time[22].

In [39] The assessment of CoAP congestion control is conducted in real time by Wishful platform. It’s is an all-inclusive platform that gives users the freedom to create custom networks and facilitates the management and execution of real time experiments. In this article, basic RTT-based algorithms and the CoAP congestion control approach are compared. The results imply that the conventional approach to congestion control might be more adaptable and reliable than the straightforward RTT-based techniques. In Internet of Things (IoT) networks a delayed gradient is created oriented congestion control method. [40] The authors aim to create IoT networks model with less congested. In order to do this,

they developed the ground-breaking CoCoA++ congestion control method. By implementing delayed gradients and probabilistic back off, the researchers were able to handle network congestion more efficiently. Either constrained Application Protocol or CoAP, is employed in conjunction with these proposed variables. The Cooja network simulation was utilized to put the suggested strategy into practice. After the authors presented their research, latency dropped and packet transfer speeds rose. By creating the solutions demonstrate in this section, the mechanism of CoAP traffic control was considered. To prevent and manage congestion, RTO beside RTT are both essential.

Table 2: Summery of Congestion Control Protocol in application Layer

Reference	Concept	Description
[30]	CoAP Congestion Control Analysis	Presents a complete analysis of the congestion control system for CoAP, focusing on the alteration of the RTO (Retransmission Time Out) estimation process. Enhances CoAP/CoCoA performance but fails to extract the congestion signal from the noisy RTT sample.
[30], [31]	CoCoA vs. CoAP Comparison	Numerous studies compare CoAP/CoCoA. CoCoA is regarded as superior in certain studies, although it may cause an increase in retransmissions as the number of requests rises.
[33], [34]	Eifel Re-transmissions Timer	Uses the Eifel re-transmissions timer to compute the RTO value, modifying RFC6298 coefficients with a new coefficient Û to adapt to larger sender loads. Does not include extracted signals of congestion from the RTT sample.
[35]	CoCoA Variants	Discusses four variants of CoCoA: CoCoA-S, CoCoA-F, & CoCoA-4 Strong. CoCoA-F improves competitiveness by decreasing back off threshold, initial values, and RTO maximum, and distinguishes between wireless and congestion losses. CoCoA-4-State-Strong adjusts to packet losses and increases throughput by 30–60%, with a 20% increase in retransmission rate.
[36]	Adaptive CoAP Congestion Method	Proposes an adaptive method to deal with CoAP congestion, considering traffic priority and packet loss rate. Includes optimized RTO, return timers, and congestion prioritization. The feasibility of the proposed strategy is not tested.
[37]	Adaptive Congestion Control Mechanism	Proposes an adaptive congestion control mechanism for highly congested networks, selecting RTT value for retransmitted packets. Increases throughput and completed transactions but is less efficient for cases where multiple retransmissions are unnecessary.
[38]	Precise CoCoA Version	Suggests a precise version of CoCoA addressing prior limitations. Analyzes CoCoA performance in burst traffic patterns, proposing new methods to set RTT measurement parameters and fix RTO back off logic to address buffer bloat issues.

Reference	Concept	Description
[39]	Fast-Slow RTO	Proposes Fast-Slow RTO to distinguish between congestion and wireless channel loss. Includes quick RTO computation, slow RTO, and a self-adaptive timer for retransmission. Efficiently controls RTO in crowded traffic and yields quicker Flow Completion time.
[39]	CoAP Congestion Control Assessment	Assesses CoAP congestion control in real-time using the Wishful platform, comparing basic RTT-based algorithms and CoAP congestion control. Suggests the conventional approach might be more adaptable and reliable than straightforward RTT-based techniques.
[40]	Delayed Gradient Congestion Control	Proposes CoCoA++ congestion control method using delayed gradients and probabilistic back off to handle network congestion efficiently. Utilizes the Cooja network simulation for implementation, resulting in reduced latency and increased packet transfer speeds.

2.4 Congestion Control that is based on offloading.

Offloading is defined as the process of shifting a particular node's load to another node in order to split the workload. Decreasing delays considers as benefits the technique, controlling traffic, and increasing success rates. Gateways and associated infrastructure have extra lines that process time to activate effective flow of traffic throughout the network. This has a direct impact on the latency observed in the service. Offloading reduces latency by redirecting traffic to less busy nodes, which can enhance network performance. Offloading requests are advised in crowded network conditions to minimize needless packet loss and communication failures.

In order to maximize user advantages and minimize operating expenses, the author of [27] suggests a game-theoretic computation offloading technique. In the atmosphere and fog domains, offloading improves resource allocation and provides benefits including reduced latency, increased energy efficiency, and better power use. The author suggests employing cooperative offloading in [41] to achieve energy conservation. This technique split the download procedure between cloud, mobile nodes, and edge. The Internet of Things network uses a variety of communication technologies to provide connectivity in an effort to enhance energy efficiency. In order to reduce energy in the setting of dense IoT networks, the author recommends employing cooperative offloading. This approach comprises. [42] Presents an approach for shifting edge computing operations in particular. This tactic aims to reduce traffic congestion and raise the network's overall efficiency. It functions systematically and is made up of two tiers: the regional and mobile edge. The duration of processing and energy usage decrease as a result of the equal allocation of arriving workloads among these tiers. This strategy demonstrates expertise in the area of Internet of Things networks that are service-oriented. The author in [43] offered a formal approach known as Stability of Green Cross Haul Orchestration to maximize unloading. This method aims to improve energy

economy, lower latency, and boost network resilience. Drift and penalty methods are constructed in the framework of offloading utilizing the Lyapunov theory in order to estimate the information processing rate in an environmentally responsible manner [44].

The lightweight request framework, proposed in [45], was designed to enhance scalability. It seamlessly incorporates various architectures and is particularly well-suited for IoT and cloud edge-based integrated systems. One of its notable features is the ability to selectively offload tasks independently at both the IoT and cloud layers. both offloading and non-offloading devices are employed with in the network by the author in reference [46]. The author examines the construction and modelling of a mobile cloud that is diverse. A remote system is used to evaluate the cloud system while the remaining systems are analyzed using a stochastic offloading approach. The investigation concludes that optimal positioning of cloudlets and appropriate distribution of the offloading process is advantageous in reducing IoT communication down time. In reference [47], the author endeavours to enhance the communication of IoT devices through the implementation of decision offloading using the K-means algorithm. This involves segregating the network to position the edge server with the K-means algorithm's assistance to regulate the offloading process. The suggested method uses decision-based offloading to reduce latency and operating costs. At [48], the aura platform executes task offloading for users by leveraging an IoT-based cloud that offers ad-hoc services. Through its distributed locations, aura facilitates the migration, processing, and initialization of tasks with the assistance of localized IoT devices. Furthermore, this model effectively manages cost and capacity to ensure load balancing.

In [49] proposed the allocation of tasks among edge nodes, with regard to the constructive syncing method, can be found in the context of IoT-based networks. This method divides up the duties according to how well-liked the process is by fog-connected edge nodes. The jobs are distributed according to personal model taken from cloudlets. Therefore offloading and queuing techniques are used together to minimize delay. [50], has introduced a load balancing technique utilizing load bot within the Internet of Things (IoT). The considerable amount of demand in the IoT network leads to traffic congestion on specific routes and nodes. As a result, the authors wanted to solve the problem of high demand in the IoT in order to reduce traffic congestion. They put up a solution in the shape of an agent called Loadbot to address this issue. By looking at the amount of user data and network loads, load bot determines the network load and makes structural modifications. Additionally, the authors achieved efficient balance of load in the Internet of Things by utilizing the Deep Belief Network approach. The suggested method was executed by Matlab. Via employing this method, the network's burden was lessened by the authors even as it grew in size. Load balancing based on deep learning. Consequently, the authors' essential target linked to the Internet of Things was load regulation. They proposed using an agent known as Loadbot to realize this, which modified the structure configuration according to user volume of data and available network strain. They also create use of their strong belief system technology to

efficiently split the load linked with the Internet of Things. They also discussed the usage of an agent named Balancebot to enable Q-learning and a neural prior ensemble-based simulated neural load estimation approach.

The Matlab software was applied to implement these proposed systems. The authors were able to enhance the IoT system's functionality by using these strategies. Researchers Soulmaz Gheisari and Ehsan Tahavori have demonstrated a technique to handle Internet of Things (IoT) traffic that they name cognitive methodology [51]. The researcher's goal was to reduce the congestion issues brought on by the restricted capacity and imprecise connectivity of the omnipresent IoT networks. They accomplished this by exploiting a learning automata-based intelligence system to combine cognition into the Internet of Things. CCCLA was created by the Author, a Learning Automata game, as a newly cognitive technique to handle congestion by employing this technology.

Implementing learning automata, each factor that may impact the congestion efficiency control were adjusted. The Cooja simulation framework was then utilized to imitate the proposed course of action. They were success to efficiently raise productivity, latency, and reliability by practicing this strategy [52].

Their research's primary objective was to address the issues of traffic congestion brought by a rise in transportation demand. They have employed a distinct traffic control technique based on the Vickrey-Clarke-Groves (VGC) method and the Rubinstein bargaining game model in order to realize this. A new pricing model has been revealed as well which considers the characteristics of Internet of Things sections and access point owners.

By strengthening communication between access point users and the IoT module throughout the data offloading process, this price structure has improve the quality of service.

In reference [53] the author proposed an algorithm based data processing and traffic control system within the IoT context. The authors aimed to increase traffic signal processing rates while decreasing deployment time and human resource needs because there were numerous sensors and intelligent equipment involved. To do this, they created a novel sophisticated traffic control system that combines the usage of a remote cloud server with a nearby traffic intelligent server. This system tracked the movement of autos, especially those that travelled swiftly, to collect multipath data. To get this data, the writers additionally developed optimized regression models. To make an intelligent choice at a four-way crossroads, they considered the number of cars that were waiting. The outcomes of the simulation demonstrated that the suggested plan of action was successful in reducing waiting times. [53] Have suggested a method for changing offloading in Internet of Things appliances. Their research aimed to improve the capabilities of Internet of Things connectivity and traffic management given the growing usage of mobile devices. To accomplish efficient traffic handling, they recommended GA-OA, a flexible offloading system that makes use of a genetic algorithm. Increases in offloading effectiveness and IoT requested success rate

resulted in less extra time in the request process. They used the Beneficial Network Environment simulator (ONE) to simulate their approach with the objective to reduce complexities, latency, and processing time.

Their results showed that the GA-OA method outperformed the offloading systems in use at the time with regard to of network production and response time. Additionally, the GA-OA technique demonstrated significant improvements in packet loss reduction and overall system reliability... The success of the plan, however, may differ based on the state of the network and the particular needs of the Internet of Things applications [54]- [55].

Table 3: Summery of Offloading Techniques in IoT Networks

Reference	Concept	Description
[27]	Game-Theoretic Computation Offloading	Suggests a game-theoretic computation offloading technique to maximize user advantages and minimize operating expenses, improving resource allocation in the atmosphere and fog domains.
[41]	Cooperative Offloading	Employs cooperative offloading to achieve energy conservation by splitting the download procedure between cloud, mobile nodes, and edge, enhancing energy efficiency in dense IoT networks.
[42]	Edge Computing Operations Offloading	Proposes an approach for shifting edge computing operations to reduce traffic congestion and increase network efficiency, using a two-tier system of regional and mobile edge.
[43]	Stability of Green Cross Haul Orchestration	Offers a formal approach to maximize unloading, improving energy economy, lowering latency, and boosting network resilience through drift and penalty methods based on Lyapunov theory.
[45]	Lightweight Request Framework	Designed to enhance scalability and seamlessly incorporate various architectures, allowing selective offloading tasks at both IoT and cloud layers.
[46]	Diverse Mobile Cloud Modelling	Examines construction and modelling of a mobile cloud, using a stochastic offloading approach to reduce IoT communication downtime.
[47]	Decision Offloading with K-means	Enhances communication of IoT devices by using the K-means algorithm to regulate the offloading process, reducing latency and operating costs.
[48]	Aura Platform	Executes task offloading for users by leveraging an IoT-based cloud, facilitating migration, processing, and initialization of tasks through localized IoT devices.

Reference	Concept	Description
[49]	Constructive Syncing Method	Allocates tasks among edge nodes based on process popularity, minimizing delay through offloading and queuing techniques.
[50]	Load Balancing with Loadbot	Introduces a load balancing technique using Loadbot, employing Deep Belief Network approach to manage network loads and structural modifications.
[51]	Cognitive Methodology	Handles IoT traffic using a learning automata-based intelligence system, efficiently raising productivity, latency, and reliability.
[52]	Vickrey-Clarke-Groves (VGC) Method	Uses VGC method and Rubinstein bargaining game model to address traffic congestion, improving quality of service through better communication between access points and IoT modules.
[53]	Algorithm-based Traffic Control	Proposes an algorithm-based data processing and traffic control system, enhancing traffic signal processing rates and reducing deployment time and human resource needs.
[54], [55]	GA-OA Offloading System	Recommends GA-OA, a flexible offloading system using a genetic algorithm to improve offloading effectiveness and IoT request success rate, reducing latency and processing time.

3. Analysis of Various strategies

Several authors have offered various strategies for reducing congestion in small-scale IoT networks. The use of an application layer protocol for congestion control is one of these strategies that is most crucial. Standard protocols are successfully used in conjunction with this approach. CoAP is typically the recommended protocol in limited situations. The compatibility of all the alterations must be maintained. Furthermore, every strategy needs to show effective operation under various traffic situations. Energy efficiency must be taken into account while building a routing-based congestion management protocol in order to manage the load. A significant amount of energy is used in the routing process itself, particularly when clusters are formed or the parent node is chosen. The author of [29] ignores mobility as a factor in clustering and fails to consider its importance in evaluating energy depletion. This omission may result in an incorrect assessment of congestion management techniques on dynamic Internet of Things networks. Thus, when assessing the efficacy of congestion control systems in dynamic Internet of Things networks, it's imperative to take movement's effect on energy consumption into account [56].

The topic covered in this paper is using different learning processes to conduct offloading. Different solutions try to reduce delays by distributing traffic throughout the network equitably. However, if the number of queries increases, it may affect efficiency

[29]. Sorting and identifying the particular packet type is crucial, as is determining congestion using that technique. The workload distribution and allocation among adjacent devices ought to be contingent upon the response time. These algorithms' primary goals are to decrease complexity, processing times, and delays. In addition, three recommended strategies have been implemented to reach load equilibrium in the face of demanding and dynamic workloads [50].However, it is imperative to recognize that this may result in increased complexity inside the (IoT) network.

4. Conclusion

The congestion control analysis mechanisms for (IoT) reveals the need for further research and development in order to effectively manage the increasing demands of connected devices and networks. Congestion control is a significant consideration in IoT networks. There are two main approaches to managing congestion: optimizing either the network or application layers, or both, in order to effectively manage network congestion and control congestion caused by packet re-transmission. Another method involves offloading traffic from congested nodes to neighbouring nodes based on their load, which can be achieved using machine learning algorithms. It is crucial to differentiate between different types of packets to reduce processing delay and improve success rates. Following shortly. It may be possible to implement intelligent learning algorithms to efficiently handle offloading and retransmission rates. Additionally, any proposed solutions should be adaptable to heterogeneous networks, offering enhanced capacity and adaptability.

References

[1] Y. Sun, Y. Xia, H. Song, and R. Bie, "Internet of things services for small towns," in *2014 International Conference on Identification, Information and Knowledge in the Internet of Things*, 2014, pp. 92-95.

[2] S. M. Alzahrani, "Sensing for the Internet of Things and its applications," in *2017 5th international conference on future internet of things and cloud workshops (FiCloudW)*, 2017, pp. 88-92.

[3] P. Agrawal and G. Chitranshi, "Internet of things for monitoring the environmental parameters," in *2016 International Conference on Information Technology (InCITe)-The Next Generation IT Summit on the Theme-Internet of Things: Connect your Worlds*, 2016, pp. 48-52.

[4] B. Ahlgren, M. Hidell, and E. C.-H. Ngai, "Internet of things for smart cities: Interoperability and open data," *IEEE Internet Computing*, vol. 20, pp. 52-56, 2016.

[5] K. Trivodaliev and B. Risteska Stojkoska, "Enabling internet of things for smart homes through fog computing," 2017.

[6] V. Govindraj, M. Sathiyanarayanan, and B. Abubakar, "Customary homes to smart homes using Internet of Things (IoT) and mobile application," in *2017 International*

Conference On Smart Technologies For Smart Nation (SmartTechCon), 2017, pp. 1059-1063.

[7] J. Rauscher and B. Bauer, "Safety and security architecture analyses framework for the internet of things of medical devices," in *2018 IEEE 20th international conference on e-health networking, applications and services (Healthcom)*, 2018, pp. 1-3.

[8] I. Chiuchisan, I. Chiuchisan, and M. Dimian, "Internet of Things for e-Health: An approach to medical applications," in *2015 International Workshop on Computational Intelligence for Multimedia Understanding (IWCIM)*, 2015, pp. 1-5.

[9] K. Gupta and S. Shukla, "Internet of Things: Security challenges for next generation networks," in *2016 International Conference on Innovation and Challenges in Cyber Security (ICICCS-INBUSH)*, 2016, pp. 315-318.

[10] V. A. Almeida, D. Doneda, and M. Monteiro, "Governance challenges for the Internet of Things," *IEEE Internet Computing*, vol. 19, pp. 56-59, 2015.

[11] P. Anitha, H. Vimala, and J. Shreyas, "Comprehensive review on congestion detection, alleviation, and control for IoT networks," *Journal of Network and Computer Applications*, p. 103749, 2023.

[12] N. H. B. Halim, N. B. Yaakob, and A. B. A. M. Isa, "Congestion control mechanism for Internet-of-Things (IOT) paradigm," in *2016 3rd International Conference on Electronic Design (ICED)*, 2016, pp. 337-341.

[13] Y. Pan, Y. Li, and J. Zhang, "Congestion-aware data acquisition for Internet of Things," in *Proceedings of 2014 International Conference on Cloud Computing and Internet of Things*, 2014, pp. 131-134.

[14] K. S. Bhandari, A. S. Hosen, and G. H. Cho, "CoAR: Congestion-aware routing protocol for low power and lossy networks for IoT applications," *Sensors*, vol. 18, p. 3838, 2018.

[15] V. K. Jain, A. P. Mazumdar, P. Faruki, and M. C. Govil, "Congestion control in Internet of Things: Classification, challenges, and future directions," *Sustainable Computing: Informatics and Systems*, vol. 35, p. 100678, 2022.

[16] C. Lim, "A survey on congestion control for RPL-based wireless sensor networks," *Sensors*, vol. 19, p. 2567, 2019.

[17] M. A. Tariq, M. Khan, M. T. Raza Khan, and D. Kim, "Enhancements and challenges in coap—a survey," *Sensors*, vol. 20, p. 6391, 2020.

[18] M. Alvi, K. M. Abualnaja, W. T. Toor, and M. Saadi, "Performance analysis of access class barring for next generation IoT devices," *Alexandria Engineering Journal*, vol. 60, pp. 615-627, 2021.

[19] E. Ojie and E. Pereira, "Simulation tools in internet of things: a review," in *Proceedings of the 1st international conference on internet of things and machine learning*, 2017, pp. 1-7.

[20] N. Yaakob, R. Badlishah, A. Amir, and S. A. binti Yah, "On the effectiveness of congestion control mechanisms for remote healthcare monitoring system in IoT environment—A review," in *2016 3rd International Conference on Electronic Design (ICED)*, 2016, pp. 348-353.

[21] N. Mishra, L. P. Verma, P. K. Srivastava, and A. Gupta, "An analysis of IoT congestion control policies," *Procedia computer science*, vol. 132, pp. 444-450, 2018.

[22] A. Maheshwari and R. K. Yadav, "Analysis of congestion control mechanism for iot," in *2020 10th international conference on cloud computing, data science & engineering (Confluence)*, 2020, pp. 288-293.

[23] H.-S. Kim, H. Kim, J. Paek, and S. Bahk, "Load balancing under heavy traffic in RPL routing protocol for low power and lossy networks," *IEEE transactions on mobile computing*, vol. 16, pp. 964-979, 2016.

[24] H. A. Al-Kashoash, H. Kharrufa, Y. Al-Nidawi, and A. H. Kemp, "Congestion control in wireless sensor and 6LoWPAN networks: toward the Internet of Things," *Wireless Networks*, vol. 25, pp. 4493-4522, 2019.

[25] H.-S. Kim, J. Ko, D. E. Culler, and J. Paek, "Challenging the IPv6 routing protocol for low-power and lossy networks (RPL): A survey," *IEEE Communications Surveys & Tutorials*, vol. 19, pp. 2502-2525, 2017.

[26] H.-S. Kim, J. Paek, D. E. Culler, and S. Bahk, "Do not lose bandwidth: Adaptive transmission power and multihop topology control," in *2017 13th international conference on distributed computing in sensor systems (DCOSS)*, 2017, pp. 99-108.

[27] H. Guo, J. Liu, and H. Qin, "Collaborative mobile edge computation offloading for IoT over fiber-wireless networks," *IEEE Network*, vol. 32, pp. 66-71, 2018.

[28] H. Shah-Mansouri and V. W. Wong, "Hierarchical fog-cloud computing for IoT systems: A computation offloading game," *IEEE Internet of Things Journal*, vol. 5, pp. 3246-3257, 2018.

[29] H.-Y. Kim, "A load balancing scheme with Loadbot in IoT networks," *The Journal of Supercomputing*, vol. 74, pp. 1215-1226, 2018.

[30] A. Pramanik, A. K. Luhach, I. Batra, and U. Singh, "A systematic survey on congestion mechanisms of CoAP based Internet of Things," in *Advanced Informatics for Computing Research: First International Conference, ICAICR 2017, Jalandhar, India, March 17–18, 2017, Revised Selected Papers*, 2017, pp. 306-317.

[31] E. Ancillotti and R. Bruno, "Comparison of CoAP and CoCoA+ congestion control mechanisms for different IoT application scenarios," in *2017 IEEE Symposium on Computers and Communications (ISCC)*, 2017, pp. 1186-1192.

[32] E. Balandina, Y. Koucheryavy, and A. Gurtov, "Computing the retransmission timeout in CoAP," in *Conference on Internet of Things and Smart Spaces*, 2013, pp. 352-362.

[33] R. Ludwig and K. Sklower, "The Eifel retransmission timer," *ACM SIGCOMM Computer Communication Review*, vol. 30, pp. 17-27, 2000.

[34] R. Bhalerao, S. S. Subramanian, and J. Pasquale, "An analysis and improvement of congestion control in the CoAP Internet-of-Things protocol," in *2016 13th IEEE Annual Consumer Communications & Networking Conference (CCNC)*, 2016, pp. 889-894.

[35] R. Hassan, A. M. Jubair, K. Azmi, and A. Bakar, "Adaptive congestion control mechanism in CoAP application protocol for internet of things (IoT)," in *2016 International Conference on Signal Processing and Communication (ICSC)*, 2016, pp. 121-125.

[36] J. J. Lee, S. M. Chung, B. Lee, K. T. Kim, and H. Y. Youn, "Round trip time based adaptive congestion control with CoAP for sensor network," in *2016 international conference on distributed computing in sensor systems (DCOSS)*, 2016, pp. 113-115.

[37] I. Järvinen, I. Raitahila, Z. Cao, and M. Kojo, "Is CoAP congestion safe?," in *Proceedings of the Applied Networking Research Workshop*, 2018, pp. 43-49.

[38] S. Bolettieri, C. Vallati, G. Tanganelli, and E. Mingozzi, "Highlighting some shortcomings of the CoCoA+ congestion control algorithm," in *Ad-hoc, Mobile, and Wireless Networks: 16th International Conference on Ad Hoc Networks and Wireless, ADHOC-NOW 2017, Messina, Italy, September 20-22, 2017, Proceedings 16*, 2017, pp. 213-220.

[39] C. Vallati, F. Righetti, G. Tanganelli, E. Mingozzi, and G. Anastasi, "ECOAP: experimental assessment of congestion control strategies for CoAP using the wishful platform," in *2018 IEEE International Conference on Smart Computing (SMARTCOMP)*, 2018, pp. 423-428.

[40] V. Rathod, N. Jeppu, S. Sastry, S. Singala, and M. P. Tahiliani, "CoCoA++: Delay gradient based congestion control for Internet of Things," *Future Generation Computer Systems*, vol. 100, pp. 1053-1072, 2019.

[41] H. Guo, J. Liu, J. Zhang, W. Sun, and N. Kato, "Mobile-edge computation offloading for ultradense IoT networks," *IEEE Internet of Things Journal*, vol. 5, pp. 4977-4988, 2018.

[42] N.-N. Dao, D.-N. Vu, W. Na, J. Kim, and S. Cho, "SGCO: Stabilized green crosshaul orchestration for dense IoT offloading services," *IEEE Journal on Selected Areas in Communications*, vol. 36, pp. 2538-2548, 2018.

[43] X. Lyu, H. Tian, L. Jiang, A. Vinel, S. Maharjan, S. Gjessing, and Y. Zhang, "Selective offloading in mobile edge computing for the green internet of things," *IEEE network*, vol. 32, pp. 54-60, 2018.

[44] L. Bracciale and P. Loreti, "Lyapunov drift-plus-penalty optimization for queues with finite capacity," *IEEE Communications Letters*, vol. 24, pp. 2555-2558, 2020.

[45] H.-S. Lee and J.-W. Lee, "Task offloading in heterogeneous mobile cloud computing: Modeling, analysis, and cloudlet deployment," *Ieee Access*, vol. 6, pp. 14908-14925, 2018.

[46] C. Zhang, H. Zhao, and S. Deng, "A density-based offloading strategy for IoT devices in edge computing systems," *IEEE Access*, vol. 6, pp. 73520-73530, 2018.

[47] R. Hasan, M. Hossain, and R. Khan, "Aura: An incentive-driven ad-hoc IoT cloud framework for proximal mobile computation offloading," *Future Generation Computer Systems*, vol. 86, pp. 821-835, 2018.
[48] M. S. Elbamby, M. Bennis, and W. Saad, "Proactive edge computing in latency-constrained fog networks," in *2017 European conference on networks and communications (EuCNC)*, 2017, pp. 1-6.
[49] M. Farahani and A. Ghaffarpour Rahbar, "Double leveled unequal clustering with considering energy efficiency and load balancing in dense iot networks," *Wireless Personal Communications*, vol. 106, pp. 1183-1207, 2019.
[50] S. Taghizadeh, H. Bobarshad, and H. Elbiaze, "CLRPL: context-aware and load balancing RPL for IoT networks under heavy and highly dynamic load," *IEEE access*, vol. 6, pp. 23277-23291, 2018.
[51] S. Gheisari and E. Tahavori, "CCCLA: A cognitive approach for congestion control in Internet of Things using a game of learning automata," *Computer Communications*, vol. 147, pp. 40-49, 2019.
[52] P. Kuppusamy, R. Kalpana, and P. Venkateswara Rao, "Optimized traffic control and data processing using IoT," *Cluster Computing*, vol. 22, pp. 2169-2178, 2019.
[53] A. Hussain, S. Manikanthan, T. Padmapriya, and M. Nagalingam, "Genetic algorithm based adaptive offloading for improving IoT device communication efficiency," *Wireless Networks*, vol. 26, pp. 2329-2338, 2020.
[54] B. Kim, J. Jang, J. Jung, J. Han, J. Heo, and H. Min, "A computation offloading scheme for uav-edge cloud computing environments considering energy consumption fairness," *Drones*, vol. 7, p. 139, 2023.
[55] A. Malik and R. Kushwah, "A survey on next generation IoT networks from green IoT perspective," *International Journal of Wireless Information Networks*, vol. 29, pp. 36-57, 2022.
[56] S. Dalal, B. Seth, V. Jaglan, M. Malik, Surbhi, N. Dahiya, U. Rani, D.-N. Le, and Y.-C. Hu, "An adaptive traffic routing approach toward load balancing and congestion control in Cloud–MANET ad hoc networks," *Soft Computing*, vol. 26, pp. 5377-5388, 2022.

Review: Information Security Based on Steganography and Cryptography

Suhair Mohammed Zeki Abd Alsammed[1], Shaima Mohammed Ali[2], Maisa'a Abid Ali Khodher[3]
Computer sciences Department[1], Computer Engineering Department[2,3]

المؤتمر العلمي الدولي الرابع عشر
لجمعية الرياضيات العراقية والمنعقد تحت شعار
الإبداع يلتقي بالتحديات من اجل التقدم العلمي والتكنولوجي
للمدة 4 - 5 اب 2024
دمشق - سورية

University of Technology-Iraq
Baghdad / Iraq
Suhiar.m.abdlsammed@uotechnology.edu.iq, Shaima.m.ali@uotechnology.edu.iq[2],
110044@uotechnology.edu.iq[3]

Abstract:

Information hiding consists of the hid of digital data within computer files. Computational security needs have been focused on vary features high security and confidentiality. This has outcomes in an explosive development of the area of information hiding. The contents picture, sound, and video can be say to as computerized information for conceal data. This paper refers review to several methods in steganography and cryptography in different media. Using steganography methods for texts is a genetic algorithm, LSB, and other manner in frames video, digital image to hide data in image or video or audio. When the cryptography methods also using to merge between steganography and cryptography, for data security increases during transmission across internet, web networks, and workstation. The outcomes obtained is the best in importance the highest security without sensitive by attackers.

Keywords: steganography, Encryption, Video, Image, LSB.

1. Introduction:

Information hiding is the science of written conceal letters in a style that no reading. This hidden message can be between sender and recipient they known this message. In today's agencies are using ciphering science addition data hiding to support or assist themselves with them aim apart from case of way, telecommunication technology and media. the text should not be sensitives to the human eye Imperceptibility, which is a principle requires that area [1,2].

Data hiding methods are divided at two parts: concealment and watermark. features for data concealing methods compare, imperceptions, survive, capacity, and secure [3].

Information hiding is a system to conceal data. It objective to hidden secure data inside a digital covering file (image, sound, video, etc.) wanting presence intrusion. presence intrusion. Steganalysis methods objective for detection the presence of secure datum that concealing in the covering file. if the intrusion was able to detection a existence or reads the hidden letter, the stenography system considered broken [4].

Information Hiding is the operation of concealing a secure letter inside a great medium like, texts, sound, vidimus and picture. That is performed in such a road this data is hiding for everybody excepting for the intentional transmitter and recipient.
Recipient. Into picture or video data hiding with a secret message is popular manner for the time being and can readily be publishing above the World Wide Web [5].

In ciphering, the data is transform to no readable form. Using the secret key providing by the channel only the authorized user can retrieve the data. This encryption data raises the

suspiciousness of attacker for existences the secure data and trying to decrypt the code to take out the data. Data conceals became extra significant which objectives to conceal presence of secure data, to avoid this problem [4].

2. Related Works:

In 2018. Reyam Jassim Essa, et. al. proposed steganography color picture using genetic algorithm (GA). Which rely on GA is using to generate random key (GRK), this represented the best arranging of secure (picture/text) blocks to be concealing in the covering picture. the outcomes are obtained from various exam, see this suggest system proves to be more efficient than another steganography method presented and in comparison with the original covering picture in terms of accuracy standard an goodness of the stego-image [5].

In 2019. Hnin Lai Nyo, and Aye Wai Oo**,** proposed is merge of information hiding and ciphering manners so as to get batter "imperceptibility, robustness, payload capacity" and to send datum security. Arnold scrambling and discrete wavelet transform (DWT) methods are used over the secure picture. these are calculated the referable values from the values of load mystery picture with the using of a secret key and embedded these referable values in the vidimus file via "least significant bit (LSB)" methods. The outcomes, execution of the system is exam with various real time pictures and different vidimus goodness files and measured via various parameters (PSNR, MSE), That is as well analyses for attacks [6].

In 2020. C. Senthilkumar, et. al. proposed a new method for increasing the vidimus safety via uses One Time Password (OTP) and sound key as password and enhancement compressing average via uses "Blind detection algorithm". The uses of blind detection algorithm contain higher computational precision, high flexibility and transfer rapid executed via an estimated higher PSNR value. This paper as well contains compressing picture, sound and vidimus files and embedded inside on vidimus [7].

In 2021. J. Jasim Zahraa, and A. Mohanad J.**,** proposed a modern manner to conceal datum in vidimus via uses 2 BitAND and BitOR operations unwanting uses the famous LSB algorithm into conceal technique. And uses a genetically algorithm via who the ciphering key is generate, confidential data is first ciphered, which is increased the power of the proposed algorithm. The outcomes see that using manner is active and safety as it supplies a PSNR range is 63, who takes the embedded capacity higher [1].

In 2021, Hiba H. Hassan, and Maisa'a A. K., proposed to password have uses to extra safety for system into hash function. Ciphering algorithm, it contains 5 stages: The primary stage: define the even point and Classify picture, the second stage: Cryptography (password using Hash Function, the third stage: transform the secure latter and secure picture for binary number uses via ACSII code, the fourth stage: It is selecting letter or picture to conceal in covering picture uses LSB, the fifth stage: execution system process. Given outcomes of proposed system are obtaining, efficiency, transparency, capacity, higher safety, and robustness. During assessed of system using MSE, PSNR, histogram, and Entropy [8].

In 2022. Miran Hikmat Mohammed, proposed a modern method to security text data while exchange between permitted users on top of the internet. Using AES and ECC are a merge

of ciphering and hiding with sound and picture multimedia, which jobs on conceal and ciphering data before transfer it on top of a networks. As outcome, this manner will add additional secure operations to the datum exchanging, and it will supply safe environment for the user to connection for the network. adding, the goodness of the datum will not be change or note through the ciphering and deciphering operation [9].

In 2022. Maisa'a Abid Ali Khodher, et. al., proposed a method to encrypt secure letters uses DNA and a 3D chaotic map at vidimus framing uses a Raster technique. The system uses third stages: First, convert vidimus frames into raster method to extraction of features from all frames. Second, encrypt of secure letters uses encode form of DNA basic, "inverse/inverse complements of DNA". And it's used 3D chaotic ma, Third, conceal encrypted secure letters into that raster vidimus frame via used a secure key at 4 corners of every all vidimus frames. This method conceals the largest size to secure datum cause the vidimus frame is a larger and agree any letter sizes. Given outcomes are efficiently, robustness, higher safety, and can afford higher capacity. These results have been obtained from a set of exams similar: "peak signal to noise ratio (PSNR), mean square error (MSE), entropy, correlation coefficient, and histogram and capacity" [10].

In 2023. Abbas Zamil Hussain, and Maisa'a Abid Ali Khodher**,** proposed three types of chaotic maps are used to construct a digital picture encrypted strategy rely on chaotic system. These are three methods to chaotic maps "the logistic map, Arnold Cat's map, and Baker's map". and uses the triple data encrypted standards (3DES) encrypted schemes with the chaotic maps aforementioned. The outcomes of the tests detected that the proposed digital picture encrypted method is both efficient and safety, makes it perfect for uses in unsafety networks [11].

In 2023. Asmaa Hasan Alrubaie, et.al., proposed a new image encryption algorithm, 2DNALM, depended on double-dynamic DNA sequence ciphering and a chaotic 2D logistic map. The three steps regarding the proposed manner are as follows: the first step: includes permuting the location of the pixels using a location key-based scrambling process. The second step includes twice DNA encoding on scrambled pictures using different rules via DNA cryptography concept to produce an encoded picture, and in the final step, the picture which has been encoded is encrypted using XOR process and chaotic keys created through a chaotic 2D logistic map. The entropy analysis and exams findings show that the proposed scheme display higher encryption and withstands several common attacks [12].

In 2023, May Alanzy, et. al., proposed Multi-Level Steganography (MLS) algorithm that uses two ciphering algorithms, AES and Blow-Fish, to security the covering image and embedded ciphering keys as key pictures within the stego image. The suggested MLS algorithm combine a robust pixel randomization function to enhance the secure of ciphered datum. the exams of outcomes explain that the proposed algorithm effectively protects datum with high Peak Signal-to-Noise Ratio (PSNR) and low Mean Square Error (MSE) values, including excellent picture quality, reliable encryption, and decryption of security letters.

The uses of hybrid ciphering with AES and BlowFish algorithms further very strong the algorithm's secure via augmenting the complexity of the encryption operation [13].

3. Steganography Method:

The steganography art is derived from the Greek words "stegos" meaning "cover" and "grafia" meaning "writing" defining it as "covered writing", using to conceal secure letter in to text, picture, vidimus, sound, and protocol. The secure letter either the picture or text, using a set of methods [14]. as shown in Fig. 1.

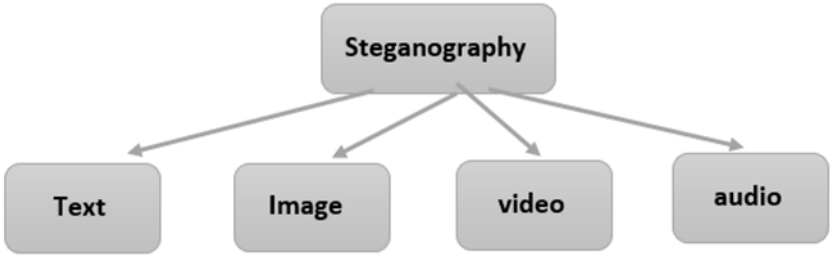

Fig.1: The steganography types [14].

The steganography consists of two kinds: letter and load. Letter is the secure datum that should be conceal and load is the covering that takes the letter in it [15]

4. Encryption Method:

data is ciphered and deciphered used a secure key (in several algorithms uses a various key to ciphering and deciphering). In missing key, the datum not ability be access and is therefore protection from unauthorized or wrongful operation [16].

There are 2 kinds of ciphering in common uses: symmetric and asymmetric ciphering. The noun driving for whether or not the same key is using for enciphering and deciphering [16].

1-Symmetric encryption

In symmetric enciphering in same key is using for enciphering and deciphering. It is then critical a secret manner is considered for transform the key among client and server, as shown in Fig. 2.

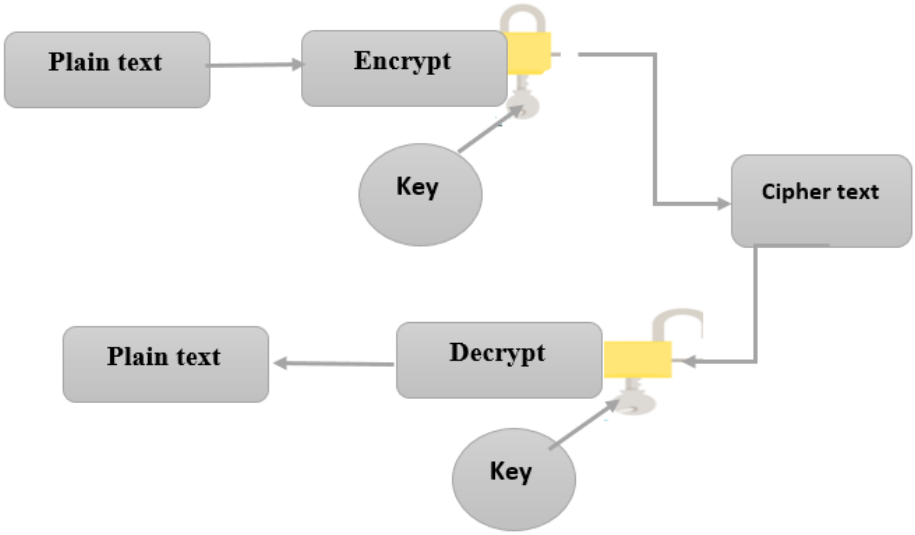

Fig. 2: The symmetric encryption in same key [16].

1- Asymmetric encryption

Asymmetric enciphering is using the notion of two keys: a various key is uses for the encrypted and decrypted operation. In Asymmetric using keys: the first is **private key**, the second is **public key**.

The **private key** is keep secure via the holder and the public key is either sharing among commissioned recipient or made ready-made to the public in big [16].

Datum encryption with the recipient's public key can only be decryption with the identical private key. Datum can be transfer without the risk of unauthorized or illegal incoming for the datum, as shown in Fig. 3.

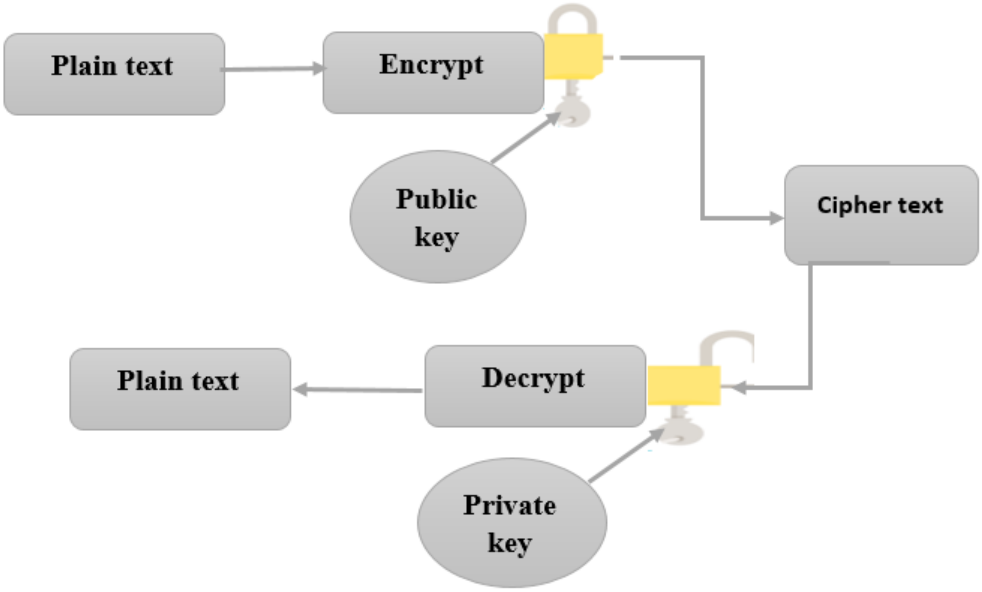

Fig. 3: The asymmetric encryption in the different key [16].

5. Cipher Methods:

The cipher methods consist of many approaches which given high security through communication many people across internet, networks web, and workstations.
Cipher is classification in three parts: **Substitution cipher, stream cipher** and **block cipher**, each them include many techniques.

Substitution Cipher, Caesar Cipher, Monoalphabetic Ciphers, Playfair Cipher, Hill Cipher, Polyalphabetic Ciphers, and One-Time Pad.

Stream Cipher: Linear feedback shift registers, Feedback polynomial, Exclusive -OR Algorithm, Hadamard Algorithm, and Berlekamp-Massey algorithm [17, 18].
Block Cipher: Electronic Codebook (ECB), Cipher Block Chaining (CBC), Cipher Feedback (CFB), Output Feedback (OFB), Counter (CTR), Digital Encryption Standard (DES), and Advance Encryption Standard (AES) [17, 18].

6. Comparison security of data in steganography and encryption:

In this section refers comparison for results of related works in this paper using several tests for these measures PSNR, MSE, security, and capacity. As shown in Table 1.

It is notes in Table 1. most researches not found values of capacity. whereas capacity is very importance in hide secret messages, and the average between PSNR and MSE, always PSNR is increase whereas MSE is reduces, because cover frame video or image before hide and after hide secret message must be similarity in different methods in hiding, and high security.

Table 1: The comparison security of data

Ref. No.	Name of authors	Methods	PSNR	MSE	Security	capacity
Ref.5	Reyam Jassim Essa, et. al. **2018**	**GA**	**0.4386**	**51.7444**	**High**	**-**
Ref.6	Hnin Lai Nyo, and Aye Wai Oo. **2019**	**DWT LSB Twisted Exchange**	**21.4558**	**469.5221**	**High**	**-**

Ref.7	C. Senthilkumar, et. al. **2020**	**OTP LSB**	**-**	**-**	**High**	**-**
Ref.1	J. Jasim Zahraa, and A. Mohanad J. **2021**	**GA LSB**	**63.56**	**0.083**	**High**	**-**
Ref.8	Hiba Hamdi Hassan, and Maisa'a Abid Ali Khodher **2021**	**Fuzzy C-mean Cluster LSB**	**63.68**	**0.0278**	**High**	**0.02083**
Ref.9	Miran Hikmat Mohammed **2022**	**AES ECC HDWT**	**-**	**-**	**High**	**-**
Ref.10	Maisa'a Abid Ali Khodher, et. al. **2022**	**DNA 3D Logistic Map Raster**	**17.4686**	**26.3210**	**High**	**0.01278**
Ref.11	Abbas Zamil Hussain, and Maisa'a Abid Ali Khodher **2023**	**Arnold Cat's map Baker's map 3DES**	**9.9718**	**20807**	**High**	**-**
Ref.12	Asmaa Hasan Alrubaie, et.al. **2023**	**2DNA 2D logistic map**	**13.0618**	**3238.1500**	**High**	**-**

Ref.13	May Alanzy, et. al. **2023**	**Multi-level AES Blow-Fish**	**80.2500**	**0.00061 387**	**High**	**480**

7. Conclusions:

In this paper, when using encryption and steganography manners to supply protection higher for data sent upon insecure channels. The encryption manner is given good outcomes, which increased the strength of encryption, as unauthorized people could not know the key. The cryptography manners helped to change plain texts to cipher text in for a more secret structure, that is not readable and detect via attackers. And the texts became high security. Therefor steganography is divided in two levels: concealing cipher text in the picture, then can be concealing the picture with cipher text into a sound file or video.

That to enhancement higher level security, the encryption keys manners are used. Data secure using data concealing in sound, video and picture to enhancement better concealing capacity and security. The major attribute of these systems are transparency, imperceptibility, security, and robustness.

References

1. J. Jasim Zahraa, and A. Mohanad J., "Improving The Security of Steganography In Video Using Genetic Algorithm", Turkish Journal of Computer and Mathematics Education, vol.12, No. 8(2021), pp. 3189-3194.

2. N. koduri, "Information security through image steganography using least significant bit algorithm," Master Thesis, Information Security and Computer Forensics University of East London, 2011.

3. M. Kavitha, Z. H. Mahmoud, Kakarla Hari Kishore, AM Petrov, Aleksandr Lekomtsev, Pavel Iliushin, Angelina Olegovna Zekiy, Mohammad Salmani, "Application of Steinberg Model for Vibration Lifetime Evaluation of Sn-Ag-Cu-Based Solder Joints in Power Semiconductors", IEEE Transactions on Components, Packaging and Manufacturing Technology, 11(3), 2021, pp. 444-450

4. M. Bilal, S. Imtiaz, W. Abdul, S. Ghouzali, and S. Asif, "Chaos based Zero-steganography algorithm," *Multimedia tools and applications*, vol. 72, No. 2, 2014, pp. 1073-1092.

5. Reyam Jassim Essa, Nada A.Z. Abdullah, Rawaa Dawoud AL-Dabbagh," Steganography Technique using Genetic Algorithm", Iraqi Journal of Science, 2018, Vol. 59, No.3A, pp. 1312-1325.

6. Hnin Lai Nyo, Aye Wai Oo, "Secure Data Transmission of Video Steganography Using Arnold Scrambling and DWT", I. J. Computer Network and Information Security, 2019, 6, pp. 45-53

7. C.Senthilkumar, K.Gayathri Devi, M.Dhivya, R.Rajkumar," A Novel Method on Enhanced Video Security using Steganography", International Journal of Recent Technology and Engineering (IJRTE), Vol.9, Issue. 1, May 2020, pp 705-709.

8. Hiba Hamdi Hassan, Maisa'a Abid Ali Khodher," Data Hiding by Unsupervised Clustering Using Fuzzy C-Mean", Design Engineering, Issue: 7, 2021, pp. 14192-14210.

9. Miran Hikmat Mohammed, " A new approach to hide texts into mages and audio files using steganography and cryptography techniques", International Journal of Advances in Applied Sciences (IJAAS), Vol. 11, No. 4, December 2022, pp. 312-323.

10. Maisa'a Abid Ali, Ashwak Alabaichi, and Ammar A. Altameemi", Steganography Encryption Secret Message in Video Raster Using DNA and Chaotic Map", Iraqi Journal of Science, 2022, Vol. 63, No. 12, pp. 5534-5548.

11. Abbas Zamil Hussain, and Maisa'a Abid Ali Khodher**,** "Medical image encryption using multi chaotic maps", TELKOMNIKA Telecommunication Computing Electronics and Control Vol. 21, No. 3, June 2023, pp. 556-565.

12. Asmaa Hasan Alrubaie, Maisa'a Abid Ali Khodher, and Ahmed Talib Abdulameer, "Image encryption based on 2DNA encoding and chaotic 2D logistic map", Journal of Engineering and Applied Science (2023) 70:60, pp 1-21.

13. May Alanzy, Razan Alomrani, Bashayer Alqarni, and Saad Almutairi, "Image Steganography Using LSB and Hybrid Encryption Algorithms", Applied Sciences (MDPI), 2023, 13, 11771, pp 1-20.

14. Masoud Nosrati, Ronak Karimi, and Mehdi Hariri," An introduction to steganography methods", World Applied Programming, Vol (1), No (3), August 2011, pp. 191-195.

15. Nagam Hamid, R. Badlishah Ahmad, Abid Yahya, and Osamah Al-qershi, "Image Steganography Techniques: An Overview",International Journal of Computer Science and Security (IJCSS), Vol. (6), Issue (3) : 2012, pp. 168-187.

16. "Data Protection, Encryption" Book, Information Commissioner's, 4 April 2017, pp. 1-36.

17. William Stallings, "Cryptography and Network Security" Prentice Hall, Edition 5th, 2011, pp. 1-900.

18. William Stallings, "Cryptography and Network Security" Prentice Hall, Edition 4th, 2005, pp. 1-983.